UNIVERSITA' VITA-SALUTE SAN RAFFAELE

CORSO DI DOTTORATO DI RICERCA INTERNAZIONALE IN MEDICINA MOLECOLARE

Curriculum in Basic and Applied Immunology and Oncology

DISSECTING MOLECULAR MECHANISMS CONTROLLING INFLAMMATORY GENE EXPRESSION IN MACROPHAGES

DoS: Renato Ostuni, PhD

Second Supervisor: Michele De Palma, PhD

Tesi di DOTTORATO DI RICERCA di Francesco Cilenti

Matr. 013834

Ciclo di Dottorato XXXIV

SSD BIO/11

Anno Accademico 2021/2022

UNIVERSITA' VITA-SALUTE SAN RAFFAELE

CORSO DI DOTTORATO DI RICERCA INTERNAZIONALE IN MEDICINA MOLECOLARE

Curriculum in Basic and Applied Immunology and Oncology

DISSECTING MOLECULAR MECHANISMS CONTROLLING INFLAMMATORY GENE EXPRESSION IN MACROPHAGES

DoS: Renato Ostuni, PhD

Second Supervisor: Michele De Palma, PhD

Tesi di DOTTORATO DI RICERCA di Francesco Cilenti

Matr. 013834

Ciclo di Dottorato XXXIV

SSD BIO/11

Anno Accademico 2021/2022

CONSULTAZIONE TESI DI DOTTORATO DI RICERCA

Il sottoscritto/ *I* FRANCESCO CILENTI

Matricola/ *registration number* 013834

Nato a/ *born at* MILANO

Il/ *on* 11/05/1993

autore della tesi di Dottorato dal titolo / *author of the PhD Thesis entitled*:

DISSECTING MOLECULAR MECHANISMS CONTROLLING INFLAMMATORY
GENE EXPRESSION IN MACROPHAGES

AUTORIZZA la Consultazione della tesi / *AUTHORIZES the public release of the thesis*

Data / *Date*   Firma / *Signature*

28/10/2021

DECLARATION

This thesis has been composed by myself and has not been used in any previous application for a degree. Throughout the text, I use both 'I' and 'We' interchangeably.

The results of this thesis have been published (Cilenti, Barbiera et al., Immunity, 2021).

Part of the text, figure, figure legends and materials and methods were taken from Cilenti, Barbiera et al., Immunity, 2021

Results in chapter 4 of the thesis were obtained with the following co-author:

Dr. Giulia Barbiera, PhD, SR-Tiget, San Raffaele Scientific Institute Milano, IT - Computational analyses (figures 1-3, 7-9, 13, 15-19, 37, 39-46, 48, 49, 51-53, 57, 59, 60, 62, 70, 71, 78-83).

All the results presented here were obtained by myself, except for:

- Dr. Nicoletta Caronni, PhD, SR-Tiget, San Raffaele Scientific Institute Milano, IT - Cell manipulation, quantitative real-time PCR and flow cytometry (figures 21-25)
- Dr. Elisa Montaldo, PhD, SR-Tiget, San Raffaele Scientific Institute Milano, IT - Cell manipulation, quantitative real-time PCR (figure 20)
- Pietro di Lucia, Division of Immunology, Transplantation and Infection Diseases, San Raffaele Scientific Institute Milano, IT - Infection with VSV (figures 75, 76)
- Dr. Paolo Miotto, Division of Immunology, Transplantation and Infection Diseases, San Raffaele Scientific Institute Milano, IT - Infection with BCG and *M.tb*. (figures 75, 76)

All sources of information are acknowledged by means of reference.

ACKNOWLEDGMENTS

DEDICATION

Ringrazio Renato Ostuni per la supervisione del lavoro in questi anni di Dottorato, per il supporto e gli indispensabili consigli che giornalmente mi ha dato e che mi hanno permesso di crescere dal punto di vista professionale e personale.

Ringrazio tutti i membri del Lab Ostuni, con i quali ho condiviso giornate di lavoro ed emozioni. Un particolare ringraziamento va a Marco Genua, che mi ha insegnato a muovere i primi passi in laboratorio e con cui ho condiviso gran parte del tempo in questi anni. Ringrazio anche particolarmente Nicoletta Caronni (la Nic) per le risate e i momenti spensierati insieme a Simona Barresi e il sostegno nei momenti un po' più difficili.

I miei amici sono sicuramente le persone a cui devo un grazie enorme perché sono riusciti a farmi sorridere e ridere in qualunque momento, a regalarmi abbracci e sguardi che ricorderò sempre.

Il grazie più grande va a Mamma e Papà, sempre al mio fianco a sostenermi. Spero siano fieri di me.

Abstract

Tight control of inflammatory gene expression by antagonistic environmental cues, namely immunostimulatory and immunomodulatory, ensures immune protection and avoid tissue damage. However, the molecular mechanisms regulating inflammatory gene expression by immunomodulatory signals remain largely uncharacterized. In this study, we dissected the genomic features of genes and *cis*-regulatory regions induced by lipopolysaccharide (LPS) and the impact of immunomodulatory signals on their activation in murine macrophages. We particularly focused on prostaglandin E_2 (PGE_2), an arachidonic derivative with a multitude and complex immunoregulatory activities, and found to counteract the activation of a set of LPS-inducible gene enhancers, including type I interferon (IFN I). Targeted gene enhancers display poorly permissive chromatin organization already in unstimulated macrophages and were marked by the transcription factor myocyte enhancer factor 2A (MEF2A). Loss of MEF2A phenocopied PGE_2 treatment, namely impaired activation of inflammatory gene enhancers and abolished IFN I production upon exposure to multiple innate immune stimuli. Mechanistically, PGE_2 interfered with LPS-induced activation of ERK5, a known interactor of MEF2. This study identifies a PGE_2-MEF2A as relevant axis involved in the control of inflammatory gene expression and IFN I response in macrophages.

TABLE OF CONTENTS

ACRONYMS AND ABBREVIATIONS

AP-1: Activator Protein 1

ASH2L: Absent, Small, or Homeotic disc 2-Like

ATAC-Seq: Assay for Transposase Accessible Chromatin coupled to Sequencing

ATP: Adenosine TriPhosphate

BAM: Border-Associated Macrophage

BET: Bromodomain and ExtraTerminal domain

bHLH: Basic Helix-Loop-Helix

BM: Bone Marrow

BMDM: Bone Marrow-Derived Macrophage

BP: Base Pair

BRD: BRomoDomain

C/EBP-α: CCAAT/Enhancer Binding Protein alpha

cAMP: Cyclic Adenosine MonoPhosphate

CBP: CREB-Binding Protein

CCL5: Chemokine C-C motif Ligand 5

CD: Cluster of Differentiation

ChIP-Seq: Chromatin ImmunoPrecipitation followed by high throughput Sequencing

CREB: cAMP Response Element-Binding

CRX: Cone-Rod homeoboX protein

DAMP: Damage-Associated Molecular Pattern

DLL4: Delta Like canonical NOTCH Ligand 4

DNMT3L: DNA MethylTransferase 3 L

EBF: Early B cell Factor

EICE: ETS-IRF Composite Element

ERK: Extracellular signal-Regulated Kinase

ETS: Erythroblast Transformation Specific

H1: Histone 1

H2A: Histone 2A

H2B: Histone 2B

H3: Histone 3

H3K4me1/me3: Mono/trimethylation of lysine 4 of H3

H3K27ac: Acetylation of lysine 27 of H3

H4: Histone 4

H5: Histone 5

HAT: Histone AcetylTransferase

HDAC: Histone DeACetylase

HSC: Hematopoietic Stem Cell

IϰB: Inhibitor of NF-kappaB

ICER: Inducible cAMP Early Repressor

ID3: Inhibitor of DNA binding 3

IFN: InterFeroN

IFN I: type I IFN

IFN-β: InterFeroN beta

IFNAR: InterFeroN Alpha Receptor

IKK: IϰB kinase

IL-1: Interleukin-1

IL-1β: Interleukin-1 beta

IL-4: Interleukin-4

IRAK: Interleukin-1 Receptor-Associated Kinase

IRF3: Interferon Regulatory Factor 3

IRF8: Interferon Regulatory Factor 8

ISGF3: IFN-Stimulated Gene Factor 3

ISRE: IFN-Stimulated Responsive Element

JAK1: JAnus Kinase 1

JNK: c-Jun N-terminal Kinase

KLF2 and **KLF4:** Kruppel-Like Factor 2 and 4

KO: Knock Out

LBP: LPS-Binding Protein

LDTF: Lineage-Determining Transcription Factor

LPS: LipoPolySaccharide

LXRα: Liver-X-Receptor alpha

M-CSF: Macrophage Colony-Stimulating Factor

MADS: MCM1, AGAMOUS, DEFICIENS, and SRF

MAPK: Mitogen-Activated Protein Kinase

MAPKK: Mitogen-Activated Protein Kinase Kinase

MEF2: Myocyte Enhancer Factor 2

MD2: Myeloid Differentiation Factor 2

MHCII: Major Histocompatibility Complex class II

mPGES-1: microsomal prostaglandin E_2 synthase 1

MYD88: MYeloid Differentiation primary response protein 88

NF-ϰB: Nuclear Factor kappa-light-chain-enhancer of activated B cells

PAMP: Pathogen-Associated Molecular Pattern

PEST: proline (P), glutamic acid (E), serine (S) and threonine (T)

PIC: Pre-Initiation Complex

PKA: Protein Kinase A

PRR: Pattern-Recognition Receptor

PTGER1-4: Prostaglandin E_2 receptor 1-4

OCT: POU domain transcription factor

PGE$_2$: Prostaglandin E_2

PLCγ2: PhosphoLipase C gamma 2

PRC: Polycomb Repressive Complex

PTM: Post-Translational Modification

RBPJ: Recombination signal Binding Protein for immunoglobulin kappa J region

RNAPII: RNA Polymerase II

RUNX1: RUNt-related transcription factor 1

SMAD: Small Mothers Against Decapentaplegic

STAT: Signal Transducer and Activator of Transcription

TAK1: TGFβ-activated kinase 1

TAM: Tumor-Associated Macrophage

TBK1: TANK Binding Kinase 1

TF: Transcription Factor

TGF-β: Transforming Growth Factor beta

Th: T helper

TIR: Toll-Interleukin Receptor

TIRAP: Toll/Interleukin-1 Receptor domain-containing Adapter Protein

TLR: Toll-Like Receptor

TNF-α: Tumor Necrosis Factor alpha

TRAF6: TNF Receptor Associated Factor 6

TRAM: TRanslocation-Associated Membrane protein

TRIF: TIR domain-containing adapter-inducing InterFeron beta

TRM: Tissue-Resident Macrophage

TYK2: TYrosine Kinase 2

TSS: Transcription Start Site

WT: wild-type

LIST OF FIGURES AND TABLES

Figure 86-92: PGE$_2$ targets MEF2A-dependent gene expression by modulating ERK5 activity.

CHAPTER 1

SELECTION OF THE MACROPHAGE-SPECIFIC REPERTOIRE OF *CIS*-REGULATORY ELEMENTS

Regulation of *cis*-regulatory elements

Eukaryotic cells display highly condensed genomic DNA complexed with proteins and non-coding RNA, referred to chromatin. Nucleosomes represent the basic repeating unit of the chromatin and consist of an octamer core comprising two copies of four histone proteins, namely histone 2A (H2A), histone 2B (H2B), histone 3 (H3) and histone 4 (H4). Each nucleosome is composed by 146 bp double-stranded DNA wrapped around the core and prevents binding to *cis*-regulatory elements of RNA polymerase II (RNAPII) and DNA-binding proteins able to modulate transcription, also known as transcription factors (TFs) (Hammond et al. 2017; Yadav, Quivy, and Almouzni 2018).

Cis-regulatory regions, such as promoters and enhancers, are DNA sequences enriched for TF binding sites and capable of driving context-dependent gene expression by recruiting components of the transcriptional machinery. Gene transcription requires the formation of the pre-initiation complex (PIC), composed by RNAPII, co-factors, and proteins with DNA binding activities, known as general transcription factors. The latter factors bind to specific DNA sequences usually located ± 50 base pairs (bp) around the transcription start site termed 'core promoter' and determine the physical location of the PIC. Other DNA-binding proteins can cooperate with general transcription factors and influence the recruitment of RNAPII. These proteins bind to DNA sequences adjacent to the core and define a larger genomic region referred to as promoter (Andersson and Sandelin 2020; Haberle and Stark 2018).

To allow PIC assembly and initiation of transcription, chromatin at core promoters and at the transcription start site (TSS) must be accessible and depleted of nucleosomes. The first nucleosomes located upstream and downstream the TSS (termed as -1 and +1 nucleosome, respectively) determine the degree of accessibility of the promoter regions since they can undergo to different structural changes that affect stability, composition, and positioning (Mavrich et al. 2008). Accessibility of promoters is also influenced by DNA sequence and increases according to the abundance of cytosine and guanine residues (Segal et al. 2006). Genomic regions with an over-representation of CG di-nucleotides, termed as CpG island, account for approximately 70% of mammalian gene promoters and display low nucleosome occupancy. CpG island usually mark housekeeping genes, and therefore identify genomic regions accessible to transcriptional machinery (Fenouil et al. 2012).

Promoter activity can be modulated by direct contact with distal *cis*-regulatory elements through chromatin loops. Enhancers are DNA sequences located up to thousands of kilobases away from target genes. These genomic regions contain multiple binding sites for cell type-restricted and environment-activated TFs and drive cell type-specific and context-dependent gene expression (Oudelaar and Higgs 2021).

The activity of the enhancers is regulated by post-translational modifications (PTMs) on the N-terminal tail of histones. For instance, histone acetyltransferases (HATs) catalyse the transfer of an acetyl group from acetyl-coenzyme A to the amino-group of lysine side chains of H3 and H4, while class I and class II histone deacetylases (HDACs) exert the opposite function (Bannister and Kouzarides 2011). The enzymatic activities of HATs and HDACs also involve non-histone proteins, among which TFs are the main members, and regulate a multitude of cellular processes, including cell cycle and DNA damage repair (Choudhary et al. 2009). For instance, acetylation of p53 by the ubiquitously expressed HATs p300 and CREB-binding protein (CBP) promotes its transcriptional activity via multiple mechanisms, as by increasing DNA binding activity (Yang and Seto 2008).

Addition or removal of acetyl group on histone proteins is a highly dynamic and tightly controlled process associated to peculiar chromatin states and transcriptional activities. *In vitro* assays allowed the study of the direct impact of histone acetylation on chromatin structure. It has been showed that PTMs affect the strength of DNA-nucleosome as well

as inter-nucleosomal interactions and the degree of permissivity of the chromatin. Addition of an acetyl group on a lysine 27 of histone H3 (H3K27ac) neutralizes the positive charge of the histone tail and reduces the strength of the interactions between DNA and nucleosomes, resulting in relaxed conformation of the chromatin and increased accessibility to the transcriptional machinery (Bannister and Kouzarides 2011; Nitsch, Zorro Shahidian, and Schneider 2021). In line with this, enrichment of H3K27ac in *cis*-regulatory elements associates to gene transcription (Lara-Astiaso et al. 2014).

However, positive regulation of gene transcription by histone acetylation mostly relies on the recruitment of several chromatin-associated factors, including proteins containing bromodomain (BRD), which recognizes and binds to acetylated lysines. BRD proteins are frequently associated to large multisubunit complexes and promote chromatin decompaction and transcriptional activity (Fujisawa and Filippakopoulos 2017). The bromodomain and extraterminal domain (BET) family consists of four proteins (namely, BRD2, BRD3, BRD4 and testis specific BRDT) characterized by two N-terminal BRDs that bind to acetylated lysine residues of histones and a C-terminal domain responsible for the interaction with TFs and other chromatin-associated factors (Shen et al. 2015)

BET proteins recruit chromatin remodelling complexes to acetylated promoters and enhancers in order to modulate nucleosome occupancy or positioning. Access to DNA sequences to *cis*-regulatory regions by TFs relies on dynamic regulation of nucleosome positioning by adenosine triphosphate (ATP)-dependent chromatin remodelling complexes (Gaykalova et al. 2011; Kujirai and Kurumizaka 2020; Kulaeva, Hsieh, and Studitsky 2010). The SWI/SNF represents an evolutionary conserved family of chromatin remodelling complexes firstly described in yeast and composed by multiple subunits (Clapier et al. 2017). Recent studies established SWI/SNF complexes as central regulator of cell fate decision since required to activate cell type-restricted enhancers through a direct interaction with p300 (Alver et al. 2017; Vierbuchen et al. 2017). Increased chromatin accessibility by remodelling complexes can be achieved by multiple mechanisms, including repositioning or eviction of nucleosomes. The ATPase subunit of SWI/SNF complexes hydrolyses ATP to progressively break interactions between DNA and histones and promote translocation of DNA along the surface of the core. The rate of ATPase activity determines the degree of alterations of nucleosome positioning. Low-to-moderate ATPase activity results in dynamic DNA-histone contacts and nucleosome

sliding, while high ATPase activity leads to disruption of DNA-histone contacts and ejection of the octamer (Clapier et al. 2016).

In this view, histone acetylation promotes the establishment of a chromatin environment permissive to gene transcription. However, it has been recently showed that inhibition of RNAPII activity caused a rapid reduction of H3K27ac at promoter and enhancer regions. These results point out that active transcription impacts on H3K27ac and identify deposition of histone acetylation as a transcription-dependent mechanism (Wang et al. 2021). The supportive rather than causative role of histone acetylation on transcription has been also suggested in mutant embryonic stem cells with reduced levels of H3K27ac selectively at enhancers. Indeed, lack of H3K27ac did not impact on chromatin accessibility at the enhancers of pluripotent genes and minimally affected the expression of the latter genes (T. Zhang et al. 2020).

Chromatin immunoprecipitation followed by sequencing (ChIP-Seq) experiments revealed the presence of p300 at active enhancers marked by H3K27ac. Consequently, binding of p300 is dynamically regulated in response to environmental cues (Ghisletti et al. 2010; Heintzman et al. 2009). Thousands of enhancers gain p300 binding in activated macrophages and associate to inflammatory genes induced upon exposure to inflammatory signal (Ghisletti et al. 2010). These studies also revealed that genomic regions of inducible p300 binding have a peculiar chromatin signature and show enrichment of monomethylation of the lysine 4 of H3 (H3K4me1). High levels of H3K4me1, in combination with low levels of trimethylated lysine 4 of H3 (H3K4me3), associate to active enhancers, and therefore identify cell-type specific regulatory repertoire, while high levels of H3K4me3 correlate to promoter regions (Heintzman et al. 2007, 2009). The presence of H3K4me1 precedes p300 binding and H3K27ac deposition during differentiation in multiple model systems, prevents recognition and binding of proteins involved in chromatin condensation, such as DNA methyltransferase 3 L (DNMT3L), and promotes incorporation of histone variants that facilitate chromatin relaxation (Lan et al. 2007; Ooi et al. 2007).

The concomitant presence of p300, H3K4me1 and trimethylation of the lysine 27 of H3 (H3K27me3) defines a set of functionally inactive enhancers with a permissive chromatin configuration that ensures rapid activation. This class of regulatory regions, termed as 'poised' enhancers, has been originally identified in human and mouse

embryonic stem cells, where marked genes that progressively lost H3K27me3 and gained H3K27ac during differentiation (Caglio, Torlai Triglia, and Pombo 2017; Rada-Iglesias et al. 2011). Deposition of H3K27me3 relies on the Polycomb Repressive Complex 2 (PRC2), which binds to poised enhancers and contributes to chromatin compaction. PRC2 participates in the establishment of the poising state of enhancers also by directly mediating contact between enhancers and promoters of target genes. This physical proximity creates a permissive environment that ensures correct activation of target genes during differentiation (Crispatzu et al. 2021; Cruz-Molina et al. 2017).

Combinatorial activity of TFs defines the *cis*-regulatory landscape in macrophages

Role of PU.1 and lineage-determining transcription factors (LDTFs)

Acquisition of cell type identity relies on combinatorial activity of TFs able to selectively activate a defined set of *cis*-regulatory regions. Selection of the repertoire of *cis*-regulatory regions implies the capacity of a group of TFs, termed as 'pioneer', to recognize their cognate binding site on nucleosomal DNA and to promote chromatin opening. A subset of pioneer factors acts as lineage-determining TFs (LDTFs) since they define the repertoire of active *cis*-regulatory regions specific for each cell type and thus drive the acquisition of cell identity (Zaret 2020). Among LDTFs, PU.1 is required to instruct macrophage identity. Indeed, PU.1 deficiency results in impaired development of tissue resident macrophages in the embryo as well as early myeloid progenitors in the bone marrow and defects in the lymphoid compartment (Dakic et al. 2005; Schulz et al. 2012). PU.1 belongs to the ETS (erythroblast transformation specific) family of TFs, one of the largest family of TFs characterized by a highly conserved DNA binding domain composed of three α-helices and four β-sheets that recognizes and binds to 5'-GGAA-3' motif, and a PEST (proline, glutamic acid, serine, and threonine) domain that mediates interactions with TFs and other chromatin-modifying proteins. The expression of PU.1 is directly regulated by TFs, such as runt-related transcription factor 1 (RUNX1)

(Hoogenkamp et al. 2009), in hematopoietic stem and progenitor cells (HSCs) and early multipotent progenitors in a macrophage colony-stimulating factor (M-CSF) manner and progressively increases during differentiation. PU.1 also directly regulates its own expression and induces the transcription of the M-CSF receptor, thus establishing a positive feedback loop that sustains its activity (Lichtinger et al. 2012; Mossadegh-Keller et al. 2013).

ChIP-Seq experiments revealed that PU.1 pervasively binds the genome of macrophages. PU.1 occupancy preferentially occurs within genomic regions characterized by high levels of H3K4me1 and low levels of HK4me3 and marks the macrophage-specific set of active enhancers, as well as within a large fraction of promoters. Reduced expression of PU.1 in bone marrow-derived macrophages (BMDMs) results in decreased level of H3K4me1 at selected enhancers, while ectopic expression of PU.1 in non-immune cells as fibroblast leads to expression of myeloid genes and increased H3K4me1 signal at macrophage-specific enhancers (Ghisletti et al. 2010). These data indicate that PU.1 establishes the identity by regulating chromatin accessibility and selects and activates macrophage-specific regulatory regions. However, PU.1 occupancy shows an additional layer of selectivity since it does not bind to all the potential sites within the genome (that are approximately hundreds of thousands), but only to a fraction of them. Selective occupancy of PU.1 relies on functional cooperation with other lineage-restricted TFs, such as interferon regulatory factor (IRF8) in macrophages, whose level of expression was recently found to determine lineage choice towards dendritic cells, monocytes, or neutrophils (Murakami et al. 2021). Interestingly, binding motifs of collaborative TFs occurs within 100 bp, but mostly at a distance higher than 20 bp, indicating that cooperative activity of TFs does not rely on protein-protein interactions in most cases (Kazemian et al. 2013). In this view, PU.1 acts as pioneer and renders genomic regions accessible to other lineage-restricted factors unable to open chromatin, thus establishing a cooperative activity that results in the activation of cell type-specific repertoire of regulatory elements. PU.1-IRF8 elements, usually referred to ETS-IRF composite elements (EICEs), control the basal expression (i.e., expression in unstimulated cells) of a broad set of genes, including genes associated to tissue repair activity, and inducible expression of immune genes, as *Ifnb1*, upon inflammatory stimulation (Mancino et al. 2015).

Motif enrichment analyses performed on genomic regions bound by PU.1 revealed a differential representation of motifs between macrophages and B cells. Resting cells display a distinct PU.1 binding profile, with only a fraction of regions occupied by PU.1 in both cell types. In macrophages, PU.1 binds in close proximity to sites occupied by CCAAT/enhancer binding protein alpha (C/EBP-α), described to regulate the entry of multipotent progenitors into myeloid lineage (Giladi et al. 2018), and activator protein 1 (AP-1), while E2A (encoded by *Tcf3* gene), EBF (early B cell factor), OCT (POU domain transcription factor) and NF-ϰB (nuclear factor kappa-light-chain-enhancer of activated B cells) TFs in B cells (Sven Heinz et al. 2010). Mutations in the C/EBP, as well as AP-1, motifs result in loss of nearby PU.1 occupancy and reduced deposition of histone marks associated to open chromatin (S. Heinz et al. 2013; Link et al. 2018). These studies provide functional evidence supporting that cooperative activity between PU.1 and other LDTFs defines the cell-specific set of active *cis*-regulatory regions and therefore cell identity.

Role of tissue-restricted TFs

Macrophages establish a profound relationship with the tissue of residence and can be considered as fully integrated and dispensable components that support the maintenance of homeostasis (Guilliams et al. 2020). Seminal studies reported the capacity of myeloid precursors as well as differentiated macrophages to engraft, adapt to environmental signals and acquire transcriptional and functional programs of resident cells (Gosselin et al. 2014; van de Laar et al. 2016; Lavin et al. 2014). This concept underpins the phenotypic diversity of macrophages across tissues. However, tissues are not uniform entities but include multiple and distinct cell types and signals that instruct different programs, and therefore different macrophage subpopulations with niche-specific functions within the same tissue. The heterogeneity of tissue-resident macrophages has been reported by several studies that describe distinct cell subsets according to the specific gene expression profile, function, and localization. Single cell transcriptomic and epigenomic allow to dissect intra-tissue heterogeneity of resident macrophages. For instance, transcriptional profiling of lung interstitial macrophages identifies two distinct populations of resident macrophages with distinct localization and functions. These two

subsets, identified as expressing high or low levels of major histocompatibility complex class II (MHCII), originate from bone marrow (BM)-derived monocytes in homeostasis and localize in close proximity to nerves or blood vessels, respectively (Chakarov et al. 2019). Similarly, two main subsets of BAMs (border-associated macrophages) were identified according to the level of expression of MHCII. These BAM populations share a core set of genes, such as *Apoe*, *Cd36* and *Pf4*, and express a set of genes selectively in MHCII^high (i.e., *Cd72* and *Cd74*) and MHCII^low (i.e., *Maf*, *Igf1* and *Mrc1*) cells (Van Hove et al. 2019).

The heterogeneity of resident macrophages has to be ascribed to functional specification in response to local environmental signals. Macrophage precursors that colonize tissues in the embryo share a common gene signature and express genes associated to cell identity, including TFs (*Maf* and *Irf8*), cytokine receptors (*Il4ra* and *Ifngr2*) and complement system (*C1qa*, *C1qb* and *C1qc*) genes. Within tissues, macrophages acquire tissue-specific expression of TFs, such as *Nr1h3* (encoding liver-x-receptor α, LXRα) and *Id3* and in liver macrophages (also known as Kupffer cells) and *Pparg* in alveolar macrophages (Mass et al. 2016). The expression of tissue-restricted TFs is required for the acquisition of tissue-specific gene expression profiles and the development of tissue-resident macrophages (TRMs). Deficiency of the TF inhibitor of DNA binding 3 (ID3) results in impaired Kupffer cell number, while development of microglia and kidney macrophages is not affected (Mass et al. 2016). Loss of Kupffer cells leads to transient production of chemokines and adhesion molecules that allow monocyte recruitment and engraftment in the liver. Here, niche-derived signals promote the expression of *Nr1h3* and *Id3*, which drive the acquisition of Kupffer cell-specific transcriptional profile in differentiating monocytes (Bonnardel et al. 2019). Therefore, specification of macrophage phenotype is not pre-determined in precursors but occurs within the tissue and is established by niche-specific signals. In this context, macrophages can acquire a multitude of identities because of the capacity to sense and integrate tissue-derived signals on the pre-existing *cis*-regulatory repertoire defined by LDTFs.

Profiling genome-wide histone modifications for active and poised distal regulatory regions reveals that resident macrophages isolated from different tissues exhibit distinct enhancer landscapes because of the differential usage of the pre-existing repertoire by tissue-restricted TFs. For instance, active enhancers in peritoneal macrophages show an

over-representation of the binding motif for the GATA TF family, while MEF2 binding motif was enriched in microglia-specific active chromatin regions (Gosselin et al. 2014; Lavin et al. 2014). These findings support that tissue-restricted TF drive the selection of tissue-specific enhancers within the available repertoire of *cis*-regulatory regions defined by PU.1 and other LDTFs.

The niche-derived signals activating tissue-restricted TFs and the underlying mechanisms are only just starting to be identified. Recent studies identified TFs and upstream regulators driving differentiation of Kupffer cells by assessing quantitative and qualitative changes of chromatin accessibility over time. Upon depletion of liver macrophages, circulating blood monocytes infiltrate the tissue and progressively acquire a chromatin profile resembling that of Kupffer cells and marked by the binding motif of the tissue-specific TF LXRα, flanked by binding motif for SMAD (small mothers against decapentaplegic) and RBPJ (recombination signal binding protein for immunoglobulin kappa J region) TFs. Mechanistically, endothelial cells of liver sinusoids and stellate cells produce transforming growth factor (TGF-β) and the NOTCH ligand DLL4 (delta like canonical NOTCH ligand 4), that activate the downstream TFs SMAD and RBPJ, respectively. These two TFs induce the expression of Kupffer cell-specific genes, including LXRα, which collaborate with PU.1 and LDTFs to select tissue-restricted enhancer landscape upon activation by desmosterol produced by hepatocytes (Bonnardel et al. 2019; Sakai et al. 2019).

CHAPTER 2

MECHANISMS OF ACTIVATION OF INFLAMMATORY GENE ENHANCERS

Signalling pathways and TFs activated by inflammatory cues

Macrophages orchestrate rapid immune responses upon recognition of pathogens and sensing of tissue damage. This capacity relies on the expression of a plethora of receptors that recognizes conserved molecular patterns of microbial and endogenous origins, termed as pathogen-associated molecular patterns (PAMPs) and damage-associated molecular patterns (DAMPs), respectively. PAMPs and DAMPs initiate immune responses through the engagement of pattern-recognition receptors (PRRs) located on plasma or endosomal membrane and cytoplasmic sensors. Toll-like receptor (TLR) is an evolutionary conserved family of PRRs consisting of an N-terminal ectodomain domain of leucine-rich repeats, which recognizes and binds to the ligand, a transmembrane domain, and a cytosolic TIR (Toll-interleukin receptor) domain responsible for the activation of downstream signalling cascades (Roers, Hiller, and Hornung 2016).

Endosomal TLRs, such as TLR3, 7, 8 and 9, display intraluminal ectodomain and cytosolic TIR. The peculiar localization of these receptors prevents aberrant activation by self-nucleic acids and allows recognition of nucleic acids of microbial origin. While TLR9 recognizes and binds to single-stranded DNA sequences containing a pattern of unmethylated CG dinucleotides (CpG), which are more frequently found in procaryotes, TLR3, TLR7 and TLR8 sense RNA molecules. In particular, TLR3 detects double-stranded RNA of viral origin, while TLR7 and TLR8 recognizes single-stranded RNA molecules enriched in uridine nucleoside (Roers, Hiller, and Hornung 2016).

TLRs located on plasma membrane, such as TLR4, recognize components of the cell surface of microbes. TLR4 and its downstream signalling pathways have been extensively characterized in immune cells, especially in macrophages. TLR4 detects LPS, the major component of the outer membrane of gram-negative bacteria. LPS is a

glycolipid composed by an oligosaccharide chain (termed as O-antigen), which differs in the number of saccharide units across bacterial species and strains, an oligosaccharide core and a glucosamine dimer linked to a varying number of acyl chains (also known as lipid A), that anchors the molecule to the wall and is responsible for the activation of TLR4 (B. S. Park and Lee 2013).

In the context of infection, the extracellular LPS-binding protein (LBP) interacts with LPS and induces alterations of the bacterial outer membrane to favour the transfer of a single molecule of LPS to CD14 (cluster of differentiation 14), which can exist as soluble or membrane-anchored forms. Soluble CD14 allows cells not expressing this protein, such as endothelial cells, to sense LPS, thus expanding the repertoire of cell types able to respond and amplify anti-microbial effects. CD14 transfers LPS to myeloid differentiation factor 2 (MD2) protein, which stably interacts with the N-terminal domain of the TLR4 and induces dimerization of the receptor (Gioannini et al. 2004; Ryu et al. 2017). Moreover, CD14 acts independently on TLR4 and induces the activation of phospholipase $C\gamma2$ ($PLC\gamma2$) and calcium influx, leading to internalization of TLR4 in the endosomes (Tan et al. 2015; Zanoni et al. 2009, 2011).

Dimerization of TLRs activates hundreds of biochemical reactions that modulate distinct biological processes. Upon receptor engagement, plasma membrane-bound TIRAP (Toll/interleukin-1 receptor domain-containing adapter protein) recognizes and binds to dimerized TIR domains and induces the assembly of a large multi-subunit complex of cytosolic proteins known as myddosome (Bonham et al. 2014). The myddosome is composed by multiple copies of the adaptor protein MYD88 (myeloid differentiation primary response protein 88), members of IRAK (interleukin-1 receptor-associated kinase) family of kinases, and the E3 ubiquitin ligase TRAF6 (TNF receptor associated factor 6), which catalyses the transfer of ubiquitins on lysine 63 residues of various adaptor proteins and induces the activation of phosphorylation cascades (Gay, Gangloff, and O'Neill 2011). Ubiquitin chains act as docking platform and recruit the kinase TAK1 (TGFβ-activated kinase 1), which then phosphorylates IKKα and IKKβ (IκB kinase α and β), leading to the interaction with IKKγ and full activation of IKK complex. IKK phosphorylates a variety of targets, including IκB proteins α and β (inhibitor of NF-κB α and β). In resting cells, IκB binds to and masks the nuclear localization signal of the TF NF-κB. Stimulus-induced phosphorylation of IκB results in

its ubiquitination and proteasomal degradation, followed by release and nuclear translocation of NF-κB as a dimer usually comprising p50 and p65 (also termed as RelA) subunits (Hinz and Scheidereit 2014; Taniguchi and Karin 2018). TAK1 also phosphorylates and activates MAPKKs (mitogen-activated protein kinase kinase), resulting in activation of MAPKs (mitogen-activated protein kinase), such as p38, ERK (extracellular signal-regulated kinase) and JNK (c-Jun N-terminal kinase), and AP-1 TF complex, composed by JUN and FOS TFs. Signal-dependent activation of NF-κB and AP-1 occurs rapidly, within minutes, and results in the expression of thousands of genes, including pro-inflammatory cytokines, in order to eliminate the invading agent and restore homeostasis (Fitzgerald and Kagan 2020).

Activation of NF-κB and AP-1 is also mediated by other inflammatory mediators as tumor necrosis factor α (TNF-α) and interleukin 1 (IL-1). The engagement of cognate receptors involves the activation of multiple adaptor proteins and the recruitment of TAK1. The downstream signalling pathways resemble the MYD88-dependent one, and results in inflammatory gene expression. Therefore, distinct signals bind to cognate receptors but activate a limited number of signalling molecules and TFs (Sabio and Davis 2014; Weber, Wasiliew, and Kracht 2010).

Deficiency of MYD88 results in abolished signalling from all TLRs, except from TLR4 and TLR3, indicating additional MYD88-independent mechanisms of signalling. Analogously to TIRAP, translocation-associated membrane protein (TRAM) anchored to plasma and endosomal membrane binds to dimerized TLR3 and TLR4 and recruits the adaptor protein TRIF (TIR domain-containing adapter-inducing interferon b) and TRAF3 and 6. The assembly of such complex, termed as triffosome, results in the activation of TAK1-dependent pathways and the kinase TBK1 (TANK binding kinase 1), which phosphorylates TRIF. This modification induces the recruitment of TBK1 in complex with interferon regulatory factor 3 (IRF3) TF and the activation of the latter by the kinase (Liu et al. 2015). Phosphorylated IRF3 dimerizes, translocates to the nucleus, and activates the expression of several genes, including the pro-inflammatory cytokine interferon β (IFN- β) in macrophages (Fitzgerald and Kagan 2020). Activation of TRIF-dependent pathway requires endosomal internalization of the TLR4. Therefore, the engagement of TLR4 induces two temporally distinct signalling pathways: TLR4 first

induces MYD88-dependent pathway from the plasma membrane and then is endocytosed and activates TRIF-dependent pathway (Kagan et al. 2008).

Production of IFN- β activates an auto/paracrine loop that induces the expression of interferon (IFN)-dependent genes, mostly anti-viral genes. IFN- β belongs to type I IFN (IFN I) family along with IFN-α and endows with antiviral activities since restricts viral replication and coordinates immune responses by triggering the production of cytokines and chemokines and promoting activation of dendritic cells and adaptive immunity. IFN I binds to interferon alpha receptor (IFNAR), a heterodimeric cell surface receptor comprising of IFNAR1 and IFNAR2 subunits, and activates tyrosine kinases, namely JAK1 (Janus kinase 1) and TYK2 (tyrosine kinase 2), which phosphorylate STAT1 and STAT2 (signal transducer and activator of transcription 1 and 2). Phosphorylated STAT1 and STAT2 dimerize, translocate to the nucleus and associate with IRF9 (interferon regulatory factor 9) to form a ternary complex termed as IFN-stimulated gene factor 3 (ISGF3). This complex binds to IFN-stimulated responsive elements (ISRE) and activates the expression of genes involved in viral restriction (*Ifit1-3*, *Oas2*, *Oas3*), TFs that reinforce inflammatory gene expression (*Irf1*, *Irf7*), cytokines and chemokines (*Tnf*, *Cxcl9* and *Cxcl10*) (Ivashkiv and Donlin 2014; Barrat, Crow, and Ivashkiv 2019).

Activation of inflammatory gene enhancers in macrophages

The immediate consequence of activation of signal-dependent TFs entails the site-specific recruitment of co-activators and other partners involved in modulation of chromatin accessibility and activity of RNAPII. Multi-subunits complexes comprising chromatin remodelling factors, histone acetyltransferase and bromodomains assemble at activated enhancers and positively regulate RNAPII activity and gene transcription (Ramirez-Carrozzi et al. 2006; Nicodeme et al. 2010). Stimulation of BMDMs with LPS induces BRD4 to bind at the promoters of a set of inflammatory genes and recruit positive transcription elongation factor b (P-TEFb), which allows processing of mature mRNA and induces activating phosphorylation at the C-terminal domain of RNAPII (Hargreaves, Horng, and Medzhitov 2009). Conditional deletion or chemical inhibition of BRD4

results in impaired induction of inflammatory genes including *Il6* and *Il10*, indicating BRD4 as required to activate inflammatory enhancers and transcription (Nicodeme et al. 2010; Dey et al. 2019).

Exposure of macrophages to LPS induces coordinated expression of hundreds of genes in temporally distinct waves and allows to study the contribution of multiple signal-activated TFs to gene transcription. Based on the sensitivity to inhibition of protein synthesis, genes induced by LPS can be classified in two main classes, namely primary and secondary response genes (Smale 2010). Genes belonging to the primary response are usually rapidly induced and do not require *de novo* protein synthesis for their expression. Therefore, transcription of these genes relies on signal-dependent TFs that are constitutively expressed but activated by post-translational modifications upon stimulation: in line with this, the induction of primary response genes (as *Tlr2*, *Nfkbia* and *Ifnb1*) is dependent on NF-κB and IRF3 TFs. Deeper analysis of the kinetics of induction of primary response genes revealed that *Ifnb1* displays unique mechanisms of regulation. Activation of NF-κB contributes to initial induction of *Ifnb1*, while IRF3 is required to sustain the expression at later time points. This dual regulation is also supported by motif enrichment analysis showing an over-representation of NF-κB and IRF3 binding sites at the *Ifnb1* promoter, suggesting a cooperative activity of these two TFs at this locus (Tong et al. 2016).

Secondary response genes are instead induced with delayed kinetics and usually require *de novo* synthesis of TFs, signalling molecules or cytokines that act in auto/paracrine manner (Smale 2010). The differences between primary and secondary response genes in kinetics of induction mostly rely on the basal chromatin accessibility at *cis*-regulatory elements and the requirement of nucleosome remodelling. Promoters of most primary response genes tend to exhibit basally high H3K27ac and H3K4me3, low nucleosome occupancy and association of SWI/SNF complex, indicating a permissive chromatin conformation already prior to stimulation. In addition, primary response genes generally display high content of CpG island at their promoters, which associate to RNAPII already in unstimulated macrophages. By contrast, high nucleosome occupancy and low CpG island content characterize the promoters of secondary response genes. Therefore, these genes require SWI/SNF-mediated chromatin remodelling because of

inaccessible chromatin configuration at basal level (Hargreaves, Horng, and Medzhitov 2009; Ramirez-Carrozzi et al. 2006, 2009).

While the induction of primary response genes occurs rapidly and it requires limited chromatin remodelling and inducible recruitment of SWI/SNF complex, a fraction of the latter genes requires SWI/SNF complex and relies on IRF3. A paradigmatic example is represented by *Ifnb1*, whose expression is tightly controlled by nucleosome barrier. *Ifnb1* promoter contains binding sites for signal-dependent TFs and a stable +1 nucleosome in unstimulated cells. Engagement of TLR4 induces sequential binding of NF-κB and IRF3 at the *Ifnb1* promoter and recruitment of nucleosome remodelling complex, resulting in sliding of the +1 nucleosome and association of RNAPII (Smale 2010).

Activation of signal-dependent TFs induces profound changes in chromatin architecture, with thousands of enhancers activated in a highly coordinated fashion and in a stimulus-specific manner. The definition and the maintenance of enhancer landscape are crucial for proper induction of inflammatory gene expression. To this regard, cohesin-deficient macrophages fail to induce inflammatory genes, including IFN-β and IFN-dependent genes, upon *in vitro* exposure to LPS. Genome-wide profiling of chromatin accessibility by ATAC-Seq (assay for transposase accessible chromatin coupled to sequencing, (Buenrostro et al. 2013)) reveals an impaired gain in accessibility at LPS-inducible enhancers and promoters, associated to reduced H3K27ac. In accordance with defective induction of IFN I response of cohesin-deficient macrophages, deregulated inducible enhancers display an over-representation of ISRE and IRF:PU.1 composite motif (Cuartero et al. 2018).

The acquisition of stimulus-specific chromatin profiles and transcriptional outputs relies on the selective activity of a limited number of signal-dependent TFs mainly on the available pre-existing repertoire of regulatory regions determined by LDTFs and other cell type-specific TFs. Such restricted activity of signal-dependent TFs depends on the inability to bind to nucleosomal DNA and requires LDTFs to make cognate motifs accessible. For this reason, the same signal-dependent TF occupies distinct genomic regions and induces various transcriptional (and functional) responses across different cell types. Exposure to LPS of distinct immune cell types (both lymphoid and myeloid) results in transcriptional induction of a shared set of genes, such as those induced by IFN

I, while the induction of other genes preferentially and selectively occurs in one cell type, as *Tlr2* in macrophages and *Gzmb* in NK cells (Jaitin et al. 2014).

Enhancers occupied by stimulus-activated TFs display peculiar chromatin features, namely a high enrichment in H3K4me1 and occupancy by LDTFs and cell type-restricted TFs. For instance, genomic regions bound by LXR in macrophages largely overlap with cell-specific pattern of H3K4me1, and display co-occurrence of PU.1 and AP-1 motifs (Sven Heinz et al. 2010). To study the impact of PU.1 on macrophage *cis*-regulatory landscape, a hematopoietic progenitor cell line derived from fetal liver of PU.1 knock out (KO) mouse has been generated. Retroviral transduction of deficient cells with a chimeric protein obtained by fusing wild-type (WT) PU.1 with the ligand-binding domain of the oestrogen receptor (PUER) allows tamoxifen-inducible reconstitution of PU.1 and differentiation in macrophages (Walsh et al. 2002). PU.1 deficiency causes reduced H3K4me1 levels as well as LXR occupancy, indicating that PU.1 is required to promote deposition of H3K4me1, maintain chromatin accessible and enable binding of signal-dependent TFs (Sven Heinz et al. 2010). In the context of TLR4 stimulation, *de novo* enhancers, namely genomic regions proximal to PU.1 ChIP-Seq peak gaining accessibility after exposure to lipid A, exhibit over-representation of motifs for NF-κB, AP-1 and ISRE and are marked by LDTFs PU.1 and C/EBP, similarly to regions of inducible p300 binding. Binding of NF-κB requires PU.1 and induces H3K4me1 deposition at *de novo* enhancers, supporting the role of LDTFs in establishing cell type-specific regulatory elements and keeping them accessible to stimulus-activated TFs. The latter TFs in turn cooperate with LDTFs to support signal-dependent chromatin remodelling and ensure proper gene transcription (Ghisletti et al. 2010; Kaikkonen et al. 2013).

The establishment of basal and LPS-inducible enhancer repertoire in macrophages also requires cooperation of IRF8 with different partners TFs. In this context, IRF8 is required not only for cell identity but also for inflammatory transcriptional response. This dual activity relies on its unique DNA binding properties: IRF8 binds to DNA with high affinity only upon interaction with other TFs and occupies distinct genomic regions according to its partner. IRF8 constitutively binds to approximately 9,000 sites in association with PU.1 in unstimulated cells and contributes to basal expression of identity and inflammatory genes, mainly IFN-dependent genes. Exposure to LPS results in

increased number of sites bound by IRF8 (approximately 15,000), mainly in regions not constitutively occupied by PU.1 and in association with signal-dependent TFs IRF1 or AP-1. In line with its dual role, IRF8 deficiency results in decreased basal chromatin accessibility at identity and inflammatory enhancers, and impaired activation and transcriptional induction of inflammatory gene enhancers (Mancino et al. 2015).

The activity of stimulus-induced TFs is not restricted to pre-existing *cis*-regulatory elements but also occurs at genomic regions that acquire enhancer features upon stimulation. Exposure of BMDMs to LPS induces the activation of enhancers that are inactive, unbound and unmarked in unstimulated cells. These regulatory regions, called latent enhancers, lack H3K4me1, H3K27ac and PU.1 binding in unstimulated cells but acquire these features upon LPS stimulation. The emergence of latent enhancers represents a common feature in response to exogenous stimuli. Indeed, as seen with LPS, pro-inflammatory mediators, such as TLR agonists, TNF-α, IL-1β and IFN-γ, and immunoregulatory cytokines, such as TGF-β and interleukin-4 (IL-4), induce small sets of latent enhancers characterized by the acquisition of H3K4me1 and H3K27ac chromatin marks and PU.1 binding. In particular, IFN-γ and IL- 4 activate two sets of unique and non-overlapping latent enhancers bound by STAT1 and STAT6 TFs, activated by IFN-γ and IL-4 respectively. These stimulus-activated enhancers are not bound by PU.1 at the basal state because of the presence of low affinity binding sites. Therefore, PU.1 is not able to bind to these closed chromatin regions, to promote nucleosome depletion and to induce enhancer formation. Mechanistically, STAT TFs translocate into the nucleus upon stimulation, bind to latent enhancers and recruit PU.1. Thus, functional cooperation with stimulus-activated TFs allows PU.1 to occupy such sites and to induce enhancer activation by recruiting chromatin remodelling and histone-modifying complexes. Although latent enhancers loose H3K27ac and PU.1 binding upon cytokine removal, H3K4me1 was maintained for days after stimulus removal, indicating that a signal-specific epigenomic signature is maintained for a short period of time, and allows faster reactivation upon re-exposure to the same signal (Ostuni et al. 2013).

Contribution of myocyte enhancer factor (MEF) family of TFs to enhancer activation

The establishment and maintenance of stimulus-responsive landscape of regulatory regions in macrophages also relies on myocyte enhancer 2 (MEF2) family of TFs. The four members of this family, namely MEF2A, -B, -C and -D, share an N-terminal domain, containing the highly conserved MADS-box domain (residues 2-57) and the MEF2-specific domain (residues 58-86), and a C-terminal transactivation domain. The MADS-box and the MEF2 domains are required for dimerization of MEF2 TFs and the DNA binding to the consensus sequence 5'-CTATTTTTGG-3' (Gossett et al. 1989; J D Molkentin et al. 1996).

The possible contribution of MEF2 in establishing the macrophage epigenome in macrophages has been provided in populations of TRMs. MEF2C expression emerged to be preferential in the most represented subset of brain macrophages, termed microglia, and contributed to select cell type-specific enhancer repertoire (Lavin et al. 2014). MEF2C knock out microglia did not show evident transcriptional differences compared to WT counterpart in homeostatic condition. However, upon inflammatory stimulus MEF2-deficient microglia expressed higher levels of inflammatory cytokines such as chemokine C-C motif ligand 5 (CCL5), TNF-α and interleukin-1 β (IL-1β), indicating the requirement of MEF2 to regulate inflammatory response in a relevant *in vivo* context (Deczkowska et al. 2017). A report in *Drosophila melanogaster* also suggests a conserved role of MEF2 TF across species. Animals with reduced expression of MEF2 displayed deficient induction of genes encoding for antimicrobial peptides. Such impaired innate immune response resulted in reduced survival upon *Listeria monocytogenes* infection (Clark et al. 2013)

The contribution of MEF2 TFs to the establishment of cell type-specific regulatory repertoire is not restricted to macrophages and relies on the association with lineage- and tissue-restricted TFs. For instance, MEF2 drives cardiac and skeletal muscle differentiation by regulating the expression of myogenic basic helix-loop-helix (bHLH) TFs and by cooperating with them to induce muscle-specific genes (T. C. Cheng et al. 1993; Creemers et al. 2006; Jeffery D. Molkentin et al. 1995; Sandmann et al. 2006). More recently it has been shown that MEF2D gene exists as two different isoforms,

namely a ubiquitously expressed (MEF2Dα1) and a muscle-specific isoform (MEF2Dα2). ChIP-Seq analysis revealed that the two isoforms shared a large set of target genomic regions but only the muscle-specific isoform was responsible for driving tissue-restricted gene expression. Mechanistically, MEF2Dα2, but not MEF2Dα1, interacts with ASH2L (absent, small, or homeotic disc 2-like) co-activator and does not with class II HDACs, thus inducing the expression of muscle-specific genes (Sebastian et al. 2013).

MEF2 TFs also contribute to neuronal differentiation and plasticity by controlling dendrite and synapse formation (Chen et al. 2016; Cole et al. 2012; Flavell et al. 2006; Shalizi et al. 2006). MEF2D is a critical regulator of photoreceptor development since knock out mice showed de-regulated expression of photoreceptor-related genes and morphologically and functionally compromised photoreceptor cells. ChIP-Seq analysis revealed that MEF2D selectively binds to enhancers and promoters controlling the expression of photoreceptor-related genes. Interestingly, genomic regions bound by MEF2D in photoreceptor cells minimally overlap with those retrieved in neuronal cells or in myocytes, indicating that MEF2D binding is selective and occurs in a cell type-specific manner. MEF2D binding at retina-specific enhancers is dependent on the interaction with the photoreceptor-specific transcription factor cone-rod homeobox protein (CRX). Mechanistically, MEF2D is recruited by CRX to photoreceptor-specific enhancers and cooperates with CRX to activate cell type-specific regulatory regions and gene expression program (Andzelm et al. 2015). In contrast, loss of MEF2D in granule neurons is partially rescued by the compensatory activity of the paralogue MEF2A. Upon MEF2D depletion, MEF2A occupancy is increased at a subset of regions bound by MEF2D, where H3K27ac levels as well as gene expression are minimally affected. These compensatory regions display more accessible chromatin than non-compensatory ones, suggesting that chromatin configuration is the main driver of MEF2A binding at these sites in MEF2D-deficient neurons (Majidi et al. 2019).

CHAPTER 3

CONTEXT-DEPENDENT MODULATION OF INFLAMMATORY GENE EXPRESSION

From stimulus-dependent to context-dependent gene expression

Macrophages are endowed with the capability of sensing a variety of environmental signals and can acquire distinct gene expression and functional profiles in a stimulus-specific manner. This ability, referred as plasticity, relies on the dynamic organization of the *cis*-regulatory repertoire and the combinatorial activity of TFs and chromatin-associated complexes. Studies on macrophage plasticity have been originally focused on the analyses of transcriptional perturbations of cells exposed *in vitro* to a single agent. In this context, the definition of the response to IFN-γ (released by T helper 1 CD4$^+$ cells) and/or LPS and IL-4 (produced, instead, by T helper 2 CD4$^+$ cells) identified opposing functional and transcriptional states associated to immunostimulatory and immunomodulatory activities, respectively. These two extremes of activation states have been originally referred to M1 and M2 and underpin differential metabolism of arginine upon exposure to LPS between macrophages derived from C57BL/6 and BALB/c mouse strains. While macrophages from C57BL/6 strain preferentially induce nitric oxide synthase (*Nos2*) and promote production of nitric oxide and T helper 1 (Th1) response, macrophages from BALB/c induce arginase (*Arg1*) to produce ornithine and T helper 2 (Th2) response. In analogy, macrophages stimulated with IFN-γ and/or LPS express high levels of *Nos2* and other inflammatory genes (i.e., *Ccl5* and *Il12b*) and display cytotoxic activities, while cells exposed to IL-4 express genes such as *Arg1* and others associated to immunomodulatory and tissue repair phenotype (i.e., *Retnla*, *Mrc1* and *Chil3*) (Mills 2012; Mills et al. 2000).

M1-M2 nomenclature is not restricted to *in vitro* stimulated macrophages but in some cases is used to define *in vivo* activation states associated with inflammatory or immunomodulatory phenotypes. Such definition is based on the expression of certain markers retrieved from *in vitro* activated cells with IFN-γ or IL-4 and therefore leads to consider only 'two types' of macrophages. For instance, macrophages resident in the white adipose tissue express genes associated to tissue reparative and M2 program, such as *Arg1*, *Pparg* and *Klf4*, while express inflammatory genes of the M1 program in obesity, including *Nos2*, *Tnf* and *Il6* (Kihwa Kang et al. 2008; Lumeng, Bodzin, and Saltiel 2007). Although this dualistic model has largely contributed to a deeper characterization of macrophage biology, it does not consider some aspects. First, macrophages display high level of transcriptional and functional heterogeneity not only across tissues but also within the same tissue. Second, macrophages face to a multitude of environmental cues. Such signals do not determine a terminal and irreversible status but drives on-demand responses. In turn, macrophages are capable of changing their activation state and rapidly adapt to the environment in a dynamic and reversible fashion. The peculiar organization of the regulatory landscape of macrophages allows adaptation and context-dependent responses. Adaptation relies on the combinatorial and integrating activity of TFs induced by multiple and different environmental signals and results in a re-organization of the *cis*-regulatory repertoire, as well as in metabolic reprogramming. The resulting chromatin state allows context-dependent gene expression and can be reverted upon stimulus removal, even though can persist long-term and affect future responses in some cases (Natoli and Ostuni 2019; Ostuni et al. 2013). For instance, repeated or persistent exposure to high dose of LPS or TNF results in a transient hypo-responsive state of macrophages to a further stimulation. Such functional state, usually referred as tolerance, represents an evolutionary conserved mechanism of defense that limits tissue damage and allows protection from infections (Seeley and Ghosh 2017). Tolerized macrophages acquire gene-specific chromatin features: genes encoding inflammatory cytokines do not display increased H3K4me3 at their promoters and are not induced at transcript level, while genes encoding antimicrobial molecules gain H3K4me3 and expression (Foster, Hargreaves, and Medzhitov 2007; Novakovic et al. 2016). Somehow in contrast, exposure of macrophages or monocytes, but also dendritic cells as recently described (Hole et al. 2019), to bacterial or fungal products leads to a faster and stronger response to unrelated

second stimulation or subsequent infection, thus providing non-stimulus-specific protection against a secondary challenge. Such stronger response to secondary stimulation has been attributed to metabolic alterations and relatively long-lasting persistence of chromatin alterations that occur after the first stimulation in myeloid progenitors in the bone marrow (S. C. Cheng et al. 2014; Kaufmann et al. 2018; Mitroulis et al. 2018; Quintin et al. 2012; Saeed et al. 2014).

In this context, the M1-M2 dualism results over-simplistic and cannot recapitulate the diverse and dynamic context-dependent activities of macrophages. Gene expression analyses of macrophages exposed *in vitro* to a panel of cytokines and TLR agonists revealed stimulus-specific gene expression programs and refined the model of macrophage activation beyond M1-M2 (Xue et al. 2014). However, the activation state of macrophages relies on the context and results from the integration of multiple environmental inputs. Such integration occurs at the level of signalling pathways (Hu and Ivashkiv 2009) as well as at chromatin level by combinatorial activities of identity and stimulus-activated TFs and drives different possible outputs ranging from neutrality, synergism, or antagonism.

Synergistic and antagonistic effects on inflammatory gene expression

Exposure to functionally coherent stimuli, such as IFN-γ and LPS, results in synergistic induction of inflammatory genes. Synergism between inflammatory cues is particularly relevant in the pathogenesis of inflammatory diseases and superinfections, where IFN-γ signature is highly expressed in activated macrophages. In this context, IFN-γ has been shown to enhance the response of macrophages to TLR4 engagement by different mechanisms. IFN-γ induces the production of inflammatory mediators and reinforce TLR signalling by promoting the expression of components of the pathway, including TLRs and MYD88 (Hu and Ivashkiv 2009). Mechanistically, exposure to IFN-γ induces the recruitment of STAT1 and IRF1 to DNA and increases chromatin accessibility at promoters and enhancers of cytokine genes as *Il6*, *Tnf* and *Il12b*. Such priming activity of IFN-γ removes nucleosome barrier and predisposes chromatin to a

faster and more robust transcription to subsequent exposure to LPS by cooperative activity of STAT1, NF-κB and other TFs (Qiao et al. 2013). Enhanced response to LPS also relies on suppressive activity of IFN-γ on feedback inhibitory mechanisms involving IL10-STAT3 pathway. IL-10 endows with immunomodulatory activities, ranging from maintenance of tissue homeostasis in the gut to activation of regulatory T cells (Ouyang and O'Garra 2019) and is produced upon TLR4 engagement as a mechanism to restrain inflammatory response via STAT3 TF (Murray and Smale 2012). IFN-γ has been shown to counteract LPS-inducible expression of *Il10* and suppress binding of STAT3 and recruitment of co-activators to enhancers of IL10-dependent genes (Kyuho Kang et al. 2019).

In contrast, stimulation with TNF-α leads to defective chromatin remodelling and transcriptional induction of a set of inflammatory gene enhancers upon secondary exposure to LPS. Tolerized state can be reverted by concomitant addition of TNF-α and IFN I, resulting in increased H3K4me3 and chromatin accessibility mediated by cooperative activity of NF-κB and IRF TFs (S. H. Park et al. 2017). Conditioning with IFN I or IFN II differentially impacts on the response to TNF-α and other TLR ligands. While IFN I increases TNF-dependent induction of inflammatory genes as *Il1a* and *Il6*, IFN II restrains such response, underlying opposing and gene-specific activities of IFN I and IFN II and signal-specific mechanisms of regulation (Q. Cheng et al. 2019).

These studies provide relevant mechanistic dissection of integration of functionally coherent stimuli administered sequentially. However, cells can be concomitantly exposed to environmental signals with opposite biological functions in several contexts, such as co-infections, tissue repair or cancer. Mouse models of combined infection with helminths and viruses have been used to study macrophage response to functionally opposing signals. Exposure to viral pathogens elicits potent immune response through multiple inflammatory mediators as IFNs, while infection with helminths evokes immunomodulatory responses mediated by cytokines as IL-4 and IL-13 (Gieseck, Wilson, and Wynn 2018). In the context of co-infection, helminths constrain effector functions of virus-specific cytotoxic T cells and promote immunomodulatory activities of macrophages in a IL-4/STAT6-dependent manner, resulting in impaired antiviral immunity (Osborne et al. 2014). A mixture of tumor- and stromal-derived signals with immunostimulatory and immunomodulatory effects contribute to shape the activation

state of tumor-associated macrophages (TAMs). Single cell transcriptomics revealed that TAMs from distinct types of tumours display a 'mixed' gene expression profiles since express genes associated to immunostimulatory and immunomodulatory activities, providing the formal proof 1) that the activation state macrophages is dictated by the context and cannot be simply reduced to M1-M2 2) of the ability of these cells to sense and integrate functionally antagonistic stimuli (Azizi et al. 2018; Lavin et al. 2017).

Integration of antagonistic signals occurs at chromatin level and relies on reciprocal repression of the opposing program. Genomic analysis of macrophages stimulated with IL-4 revealed a selective transcriptional suppression of a set of genes, including inflammatory genes, and decreased histone acetylation, chromatin accessibility and occupancy by LDTFs at their enhancers. The suppressive activity at these enhancers relies on STAT6 and occurs without direct binding to DNA but likely through recruitment of HDAC3 and transcriptional repressor complexes. Subsequent exposure to LPS results in diminished enhancers activation, suggesting the ability of IL-4 to induce durable chromatin re-organization at a set of enhancers and prevent fully activation upon inflammatory cue (Czimmerer et al. 2018).

In a reciprocal way, IFN-γ induces the selective recruitment of PRC2 and the deposition of H3K27me3 at *cis*-regulatory elements of genes with immunomodulatory activities and prevents subsequent activation (Qiao et al. 2016). Therefore, IL-4 and IFN-γ employs durable suppression at selected regulatory regions activated by the opposite program. Enhancers suppressed by IFN-γ are marked by the binding site of MAF. Prolonged exposure to IFN-γ suppresses MAF occupancy at the enhancers but, interestingly, not at the promoters of immunomodulatory genes, including *Il10* and *Sepp1*. The functional inactivation of these enhancers indicates that the antagonism exerted by IFN-γ on immunomodulatory program also relies on the interference with the activity of TFs involved in the definition of the basal enhancer landscape of macrophages (Kyuho Kang et al. 2017).

The concept of chromatin as hub of integration of antagonistic signals is further supported by studies in which macrophages have been concomitantly exposed to IFN-γ and IL-4 for a short period of time. RNA-Seq analyses of co-stimulated cells revealed that these two cytokines antagonize each other's transcriptional program, exemplified by the impaired induction of *Nos2* and *Ccl5* by IL-4 and *Arg1* and *Retnla* by IFN-γ. However,

the mutual repressive effect occurs selectively for a set of induced genes, since the expression of most of the genes is largely unaffected or, in some cases, increased. The lack of alterations at the signaling pathway level supports the existence of selective mechanisms of mutual repression. Indeed, transcriptional antagonism is reflected in a global attenuation of H3K27ac deposition and an impaired inducible histone acetylation at a subset of *cis*-regulatory regions with peculiar genomic features and distinct representation of TF binding sites (Piccolo et al. 2017). Such data indicate that antagonistic activation programs can largely co-exist and converge on chromatin. Similar findings were recently described also in T cells, able to concomitantly express genes of antagonistic differentiation programs, namely type 17 and type 2 helper T cells (Harrison et al. 2019).

PGE$_2$ as emerging key modulator of inflammatory response

The lipid metabolite PGE$_2$ has emerged to contribute to a variety of biological processes, ranging from maintenance of tissue homeostasis to complex immunoregulatory activities. Synthesis of PGE$_2$ starts from membrane phospholipids, which are processed by phospholipase A2 to generate arachidonic acid. The latter molecule is converted by cyclooxygenase 1 and 2 (COX-1 and -2) in PGH$_2$, then processed in PGE$_2$ by microsomal prostaglandin E$_2$ synthase 1 (mPGES-1). PGE$_2$ induces distinct cellular responses depending on the receptor engaged on target cells. Prostaglandin E$_2$ receptors (PTGER or EP) are membrane receptors coupled to distinct G proteins and intracellular signalling pathways. EP1 activates PLC and induces release of calcium from endoplasmic reticulum, while EP3 increases intracellular levels of calcium and inhibits the cyclic adenosine monophosphate (cAMP)-dependent pathway. By contrast, EP2 and EP4 trigger adenylyl cyclase activity and cAMP-dependent activation of protein kinase A (PKA) and cAMP response element-binding (CREB) TF.

The definition of PGE$_2$ as a pro-inflammatory mediator derives from its role in orchestrating the early phases of the inflammatory response, namely vasodilatation and recruitment of innate immune cells to the damaged site (Nakanishi and Rosenberg 2013).

Somehow in contrast, PGE_2 has been also emerged as immunomodulatory molecule able to restrain adaptive and innate immune responses. Such effect in myeloid cells has been mainly attributed to the activation of the cAMP pathway. In this context, it has been shown that PGE_2 synergizes with IL-4 to induce tissue repair program via cAMP/CREB pathway. Macrophages treated *in vitro* with the combination of IL-4 and PGE_2 resulted in potentiated expression of genes associated to reparative phenotype, such as *Arg1*, *Mrc1* and *Ym1* (Luan et al. 2015). The synergistic effect of PGE_2 also relies on cAMP-dependent modulation of mitochondrial metabolism. In particular, PGE_2 alters the expression of mitochondrial genes, resulting in dissipation of mitochondrial membrane potential and increased expression of genes associated to tissue repair and proliferation (Sanin et al. 2018). Activation of the cAMP pathway has been shown to modulate macrophage response *in vivo*. In homeostatic conditions, norepinephrine, produced by sympathetic neurons innervating the gut, drive a subset of resident-macrophages to express genes of the tissue repair program through the β2 adrenergic receptor-cAMP pathway. Enteric infection causes an hyperactivation of the sympathetic system and increased production of norepinephrine, resulting in exacerbation of the protective program (Gabanyi et al. 2016; Matheis et al. 2020). Furthermore, PGE_2-EP4 axis has recently found to modulate the composition of the intestinal microbiota and, in turn, affects tissue homeostasis. Chemical inhibition of COX enzymes leads to increased expression of IFN I by resident myeloid cells and decreased number of regulatory T cells, resulting in enhanced intestinal inflammation (Crittenden et al. 2021).

In vitro studies also support the ability of PGE_2 to reprogram epigenome of myeloid cells to acquire suppressive phenotype. Differentiation of monocytes in the presence of PGE_2 results in increased expression of DNMT3A, hypermethylation of immune genes and suppression of cytotoxic T cell responses (Rodríguez-Ubreva et al. 2017). Furthermore, PGE_2 has been found to modulate inflammatory response in macrophages by restraining endosomal internalization of TLR4 and enhancing IL-10 production by activated macrophages (MacKenzie et al. 2013; Perkins et al. 2018).

Among tumor-associated signals, PGE_2 and cAMP-eliciting stimuli, such as lactate, emerged as driver of tumor progression since sustains proliferation and immune evasion of cancer cells, induces detrimental and tumor-promoting inflammation, and promotes immunomodulatory activities of T and myeloid cells. Tumor-derived PGE_2 fuels tumor

growth by different mechanisms. On one hand, PGE_2 produced by melanoma cells promotes the expression of genes associated to tumor-promoting inflammation, such as *Il6*, *Il1b* and *Cxcl1*. Genetic ablation of COX enzymes shifts the intra-tumoral inflammatory profile since leads to reduced expression of the latter genes and the appearance of the IFN-induced signature, (i.e., *Cxcl10*, *Ifit1* and *Ifit2*), indicating the activation of anti-tumor immune responses. On the other hand, PGE_2 inhibits the activation of protective immunity. In line with this, PGE_2-deficient tumours fail to support the differentiation of myeloid cells with immunomodulatory properties and promotes early infiltration of activated NK cells, followed by an intra-tumor accumulation of conventional dendritic cells and cytotoxic T cells and tumor eradication (Bonavita et al. 2020; Böttcher et al. 2018; Porta et al. 2020; Zelenay et al. 2015). Activation of the cAMP pathway by the high glycolytic rate of tumor cells imparts an immunosuppressive and tumor-promoting phenotype of tumor-associated macrophages. Acidification of tumor microenvironment triggers intracellular accumulation of cAMP and expression of the TF ICER (inducible cAMP early repressor), known to suppress inflammatory gene expression in myeloid cells (Harzenetter et al. 2007). ICER-deficient tumor-associated macrophages produce higher levels of TNF-α and other inflammatory cytokines and contribute to tumor rejection in mouse models of melanoma and colorectal cancer (Bohn et al. 2018). The relevance of PGE_2 in human cancer has been provided by several correlation studies. Expression levels of inflammatory genes as *Il6* and *Cxcl1* positively correlate with those of *Ptgs2* (encoding COX-2) in human melanoma tumours. In contrast, *Ptgs2* levels negatively associate with the T cell markers *Cd8a* and *Cd8b*, as well as with that of IFN response (i.e., *Cxcl9* and *Cxcl10*) (Zelenay et al. 2015). Furthermore, clinical data in patients affected by colorectal cancer showed that daily treatment with aspirin (an irreversible inhibitor of COX enzymes) reduces the risk of developing an hereditary form of colorectal cancer, suggesting the critical role of prostanoids in tumour initiation and progression (Burn et al. 2011).

AIM OF THE WORK

Regulation of inflammatory gene expression relies on the co-existence in the same local milieu of signals with antagonistic biological functions (namely, immunostimulatory and immunomodulatory) to ensure immune protection and avoid tissue damage. However, immunomodulatory signals may also dampen protective inflammatory response and instruct macrophages to further sustain and reinforce an immunosuppressive environment.

The aim of this study is to characterize the molecular mechanisms through which immunomodulatory agents restrain inflammatory gene expression in macrophages, with a particular focus on PGE_2. To this aim, we exploited a reductionist approach consisting of *in vitro* differentiated mouse bone marrow-derived macrophages stimulated for 4 hours with LPS, as paradigmatic inflammatory signal, alone or in combination with relevant immunomodulatory agents, as PGE_2, IL-10 and IL-4, and performed systematic genomic studies (Figure 1). Bulk and single cell RNA-Seq analyses, as well as profiling of active *cis*-regulatory regions and genomic occupancy by LDTF and stimulus-dependent TFs, provided principles underlying control of inflammatory gene expression and identified determinants of immunomodulation by PGE_2. We also extended our studies to the analysis of the response to other relevant innate immune signals, as additional TLR ligands and viral and bacterial pathogens, and identified a conserved mechanism of immunomodulation by PGE_2 in macrophages.
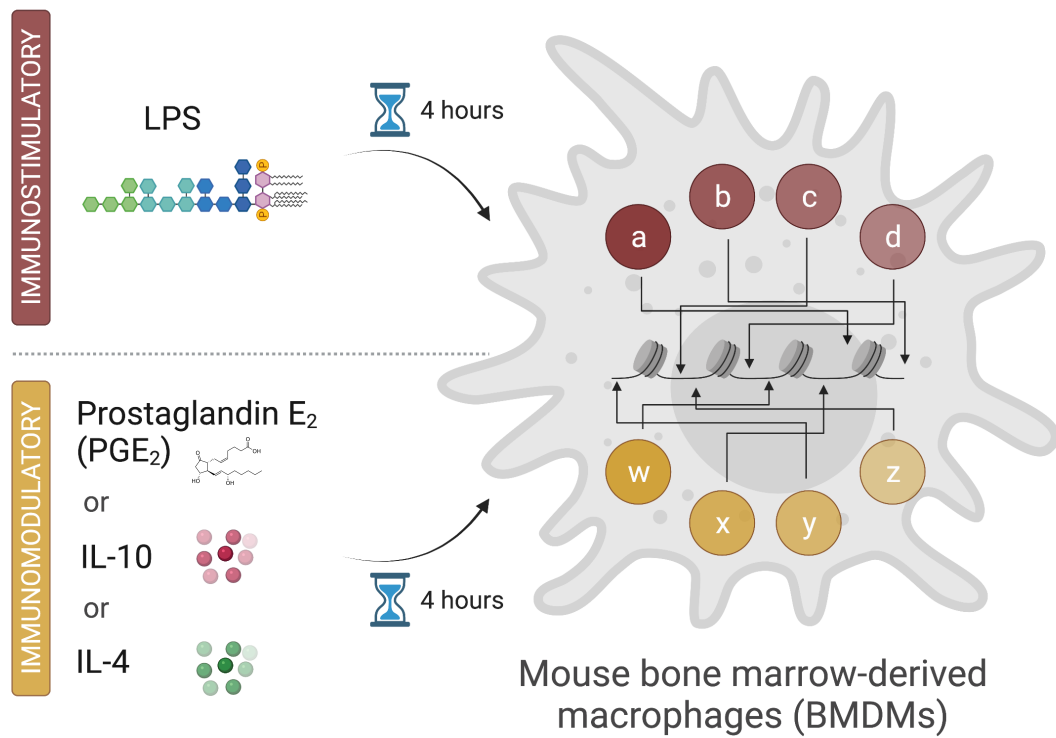
Schematic representation of the experimental model used in this study.
Figure 1: Bone marrow-derived macrophages (BMDMs) were stimulated *in vitro* for 4 hours with LPS alone or in combination with relevant immunomodulatory signals, as prostaglandin E2 (PGE2), interleukin-10 (IL-10) or interleukin-4 (IL-4)

RESULTS

Immunomodulatory signals target distinct sets of inflammatory genes

To assess the impact of immunomodulatory signals on inflammatory gene expression, we stimulated bone marrow-derived macrophages (BMDMs) for 4 hours with LPS or the combination of LPS and PGE_2 (LPS+PGE_2), IL-10 (LPS+IL-10) or IL-4 (LPS+IL-4) and processed for bulk RNA-Seq. We selected genes induced by LPS and defined as 'PGE_2-sensitive' (n=70), 'IL-10-sensitive' (n=72) or 'IL-4-sensitive' (n=42) those with reduced level of expression in costimulated cells compared to LPS-treated cells (see Methods), and 'resistant' (n=72) those with preserved expression in costimulated cells (see Methods) (Figure 2, 3). Immunomodulatory signals suppressed the induction of key inflammatory genes, including cytokines and chemokines such as *Ifnb1*, *Tnf*, *Il12b*, *Cxcl9*, *Cxcl10*, *Ccl3*, *Ccl4*, and transcription factors such as *Irf1* (Figure 2). By contrast, resistant genes included components of the TLR4 signalling pathway, as *Myd88*, *Junb* and *Relb* (Figure 3). Re-analyses of published RNA-Seq datasets (Tong et al. 2016) revealed a selective enrichment of sensitive genes in TRIF-, IRF3- and IFN-α/IFNAR-dependent transcripts, while resistant genes were enriched in AP-1- and NF-κB-dependent transcripts (Figure 1, 2, 3, see Methods)

Interestingly, PGE_2, IL-10 and IL-4 targeted distinct inflammatory genes, as exemplified by *Ifnb1* (Figure 2). PGE_2 and IL-10, but not IL-4, suppressed the induction of IFN I at the mRNA (Figure 2, 5) and protein levels (Figure 6), as well as secondary activation of STAT1, STAT2 and IRF1 (Figure 7). The suppressive activity of PGE_2 and IL-10 on IFN I response relied on direct inhibition of *Ifnb1* induction. Indeed, PGE_2 or IL-10 had a minimal impact when co-administered with IFN-α on IFN I-induced gene expression (Figure 8). In support to this, exogenous administration of recombinant IFN-β to costimulated BMDMs resulted in restored induction of most of PGE_2-sensitive genes (Figure 9, 10, see Methods). However, a fraction of sensitive genes, such as *Tnf* and *Il12b*,

remained still suppressed upon IFN-β reconstitution, indicating additional mechanism(s) of suppression (Figure 10).

Figure 2
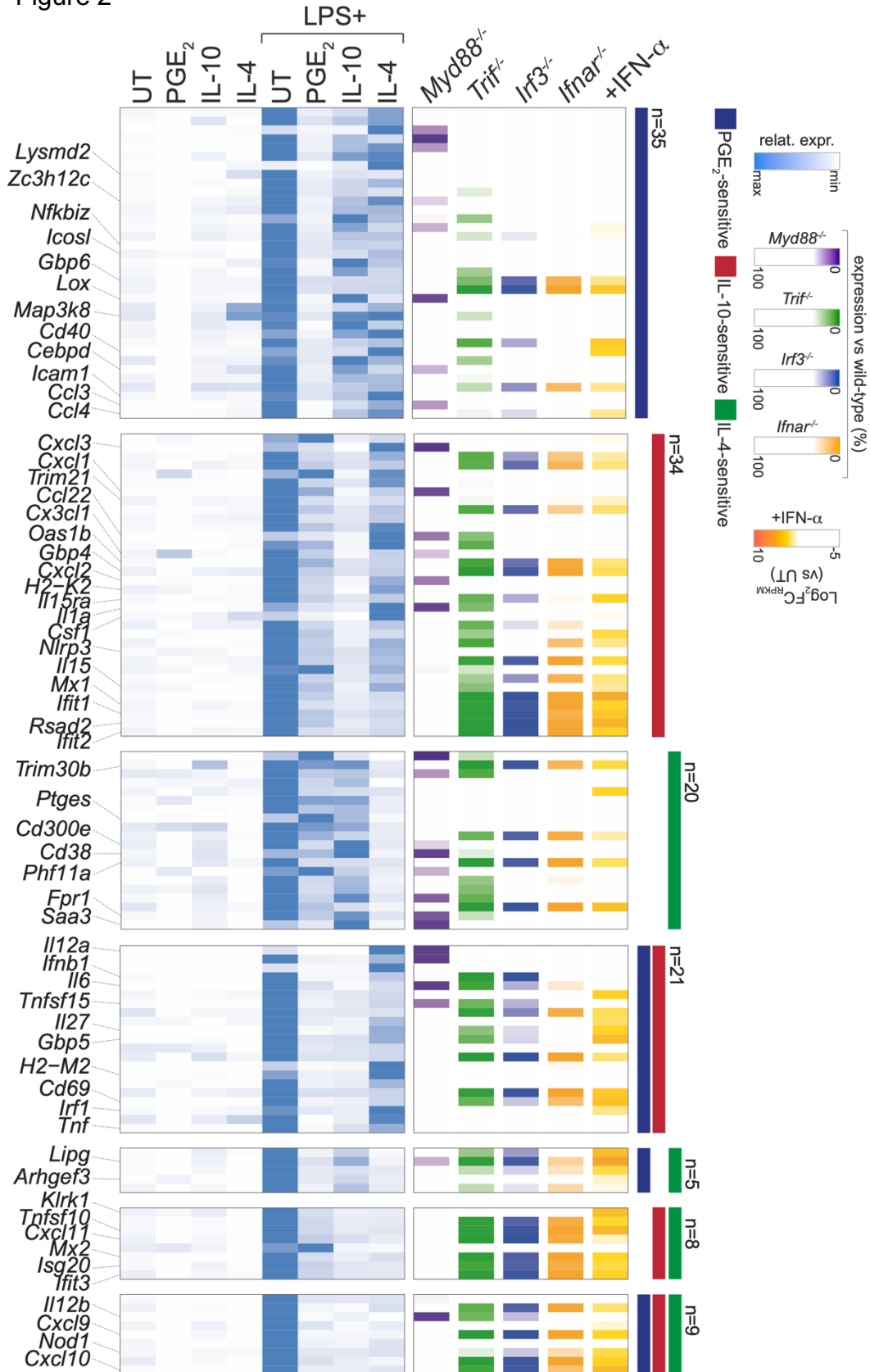
Immunomodulatory signals target distinct sets of LPS-inducible genes.
Figure 2 - Heatmap showing the behavior of LPS-inducible genes in BMDMs that are sensitive to costimulation with PGE_2 (blue), IL-10 (red) or IL-4 (green). Left panel: row-normalized percentage of gene expression across experimental conditions with minimum and maximum values set to 0 and 100, respectively. Right panel: percentage of gene expression in lipid A-stimulated $Myd88^{-/-}$, $Ticam1^{-/-}$, $Irf3^{-/-}$, $Ifnar1^{-/-}$ versus wt BMDMs (data from Tong et al., Cell 2016), as well as $log_2FC(RPKM_{IFN-a}/RPKM_{UT})$ values. Selected gene names are shown on the left, legends are shown on the right. Data from two biological replicates. Pearson correlation > 0.97 for all replicates.
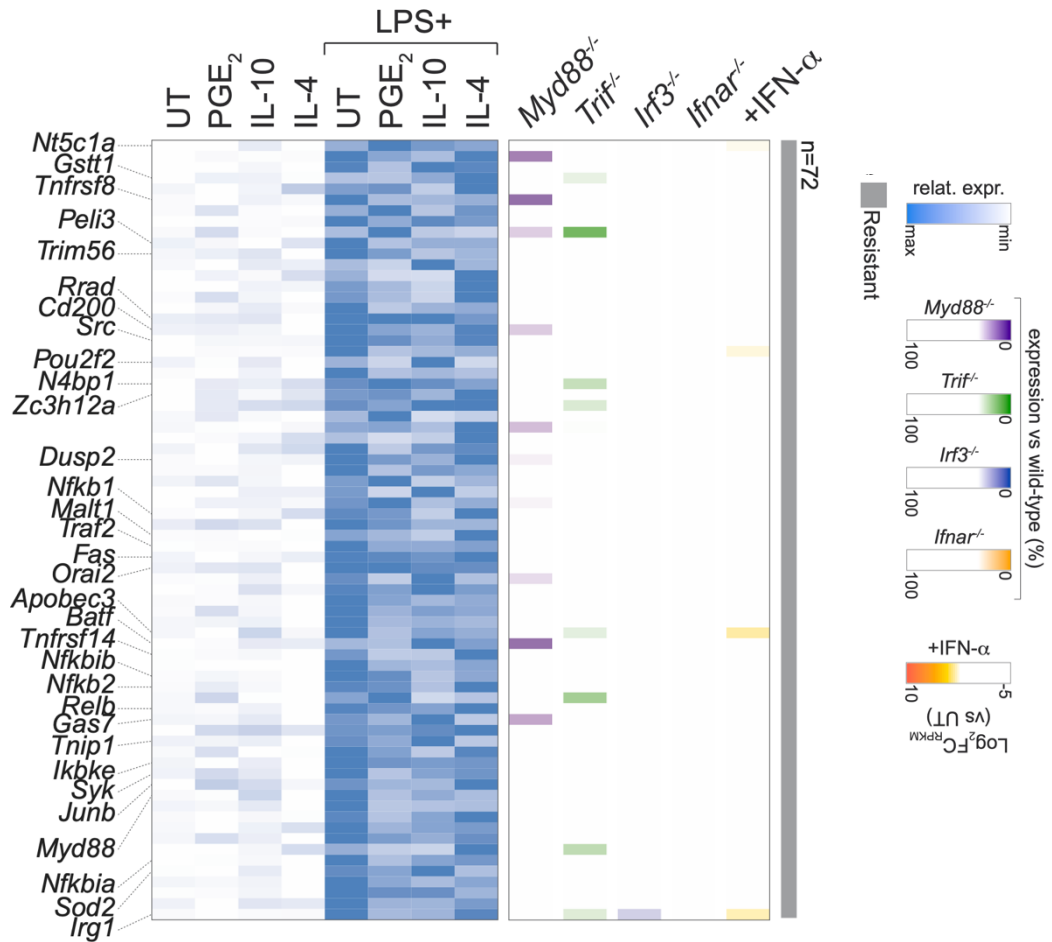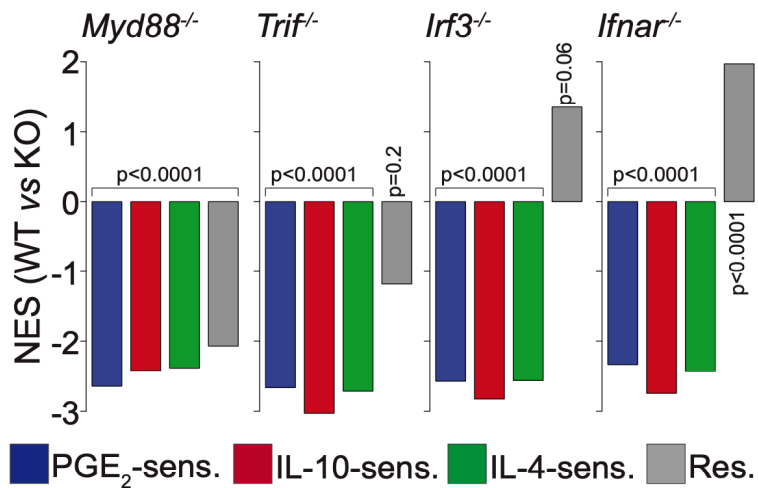
Figure 3

Figure 4

Immunomodulatory signals target distinct sets of LPS-inducible genes.

Figure 3 - Heatmap showing the behavior of LPS-inducible genes in BMDMs that are resistant to costimulation (grey). Left panel: row-normalized percentage of gene expression across experimental conditions with minimum and maximum values set to 0 and 100, respectively. Right panel: percentage of gene expression in lipid A-stimulated $Myd88^{-/-}$, $Ticam1^{-/-}$, $Irf3^{-/-}$, $Ifnar1^{-/-}$ versus wt BMDMs (data from Tong et al., Cell 2016), as well as $log_2FC(RPKM_{IFN-a}/RPKM_{UT})$ values. Selected gene names are shown on the left, legends are shown on the right. Data from two biological replicates. Pearson correlation > 0.97 for all replicates.

Figure 4 - Gene Set Enrichment Analysis (GSEA) of PGE_2-sensitive (blue), IL-10-sensitive (red), IL-4-sensitive (green) or resistant (grey) transcripts (gene sets) in ranked gene lists obtained comparing lipid A-stimulated $Myd88^{-/-}$, $Ticam1^{-/-}$, $Irf3^{-/-}$, $Ifnar1^{-/-}$ versus wt BMDMs (data from Tong et al., Cell 2016). Normalized enrichment score (NES) and p-values are shown for each plot.
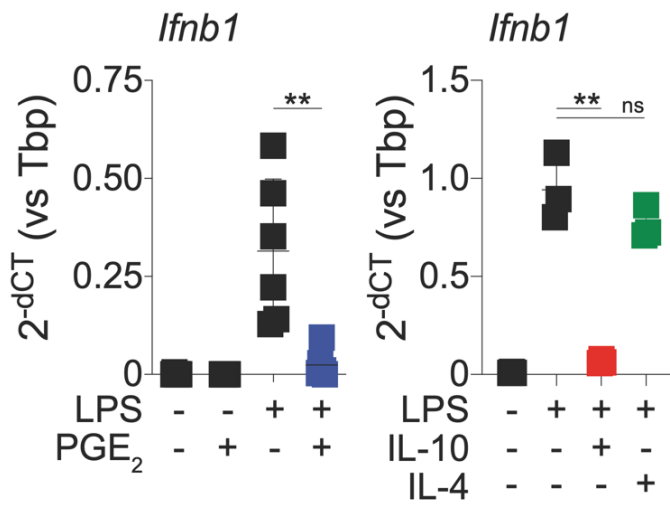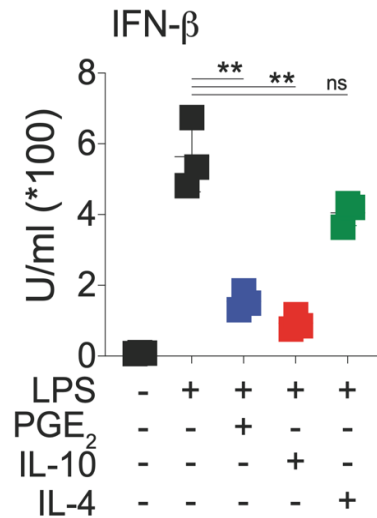
Figure 5

Ifnb1 (left panel)

2^{-dCT} (vs Tbp), y-axis 0–0.75

** above LPS + PGE$_2$ + condition

| LPS | - | - | + | + |
| PGE$_2$ | - | + | - | + |

Ifnb1 (right panel)

2^{-dCT} (vs Tbp), y-axis 0–1.5

** ns

LPS	-	+	+	+
IL-10	-	-	+	-
IL-4	-	-	-	+

Figure 6

IFN-β

U/ml (*100), y-axis 0–8

** ** ns

LPS	-	+	+	+	+
PGE$_2$	-	-	+	-	-
IL-10	-	-	-	+	-
IL-4	-	-	-	-	+

Figure 7

LPS   LPS+PGE$_2$
(h) - .25 .5 1 2 4   .25 .5 1 2 4
pSTAT1
ACTB
pSTAT2
VCL
IRF1
VCL

LPS   LPS+IL-10
(h) - .25 .5 1 2 4   .25 .5 1 2 4
pSTAT1
VCL

Figure 8

IFN-α-induced genes

Sensitive / Resistant

Density (y-axis 0–1.5)

+PGE$_2$ (blue)
+IL-10 (red)

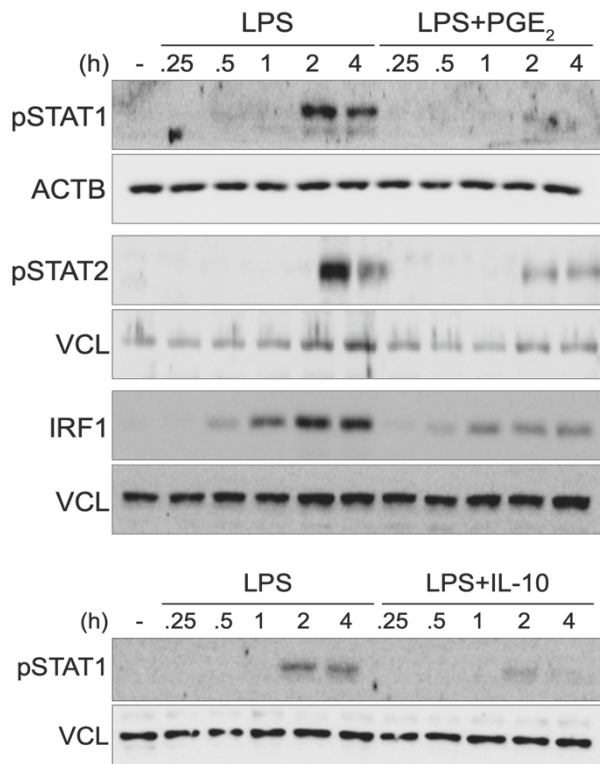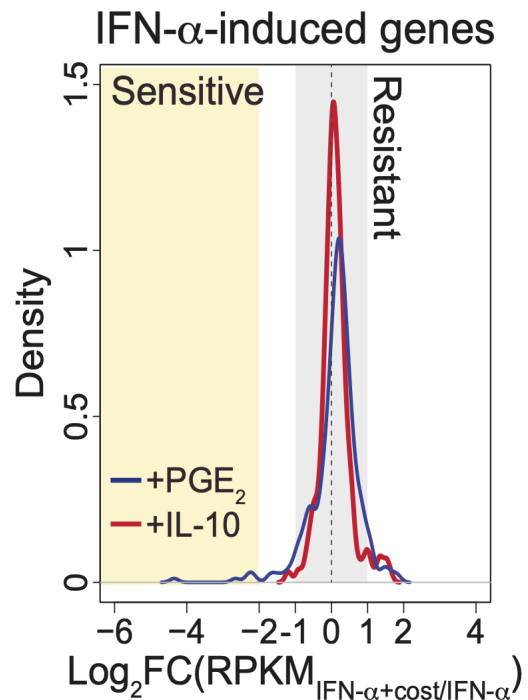Log$_2$FC(RPKM$_{IFN-α+cost/IFN-α}$), x-axis -6 -4 -2 -1 0 1 2 4

PGE$_2$ and IL-10, but not IL-4, suppress IFN-β production by activated macrophages.

Figure 5 - Expression of *Ifnb1* in BMDMs stimulated with LPS in the absence or presence of PGE$_2$ (left), IL-10, or IL-4 (right). Dot plots represent mean ± SD. Data from six (left) or three (right) biological replicates. ** p<0.01, ns not significant (unpaired *t*-test).

Figure 6 - IFN-β release by BMDMs in the indicated conditions. Dot plot represents mean ± SD. Data from three biological replicates. ** p<0.01; ns, not significant (unpaired *t*-test).

Figure 7 - (top) Western blot analyses for phosphorylated STAT1 (Tyr701), STAT2 (Tyr689), IRF1 and loading controls in BMDMs stimulated with LPS or LPS+PGE$_2$ for the indicated time points. (bottom) Western blot analyses for phosphorylated STAT1 (Tyr701) in BMDMs stimulated with LPS or LPS+IL-10 for the indicated time points.

Figure 8 - Density plot showing the effect of costimulation with PGE_2, or IL-10 on $IFN\alpha$-induced gene expression. Dotted line indicates lack of effect of the costimulation; yellow or grey shaded areas indicate values used to define costimulation-sensitive or resistant genes, respectively.
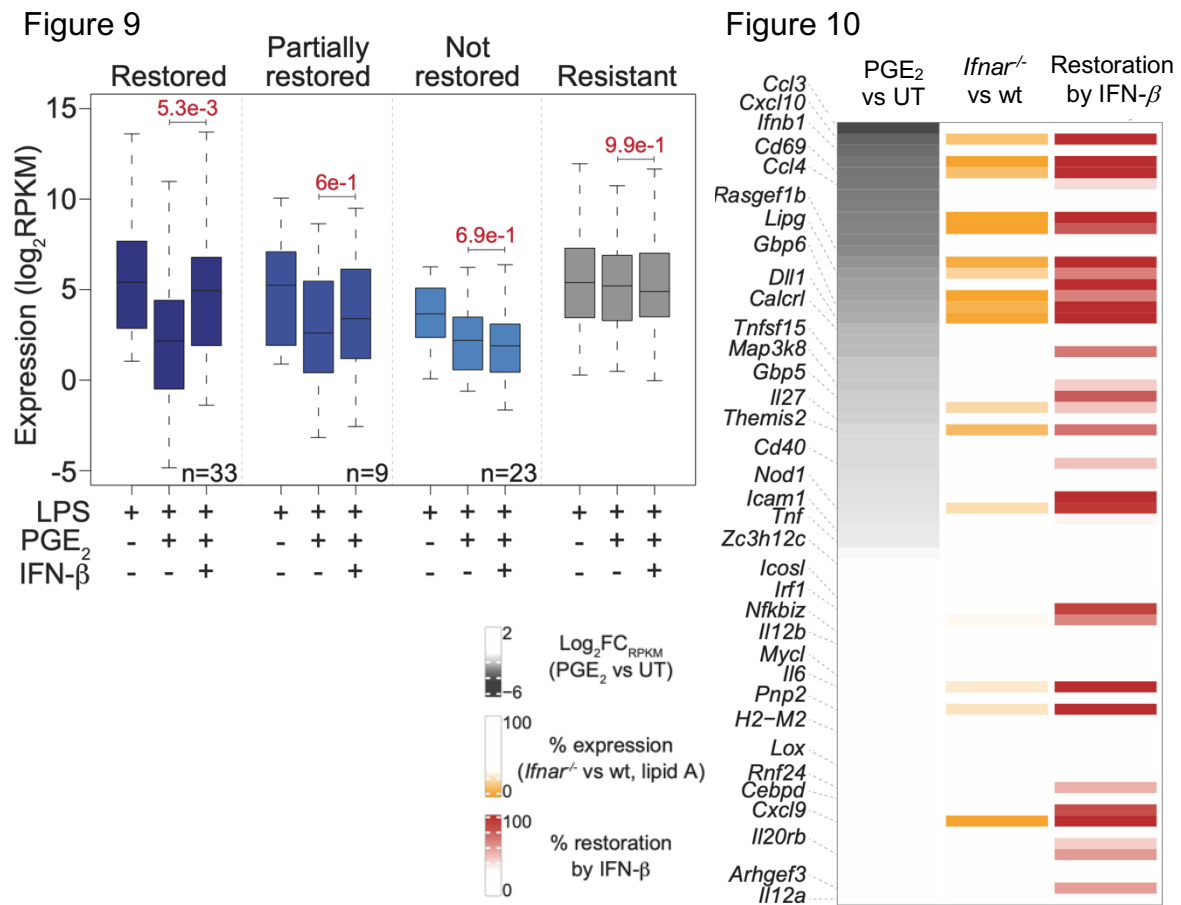
Exogenous IFN-β restores the induction of a set of PGE₂-sensitive genes.

Figure 9 - Mean expression values of resistant genes (grey) or PGE₂-sensitive genes, classified as IFN-β restored (dark blue), partially restored (blue) or not restored (light blue) in the indicated conditions. Numbers indicate p-values for the corresponding comparisons (Mann-Whitney U test). Data from three biological replicates. Pearson correlation > 0.95 for all replicates.

Figure 10 - Heatmap showing the behavior of PGE₂-sensitive genes. Genes are ranked by ascending values of $\log_2 FC_{RPKM}$ in the PGE₂ vs UT condition (left lane, grey scale). Right lanes represent the percentage of gene expression in lipid A-stimulated *Ifnar1⁻/⁻* vs wt BMDMs (data from Tong et al., Cell 2016) (orange scale), as well as percentage of restoration by IFN-β (red scale) treatment in BMDMs costimulated with LPS+PGE₂. Selected gene names are shown on the left, legends are shown on the bottom left. Data from two or three biological replicates. Pearson correlation > 0.97 for all replicates.

PGE₂ suppresses inflammatory gene expression partly via boosting IL-10 release by activated macrophages

Macrophages exposed to LPS produce IL-10 and PGE$_2$ as counter-regulatory mechanisms to avoid excessive inflammatory response (Murray and Smale 2012; Uematsu et al. 2002). We next asked whether PGE$_2$ and IL-10 influenced each other's action in costimulated BMDMs. PGE$_2$ levels did not differ between LPS+IL-10- and LPS-treated cells (Figure 11), while IL-10 release increased upon co-exposure to PGE$_2$ at the mRNA and protein levels (Figure 12, 13). To evaluate the contribution of released IL-10 on PGE$_2$-mediated suppression, we treated costimulated BMDMs in the presence of a blocking antibody targeting IL-10 receptor (IL-10R) and performed bulk RNA-Seq (see Methods). Blockade of IL-10 signalling resulted in completely recovered expression of a small group of PGE$_2$-sensitive genes, including *Il12b* and *Il6*, indicating that the suppression of these genes is entirely dependent on the paracrine/autocrine activity of IL-10 (Figure 14, 15). However, most of PGE$_2$-sensitive genes, including *Ifnb1*, was minimally affected by anti-IL10R treatment (Figure 14, 15). Collectively, these data indicate that PGE$_2$ suppresses inflammatory gene expression by direct inhibition of IFN I response and hyper-induction of IL-10.
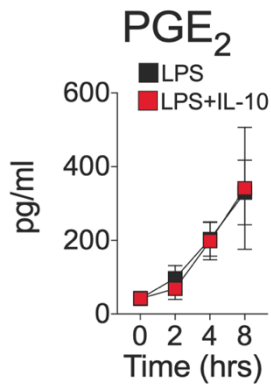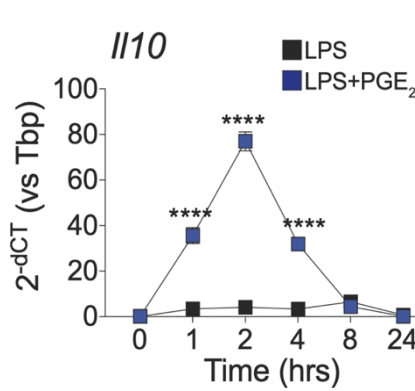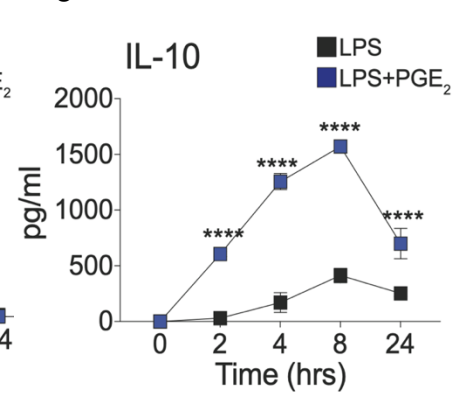
Figure 11

PGE$_2$

Figure 12

Il10

Figure 13

IL-10

Figure 14

IL-10R blockade

Figure 15
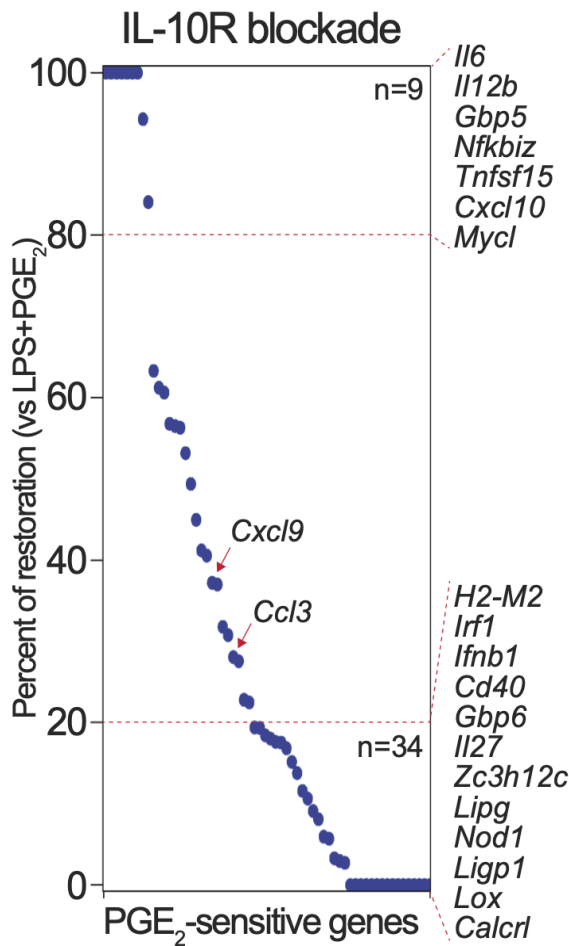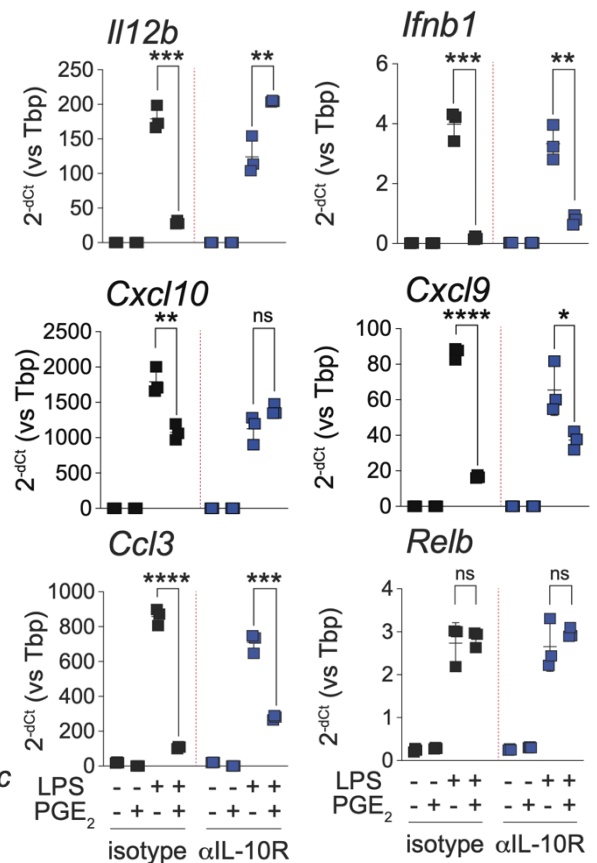
Il12b

Ifnb1

Cxcl10

Cxcl9

Ccl3

Relb

PGE$_2$ suppresses inflammatory gene expression partly via hyper-induction of IL-10 by activated macrophages.

Figure 11 - PGE$_2$ release by BMDMs stimulated as indicated. Line plot represents mean ± SD. Data from three biological replicates.

Figure 12 - Expression of *Il10* in BMDMs stimulated with LPS in the absence or presence of PGE$_2$ for the indicated time points. Dot plots represent mean ± SD. Data from three biological replicates. **** p<0.0001 (two-way ANOVA test).

Figure 13 - IL-10 release by BMDMs stimulated as indicated. Dot plots represent mean ± SD. Data from three biological replicates. **** p<0.0001 (two-way ANOVA test).

Figure 14 - Percentage of restoration of PGE$_2$-sensitive genes in the presence of IL-10R blocking antibody. Selected gene names are shown on the right. Data from three biological replicates. Pearson correlation > 0.98 for all replicates.

Figure 15 - RT-qPCR analysis of a set of resistant and PGE$_2$-sensitive genes in BMDMs stimulated as indicated. Dot plots represent mean ± SD. Data from three biological replicates. **** p<0.0001, *** p<0.001, ** p<0.01, * p<0.05, ns not significant; (unpaired *t*-test).

PGE₂ suppresses LPS-inducible gene expression at single-cell level

We asked whether the transcriptional profile of costimulated cells was due to the integration of antagonistic signals in individual cells or to the concomitant existence of cells responding to a single stimulus. We stimulated BMDMs for 4 hours with LPS, PGE_2 or LPS+PGE_2 and performed single cell RNA-sequencing (scRNA-Seq). UMAP (Uniform Manifold Approximation and Projection) analyses defined clusters corresponding to the experimental conditions (Figure 16), with virtually no costimulated cells falling in cluster corresponding to LPS or PGE_2 treatment (Figure 17). Cells belonging to cluster of costimulated cells (cluster 4) co-expressed genes induced by LPS as well as by PGE_2 (Figure 18), further supporting the indication that the resulting transcriptional profile of costimulated BMDMs was due to the integration of antagonistic signals. Moreover, genes defined as PGE_2-sensitive in bulk RNA-Seq data showed reduced induction also at single cell level in costimulated BMDMs, while PGE_2-resistant genes were less affected (Figure 19). In line with bulk RNA-Seq data, PGE_2 had a limited impact on IFN-α-induced gene expression also at single cell level. BMDMs stimulated with IFN-α+PGE_2 co-expressed genes induced by IFN-α and PGE_2 and clustered separately from PGE_2 or IFN-α-treated cells, even if the distance between these cluster was small (Figure 16, 20).
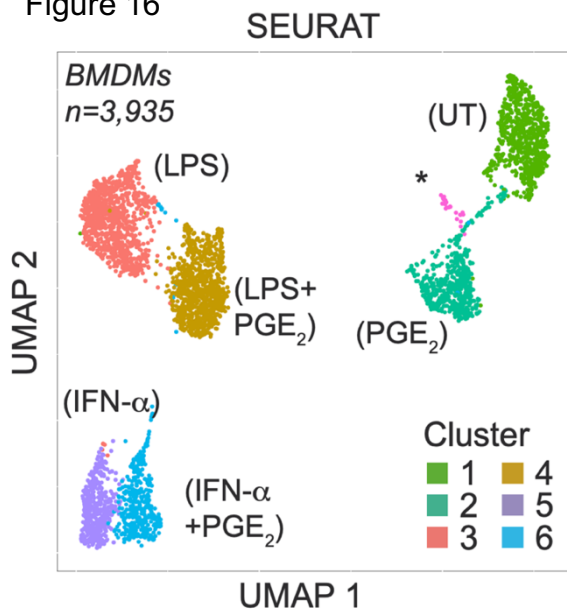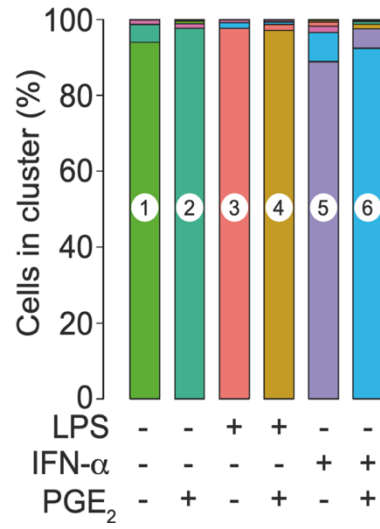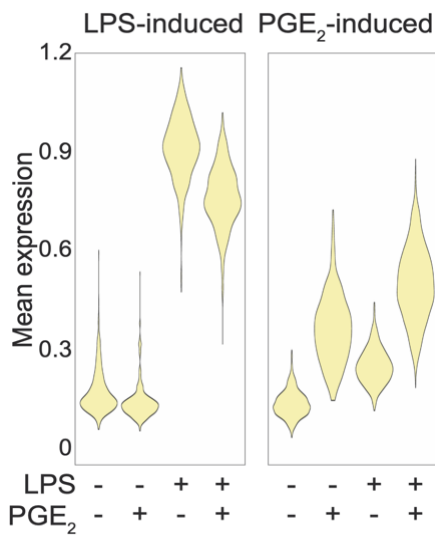
Figure 16

SEURAT

BMDMs
n=3,935

(UT)

(LPS)

*

UMAP 2

(LPS+
PGE$_2$)

(PGE$_2$)

(IFN-α)

(IFN-α
+PGE$_2$)

Cluster
- 1
- 4
- 2
- 5
- 3
- 6

UMAP 1

Figure 17

| Cells in cluster (%) | | | | | |

LPS   -   -   +   +   -   -
IFN-α -   -   -   -   +   +
PGE$_2$ -   +   -   +   -   +

Figure 18

LPS-induced   PGE$_2$-induced

Mean expression

LPS   -   -   +   +   -   -   +   +
PGE$_2$ -   +   -   +   -   +   -   +

Figure 20

IFN-α-induced   PGE$_2$-induced

Mean expression

IFN-α   -   -   +   +   -   -   +   +
PGE$_2$ -   +   -   +   -   +   -   +

Figure 19

Mean expression

9.4e-189
3.6e-94
0.59
1.5e-49
2.6e-271

UT   PGE$_2$ LPS   LPS+PGE$_2$
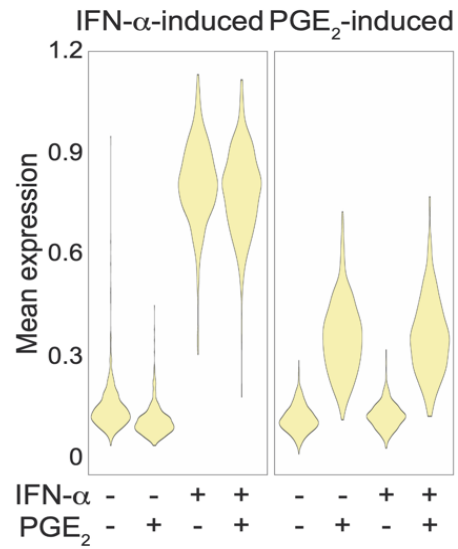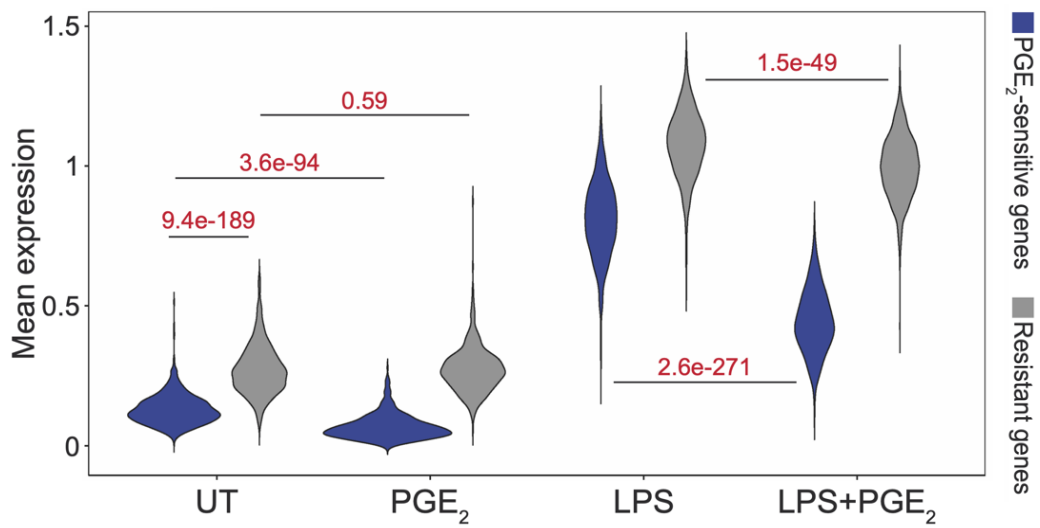
PGE$_2$-sensitive genes
Resistant genes

50

PGE$_2$ antagonizes LPS-induced gene expression at the single-cell level.
Figure 16 – UMAP plot of scRNA-Seq BMDMs stimulated as indicated. Colors represent Leiden graph clustering and treatments are shown in brackets. The asterisk indicates a small cluster (n=35) of contaminant cells that were excluded from analyses.
Figure 17 – Stacked bar plot showing the percentage of cells from each experimental condition within each cluster.
Figure 18 – Mean expression values of LPS-induced or PGE$_2$-induced genes (see Methods) in the indicated conditions.
Figure 19 – Violin plot showing mean expression values of PGE$_2$-sensitive (blue) or resistant (grey) genes in the indicated conditions. Numbers indicate p-values for the corresponding comparisons (Mann-Whitney U test).
Figure 20 – Mean expression values of IFNα-induced or PGE$_2$-induced genes (see Methods) in the indicated conditions.

PGE$_2$ suppresses inflammatory gene expression *ex vivo* and *in vivo*

We next assessed whether the suppressive activity of PGE$_2$ also occurred in relevant myeloid cell populations other than BMDMs. Human monocyte-derived macrophages, mouse bone barrow-derived dendritic cells and mouse peritoneal macrophages stimulated with LPS+PGE$_2$ showed impaired induction of *Ifnb1* and other PGE$_2$-sensitive genes such as *Il12b* and *Tnf*, while selected resistant genes were less affected (Figure 21-23). Collectively, these data indicate that the suppressive effect of PGE$_2$ on LPS-inducible gene expression is conserved across species and myeloid cells.

PGE$_2$ suppressed inflammatory gene expression also *in vivo*. Intraperitoneal administration of a sublethal dose of LPS in combination with PGE$_2$ resulted in reduced expression of PGE$_2$-sensitive genes, even though the induction of *Ifnb1* was not observed at that time point (Figure 24). We then injected LPS and PGE$_2$ intranasally and collected bronchoalveolar lavage fluid (BALF), which was mainly composed by CD11c$^+$ SiglecF$^+$ alveolar macrophages (Figure 25). *In vivo* exposure of alveolar macrophages to LPS+PGE$_2$ resulted in reduced induction of *Ifnb1*, IFN-dependent genes such as *Cxcl9* and inflammatory cytokines such as *Tnf* and *Il12b* (Figure 26). These data establish PGE$_2$ as a potent immunomodulatory molecule able to suppress IFN I response also *in vivo*.
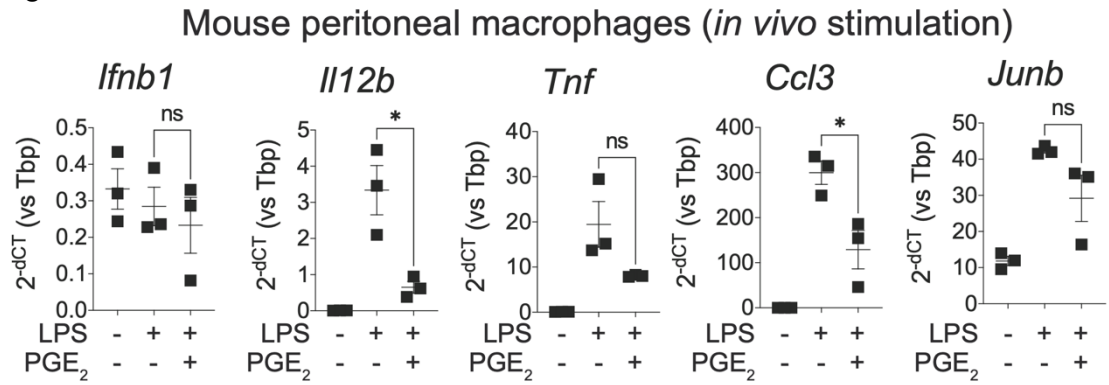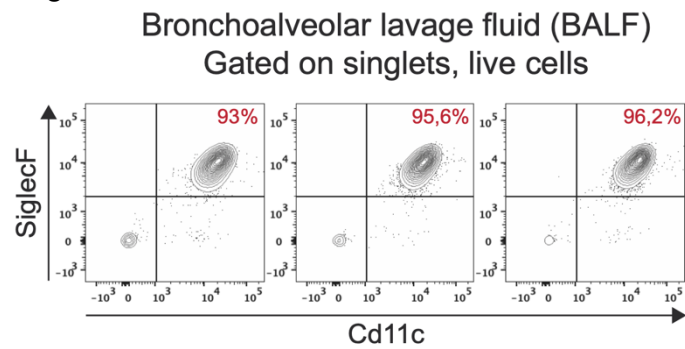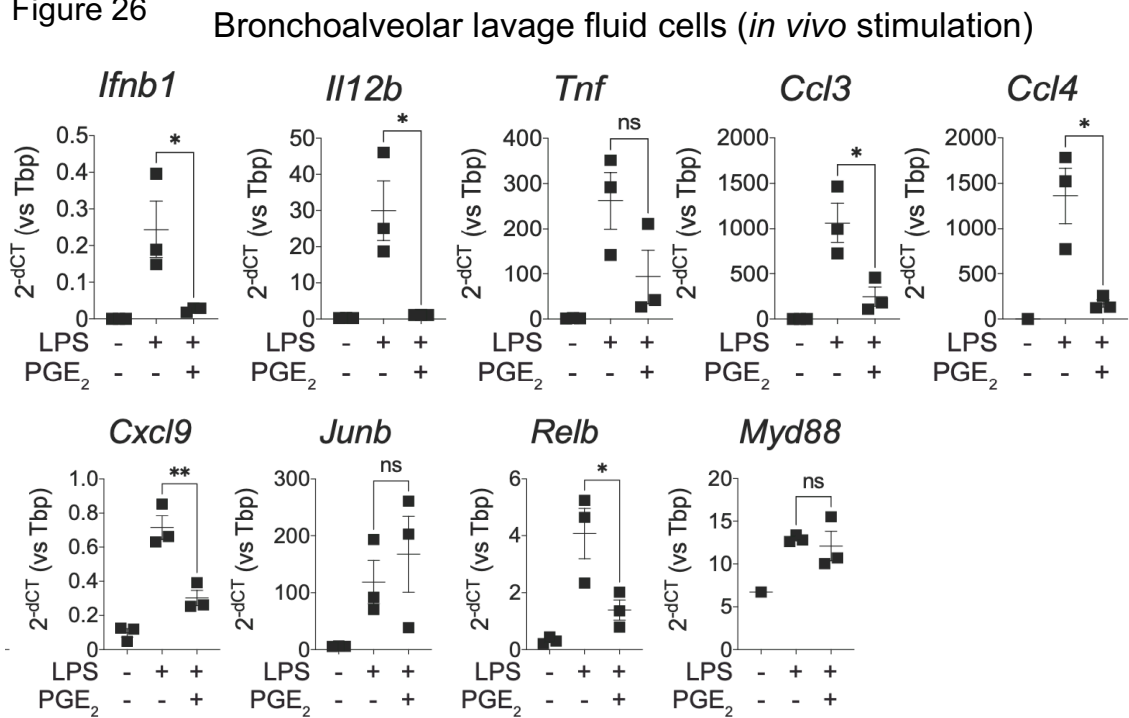
Figure 21

Human monocyte-derived macrophages (*ex vivo* stimulation)

Figure 22

Mouse bone marrow dendritic cells (*ex vivo* stimulation)

Figure 23   Mouse peritoneal macrophages (*ex vivo* stimulation)

Figure 24

Mouse peritoneal macrophages (*in vivo* stimulation)

Figure 25

Bronchoalveolar lavage fluid (BALF)
Gated on singlets, live cells

Figure 26   Bronchoalveolar lavage fluid cells (*in vivo* stimulation)

PGE$_2$ antagonizes LPS-induced gene expression *ex vivo* and *in vivo*.

Figure 21 – RT-qPCR analysis of a set of PGE$_2$-sensitive or resistant genes in human monocyte-derived macrophages stimulated as indicated. Dot plots represent mean ± SD. Data from seven biological replicates. **** p<0.0001, *** p<0.001, ** p<0.01, ns not significant (unpaired *t*-test).

Figure 22 - RT-qPCR analysis of a set of PGE$_2$-sensitive or resistant genes in mouse bone marrow-derived dendritic cells stimulated as indicated. Dot plots represent mean ± SD. Data from five biological replicates. **** p<0.0001, ** p<0.01, ns not significant (unpaired *t*-test).

Figure 23 - RT-qPCR analysis of a set of PGE$_2$-sensitive or resistant genes in mouse peritoneal macrophages stimulated as indicated. Dot plots represent mean ± SD. Data from three biological replicates. * p<0.05, ns not significant (unpaired *t*-test).

Figure 24 - RT-qPCR analysis of a set of PGE$_2$-sensitive or resistant genes in mouse peritoneal macrophages upon *in vivo* stimulation (4 hours). Dot plots represent mean ± SD. Data from five to eight biological replicates. **** p<0.0001, ** p<0.01, * p<0.05, ns not significant (unpaired *t*-test).

Figure 25 - Selected flow cytometry plots showing the expression of Cd11c and SiglecF in BALF cells of untreated mice.

Figure 26 - RT-qPCR analysis of a set of PGE$_2$-sensitive or resistant genes in bronchoalveolar lavage fluid cells upon *in vivo* stimulation (2 hours). Dot plots represent mean ± SD. Data from three biological replicates. ** p<0.01, * p<0.05, ns not significant (unpaired *t*-test).

Activation of the cAMP pathway phenocopies PGE$_2$ treatment

We aimed to dissect the mechanisms of regulation of inflammatory response by PGE$_2$. Exposure to PGE$_2$ induced a fast and transient increased in intracellular levels of the second messenger cAMP (Figure 27). To assess the relevance of cAMP in modulating inflammatory gene expression, we used chemical activators of this pathway. Treatment of BMDMs with an activator of adenylyl cyclase (forskolin, FSK) (Figure 28), a cell permeable analogue of cAMP (dibutyryl-cAMP, db-cAMP) or an activator of PKA (6-Bnz-cAMP) (Figure 29) resembled exposure to PGE$_2$. Indeed, BMDMs co-exposed to LPS and cAMP activators failed to induce *Ifnb1* and other PGE$_2$-sensitive genes (Figure 28, 29). In line with this, other cAMP-eliciting stimuli, such as agonists of the β2 adrenergic receptor (Salmeterol Xinafoate) or of the adenosine 2B receptor (BAY60-6583), suppressed LPS-induced expression of IFN I and PGE$_2$-sensitive genes (Figure 30), pointing out the cAMP pathway as relevant modulator of IFN I response and inflammatory gene expression in macrophages. We next asked whether CREB, the TF ultimately activated by PKA, contributed to the suppression of inflammatory gene expression by PGE$_2$. Surprisingly, gene disruption by CRISPR/Cas9 of CREB (Figure 31) did not restore the induction of inflammatory genes in costimulated BMDMs (Figure 32), indicating that PGE$_2$-mediated suppression of LPS-inducible gene expression was CREB-independent.
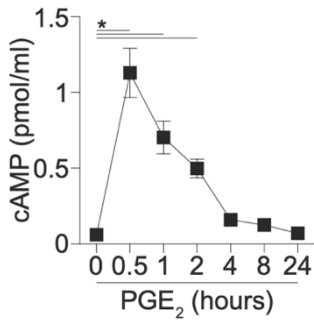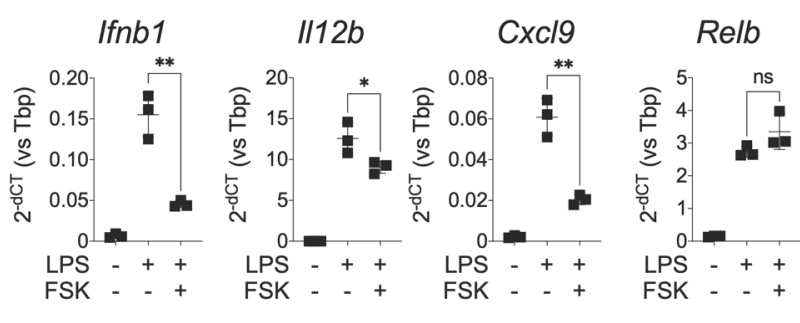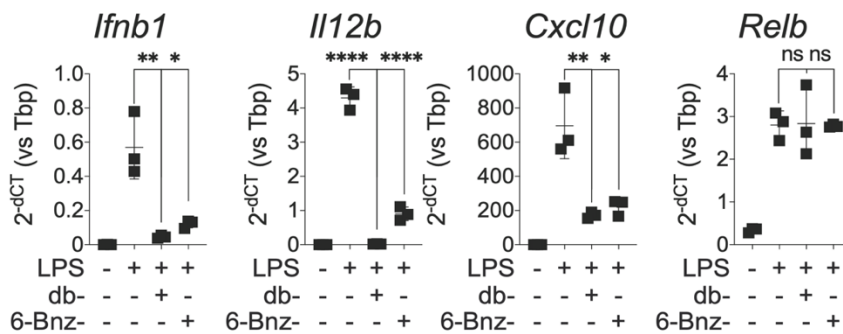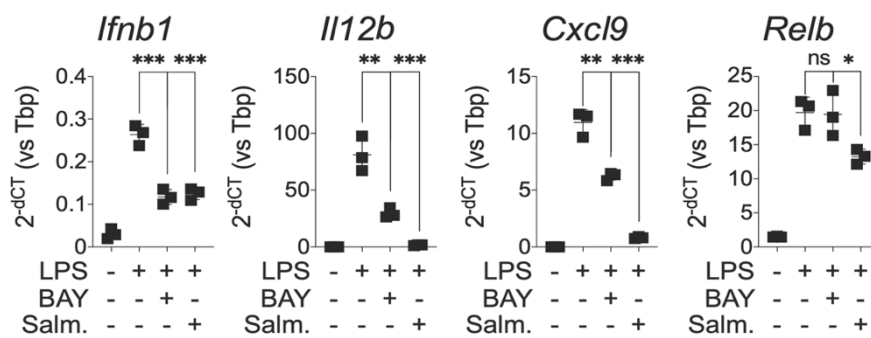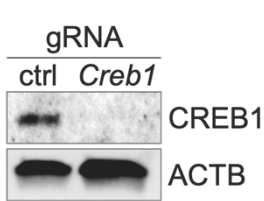
Figure 27

Figure 28

Figure 29
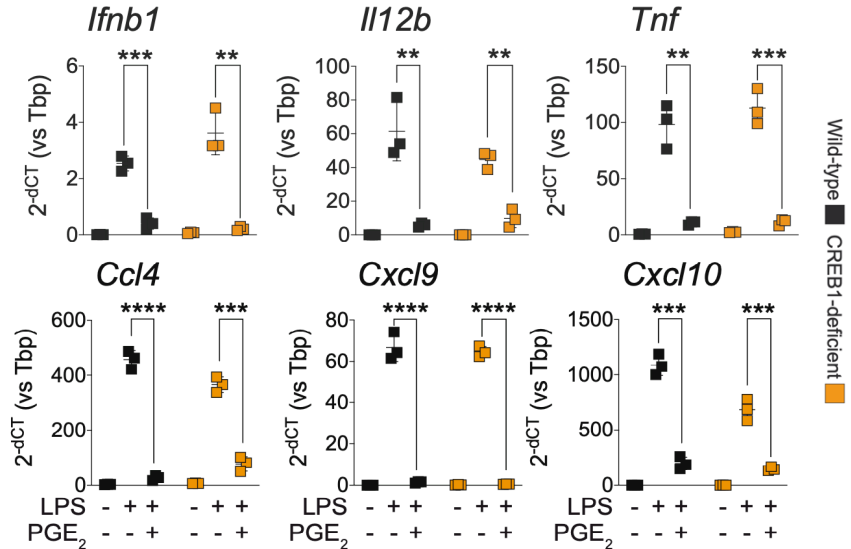
Figure 30

Figure 31

Figure 32

57

Activation of the cAMP pathway phenocopies PGE$_2$ treatment.

Figure 27 - Intracellular cAMP in BMDMs treated with PGE$_2$ for the indicated time points. Line plot represents mean ± SD. Data from two biological replicates. * p<0.05 (unpaired *t*-test).

Figure 28 - RT-qPCR analysis of a set of PGE$_2$-sensitive or resistant genes in BMDMs treated for 4 hours with LPS in the absence or presence of forskolin (2-hours pre-treatment). Dot plots represent mean ± SD. Data from three biological replicates. ** p<0.01, * p<0.05, ns not significant (unpaired *t*-test).

Figure 29 - RT-qPCR analysis of a set of PGE$_2$-sensitive or resistant genes in BMDMs treated for 4 hours with LPS in the absence or presence of db-cAMP or 6-Bnz-cAMP (2-hours pre-treatment). Dot plots represent mean ± SD. Data from three biological replicates. **** p<0.0001, *** p<0.001, ** p<0.01, * p<0.05, ns not significant (unpaired *t*-test).

Figure 30 - RT-qPCR analysis of a set of PGE$_2$-sensitive or resistant genes in BMDMs treated for 4 hours with LPS in the absence or presence of BAY60-6583 (BAY) or salmeterol xinafoate (Salm.). Data from three biological replicates. *** p<0.001, ** p<0.01, * p<0.05, ns not significant (unpaired *t*-test).

Figure 31 - Western blot analysis for CREB1 in BMDMs upon CRISPR-Cas9-mediated targeting of *Creb1*. β-Actin (ACTB) is reported as loading control.

Figure 32 - RT-qPCR analysis of a set of PGE$_2$-sensitive genes in wt (black) and CREB1-deficient (orange) BMDMs. Dot plots represent mean ± SD. Data from three biological replicates. **** p<0.0001, *** p<0.001, ** p<0.01, (unpaired *t*-test).

Poorly permissive chromatin underlies sensitivity to PGE₂

As a mechanism of modulation of inflammatory response, we first hypothesized that PGE$_2$ may interfere with the signalling pathways elicited by LPS. LPS-induced degradation of IκBα and nuclear translocation of NF-ϰB p65 were preserved in costimulated BMDMs, as well as internalization of TLR4, phosphorylation of TBK1, and nuclear translocation of IRF3 (Figure 33-37). These data indicate that PGE$_2$-mediated suppression of inflammatory gene expression does not occur by altering the magnitude of the LPS-induced signalling pathways.

Since chromatin represents the platform where external signals converge to modulate gene expression, we assessed whether PGE$_2$ may act at epigenomic level and performed ChIP-Seq for H3K27ac and PU.1, as well as ATAC-Seq. We first defined the set of enhancers induced by LPS and evaluated the impact of PGE$_2$ on the latter regions (see Methods). A large fraction of LPS-inducible enhancers (n=848) displayed reduced H3K27ac deposition in costimulated cells (Figure 38), such as those at the *Ifnb1* and *Cxcl10* loci (Figure 39), and was classified as 'PGE$_2$-sensitive enhancers', while another fraction of enhancers, namely 'PGE$_2$-resistant enhancers' (n=322), was largely unaffected by PGE$_2$ (Figure 38, see Methods). PGE$_2$-sensitive enhancers displayed poorly accessible chromatin at basal level (namely in untreated BMDMs), as defined by low signal of H3K27ac, H3K4me1, PU.1 and ATAC-Seq (Figure 38, 40, 41, 42). Poorly basal chromatin accessibility of the latter regions was also reflected by low basal expression of sensitive genes (Figure 43, 44), low signal of H3K27ac, H3H4me3, PU.1 and ATAC-Seq at their promoters, as assessed by re-analyses of published datasets (Cuartero et al. 2018; Ostuni et al. 2013) (Figure 45), and high sensitivity to BET or CBP and p300 inhibitors (Figure 46, see Methods).

Interestingly, PGE$_2$ alone further reduced basal expression of sensitive genes and H3K27ac selectively at sensitive enhancers (Figure 38). Notably, sensitive regions displayed persistent (up to eight hours) reduced chromatin accessibility (Figure 47, 48) and PU.1 binding (Figure 47). These data indicate that PGE$_2$ disassembles basal chromatin organization selectively at a set of poorly permissive chromatin regions, including *Ifnb1* and IFN-dependent gene enhancers, and limits their full activation upon exposure to LPS.
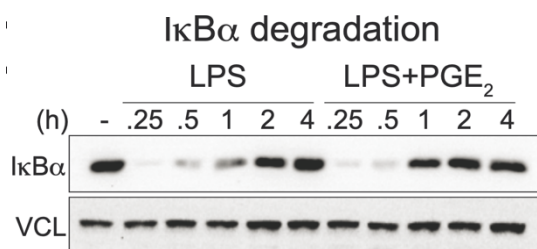
Figure 33

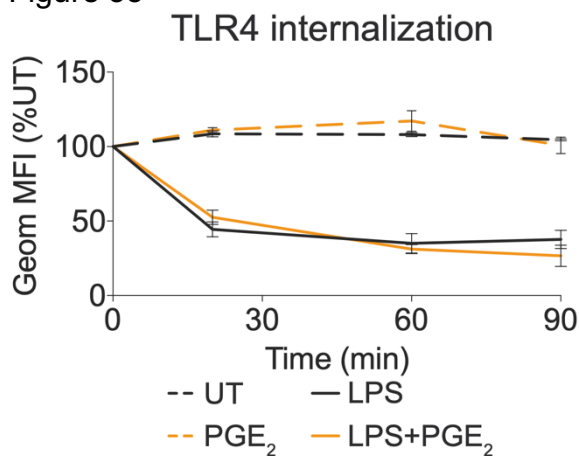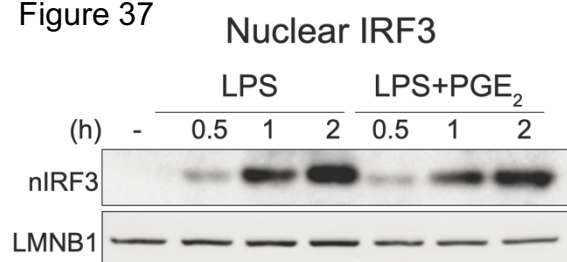**IκBα degradation**

LPS   LPS+PGE$_2$

(h)	-	.25	.5	1	2	4	.25	.5	1	2	4
IκBα											
VCL											

Figure 34

Nuclear p65

Figure 35

TLR4 internalization

-- UT   — LPS
-- PGE$_2$ — LPS+PGE$_2$

Figure 36

Phospho-TBK1

Figure 37

Nuclear IRF3

LPS   LPS+PGE$_2$

(h)	-	0.5	1	2	0.5	1	2
nIRF3							
LMNB1							

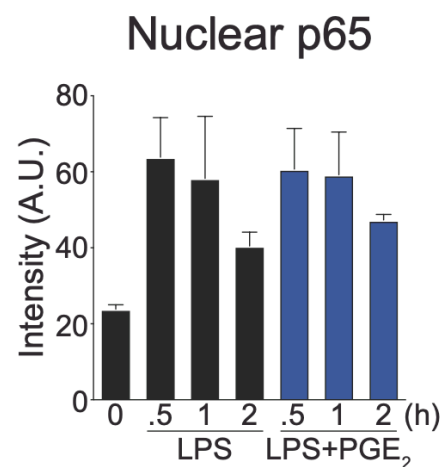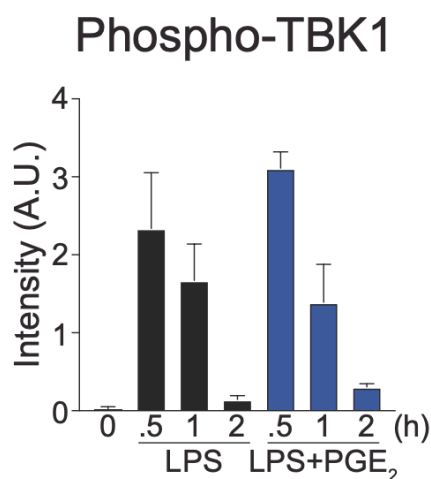**PGE$_2$ does not interfere with the LPS-induced signalling pathways.**

Figure 33 – Western blot analyses of IκBa in whole cell extracts in BMDMs stimulated as indicated.

Figure 34 – Immunofluorescence analyses of nuclear NF-κB p65 in BMDMs stimulated as indicated. Bar plots represent mean ± SD. Data from three biological replicates.

Figure 35 – Flow cytometry analysis of TLR4 internalization showing percentage of geometric Mean Fluorescence Intensity relative to the untreated condition in BMDMs stimulated as indicated. Line plot represents mean ± SD. Data from three biological replicates.

Figure 36 – Immunofluorescence analyses of phosphorylated TBK1 in BMDMs stimulated as indicated. Bar plots represent mean ± SD. Data from three biological replicates.

Figure 37 – Western blot analyses of IRF3 in nuclear extracts in BMDMs stimulated as indicated.
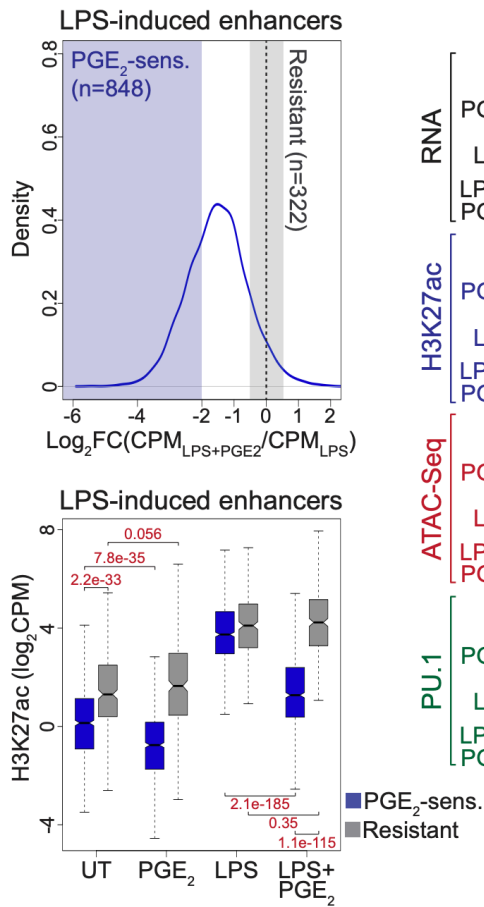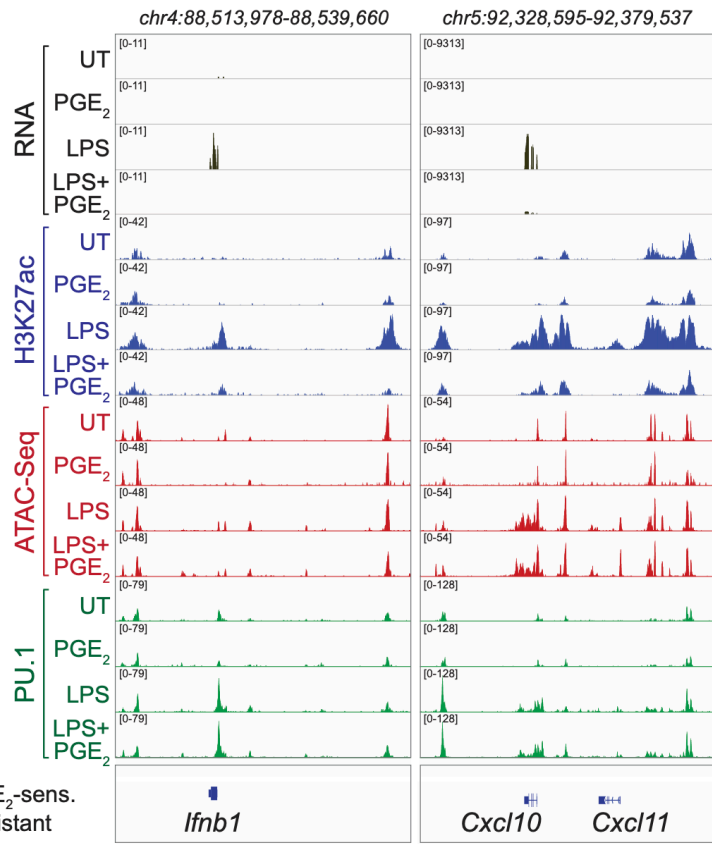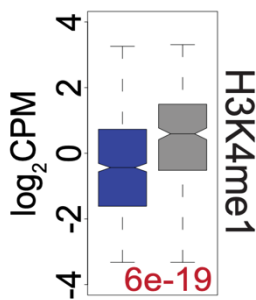
Figure 38

LPS-induced enhancers

LPS-induced enhancers

Figure 39

Figure 40

Figure 41

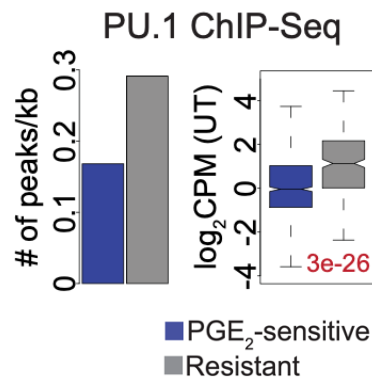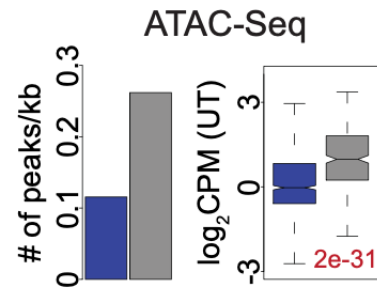## PU.1 ChIP-Seq

Figure 42

ATAC-Seq

Genomic features of PGE$_2$-sensitive and PGE$_2$-resistant gene enhancers.

Figure 38 – (top) Density plot showing the effect of PGE$_2$ costimulation on LPS-induced H3K27ac. Dotted line indicates lack of effect of the costimulation; blue or grey shaded areas indicate values used to define PGE$_2$-sensitive or resistant enhancers, respectively. Data from two biological replicates. Pearson correlation > 0.94 for all replicates. (bottom) H3K27ac ChIP-Seq mean signal intensity within PGE$_2$-sensitive (blue) or resistant enhancers (grey) in the indicated conditions. Numbers indicate p-values (Mann-Whitney U test) for the indicated comparisons. Data from two biological replicates. Pearson correlation > 0.94 for all replicates.

Figure 39 – Integrative Genome Viewer (IGV) snapshots showing read coverage of the indicated datasets at selected PGE$_2$-sensitive genomic loci in costimulated BMDMs.

Figure 40 – Box plot showing H3K4me1 ChIP-Seq signal intensity in unstimulated BMDMs of PGE$_2$-sensitive (blue) or resistant (grey) enhancers (data from Ostuni et al., Cell 2013)

Figure 41 – Number of PU.1 ChIP-Seq peaks/kb (bar plot, left) or respective signal intensities (box plots, right) within PGE$_2$-sensitive (blue) or resistant enhancers (grey). Data refer to untreated BMDMs. Numbers indicate p-values (Mann-Whitney U test) for the indicated comparisons.

Figure 42 - Number of ATAC-Seq peaks/kb (bar plot, left) or respective signal intensities (box plots, right) within PGE$_2$-sensitive (blue) or resistant enhancers (grey). Data refer to untreated BMDMs. Numbers indicate p-values (Mann-Whitney U test) for the indicated comparisons.

Figure 43
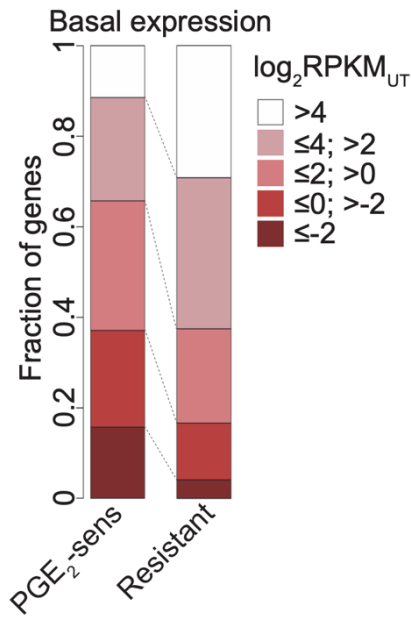
Basal expression

log$_2$RPKM$_{UT}$
- >4
- ≤4; >2
- ≤2; >0
- ≤0; >-2
- ≤-2

Fraction of genes

PGE$_2$-sens   Resistant

Figure 44

RNA-Seq

Expression (log$_2$RPKM)

1.1e-4   0.006   4e-8   2e-9

- PGE$_2$-sens.
- Resistant

UT   PGE$_2$ LPS   LPS+ PGE$_2$

Figure 45

H3K4me3
0.0008
4e-5
8e-9

CPM (in UT)

-3   +3

H3K27ac
4e-6
6e-7
1e-9

-5   +5

PU.1
0.001
0.0007
2e-5

CPM (in UT)

-1   0   +1

ATAC-Seq
0.002
0.009
4e-5

-1   0   +1

distance from TSS (kb)

- PGE$_2$-sens.
- IL-10-sens.
- IL-4-sens.
- Resistant

Figure 46

BRD2/4-dep (%)

BRD2/4 inhibitor

CBP/p300-dep (%)

CBP/p300 inhibitor

Genomic features of PGE$_2$-sensitive and PGE$_2$-resistant gene enhancers.
Figure 43 – Stacked bar plot showing the fraction of PGE$_2$-sensitive or resistant genes, within the basal expression values (namely, in unstimulated BMDMs) indicated in the legend.
Figure 44 – Mean expression values of PGE$_2$-sensitive (blue) or resistant (grey) genes in the indicated conditions. Data from two biological replicates. Pearson correlation > 0.97 for all replicates. Numbers indicate p-values for the corresponding comparisons (Mann-Whitney U test).
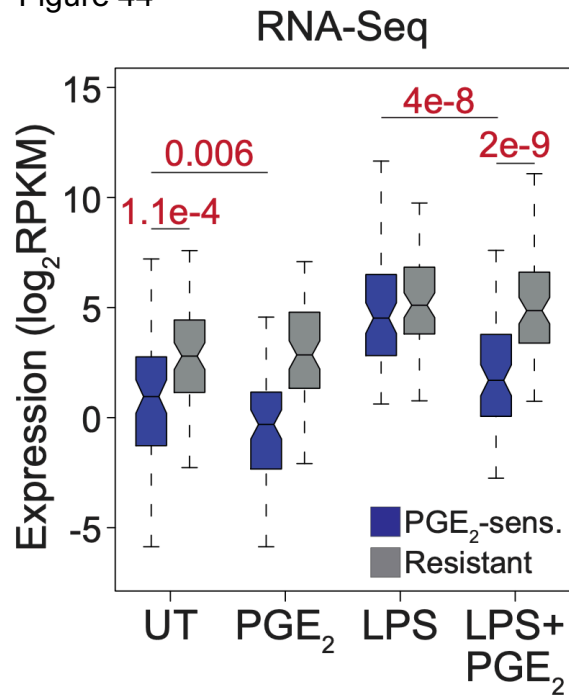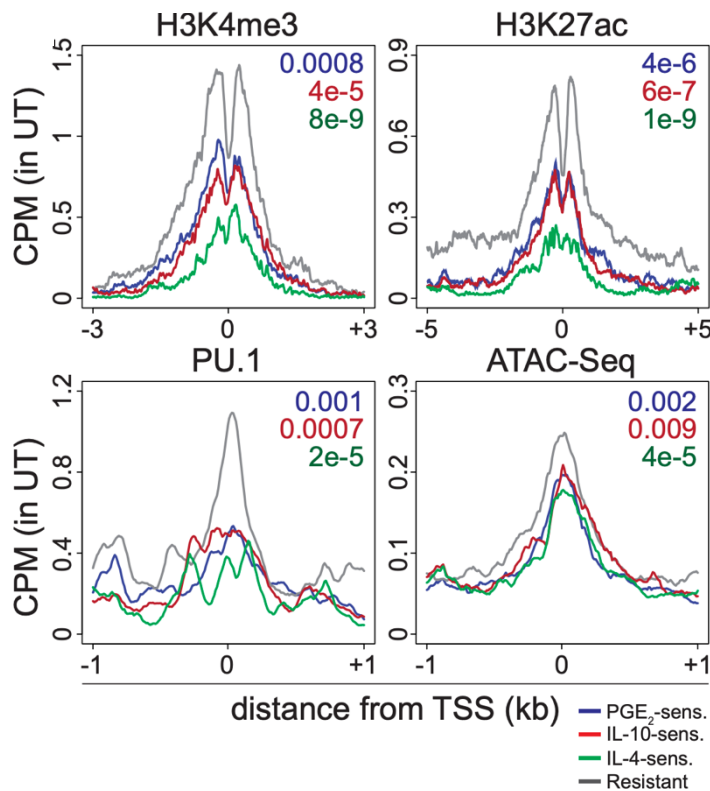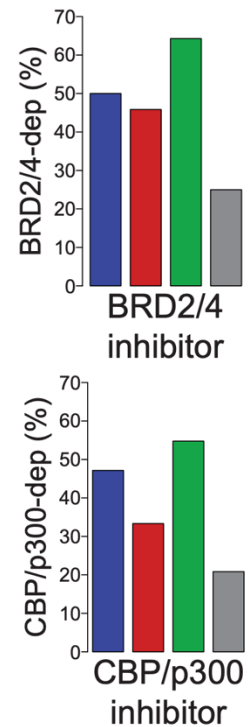**Figure 45 –** Mean intensities (CPM) of H3K4me3, H3K27ac, PU.1 ChIP-Seq or ATAC-Seq signals in genomic regions spanning the transcription start site (TSS) of PGE$_2$-sensitive (blue), IL-10-sensitive (red), IL-4-sensitive (green) or resistant (grey) genes in unstimulated BMDMs (data from Ostuni et al., Cell 2013 and Cuartero et al., Nat Immunol 2018). Numbers indicate p-values (Mann-Whitney U test) comparing coverages (CPM) computed on the displayed genomic regions.
Figure 46 – Percentage of PGE$_2$-sensitive (blue), IL-10-sensitive (red), IL-4-sensitive (green) or resistant (grey) genes whose induction by LPS was reduced (see Methods) by inhibition of BRD2-4 (left) or CBP-p300 (right). Data from three biological replicates. Pearson correlation > 0.98 for all replicates.

Figure 47
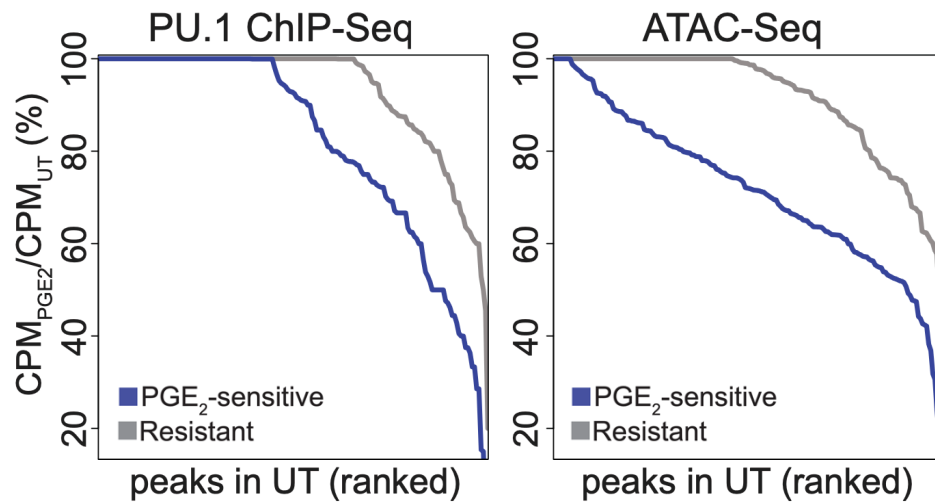
Figure 48
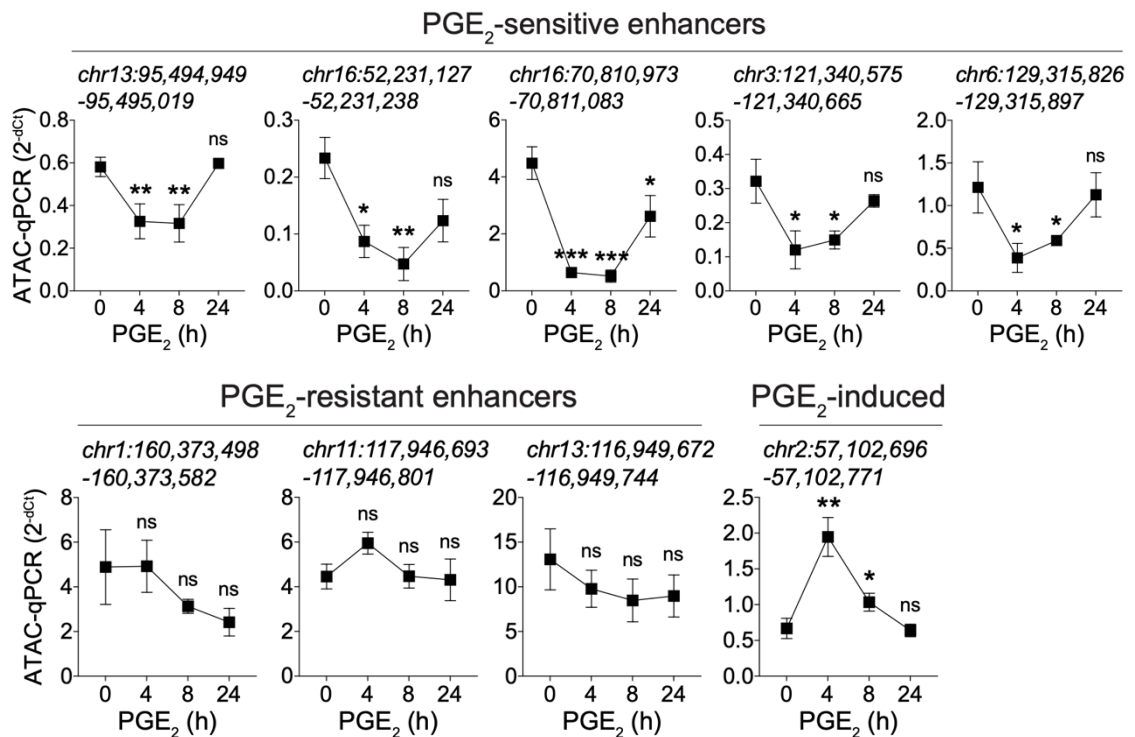
PGE$_2$ further reduces basal chromatin accessibility at PGE$_2$-sensitive enhancers.
Figure 47 – Line plots showing PU.1 ChIP-Seq or ATAC-Seq signal intensities as percent ratio in BMDMs treated with PGE$_2$ to untreated controls. Data refer to PGE$_2$-sensitive (blue) or resistant (grey) enhancers.
Figure 48 - ATAC-qPCR analysis of selected PGE$_2$-sensitive, resistant, and PGE$_2$-induced enhancers in BMDMs stimulated with PGE$_2$ for the indicated time points. Line plots represent mean ± SD. Data from three biological replicates. *** $p<0.001$, ** $p<0.01$, * $p<0.05$, ns not significant (unpaired t-test).

AP-1 and IRF TFs mark resistant and *de novo* PGE$_2$-sensitive enhancers, respectively

To define sequence determinants responsible for sensitivity or resistance to PGE$_2$, we performed motif enrichment analysis on H3K27ac dataset and found binding motif for AP-1 as the top represented within resistant enhancers (Figure 49). We validated this analysis by ChIP-Seq for JUNB and found an increased occupancy of this TF at resitant regions in costimulated BMDMs (Figure 50). We explained this behaviour by the evidence of hyper-activation of the upstream MAPK p38 and JNK upon treatment with LPS and PGE$_2$ (Figure 51). We also found an increased occupancy of NF-$\varkappa$B at resistant regions (Figure 52), in line with the enrichment of resistant genes in NF-$\varkappa$B-dependent transcripts (Figure 3, 4).

Instead, *de novo* PGE$_2$-sensitive enhancers (see Methods) showed enrichment in IRF and PU.1:IRF binding sites (Figure 49). Accordingly, occupancy of IRF1 increased upon stimulation with LPS and was strongly inhibited upon co-exposure to PGE$_2$ selectively at sensitive regions (Figure 50). Similar behaviour was observed for STAT1 occupancy, likely reflecting the impaired IFN-β production in costimulated BMDMs (Figure 50).

Figure 49

PGE$_2$-sensitive enhancers

Pre-existing	MEF2	p-val 1e-5 q-val 0.001
de novo	IRF	p-val 1e-10 q-val <0.001
	PU.1-IRF	p-val 1e-5 q-val 0.001
	EGR	p-val 1e-3 q-val 0.04

Resistant enhancers

Pre-existing	AP-1	p-val 1e-5 q-val 0.001
de novo	AP-1	p-val 1e-7 q-val <0.001
	BACH	p-val 1e-3 q-val 0.02
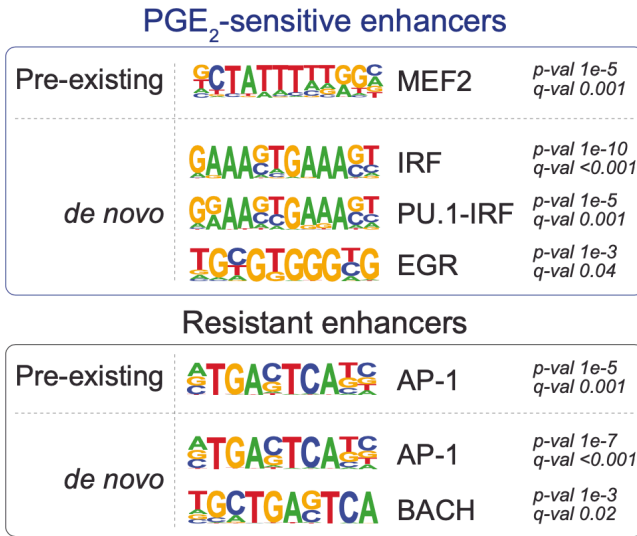
Figure 51

Figure 52

Figure 50

Distance (+/- 1 kb) from ATAC peak summit

67

MEF2 TFs mark pre-existing PGE$_2$-sensitive enhancers, while AP-1 and IRF TFs mark PGE$_2$-resistant and *de novo* PGE$_2$-sensitive enhancers, respectively.

Figure 49 - Motif enrichment analysis showing top-ranking motifs identified within pre-existing or *de novo* OCRs (see Methods) at PGE$_2$-sensitive or resistant enhancers. Putative cognate TF families and associated p-values and q-values are shown.

Figure 50 – (top) ChIP-Seq signal intensities for the indicated TFs at pre-existing or *de novo* OCR within PGE$_2$-sensitive (colored) or resistant (grey) enhancers in the indicated conditions. Numbers denote p-values (Mann-Whitney U test) for the indicated comparisons. (bottom) Heatmap showing the intensity of ChIP-Seq signals for the indicated TFs and the indicated experimental conditions at pre-existing or *de novo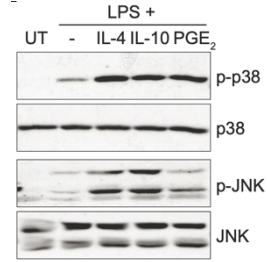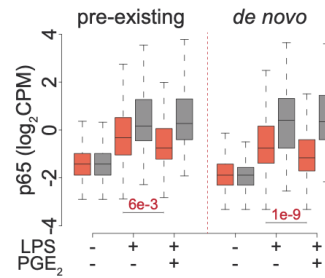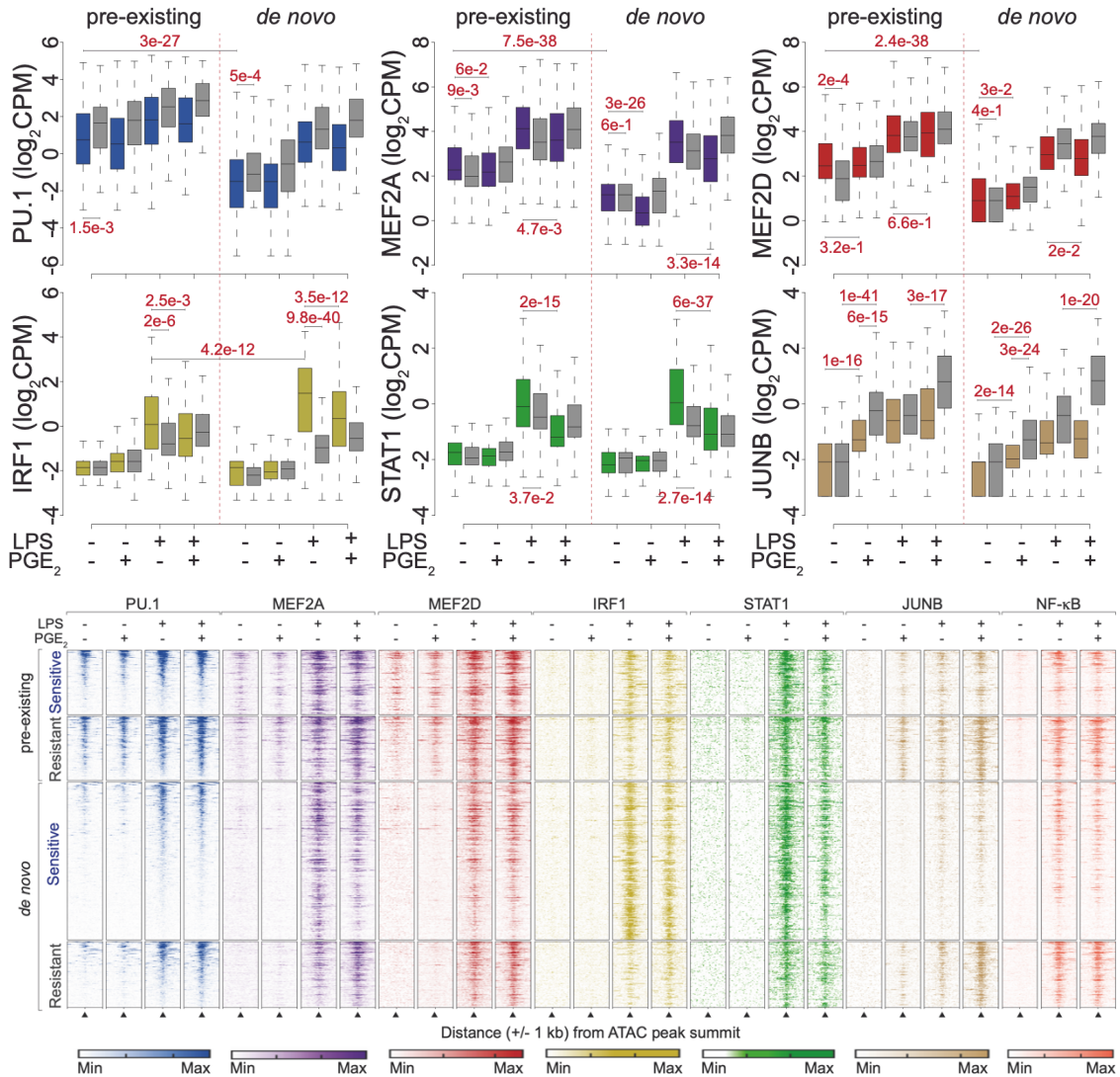* OCRs within PGE$_2$-sensitive or resistant enhancers. Signal intensities are represented over a 2 kb genomic region spanning the ATAC-Seq peak summit. Legends are shown on the bottom.

Figure 51 - Western blot analyses in BMDMs for phosphorylated p38 (Thr180/Tyr182) or JNK (Thr183/Tyr185) as well as non-phosphorylated forms in the indicated conditions. Data shown refer to a stimulation of 30 minutes.

Figure 52 - p65 ChIP-Seq signal intensities at pre-existing or *de novo* OCRs within PGE$_2$-sensitive (orange) or resistant (grey) enhancers in the indicated conditions. Numbers denote p-values (Mann-Whitney U test) for the indicated comparisons.

MEF2 TFs mark pre-existing PGE$_2$-sensitive enhancers

Motif enrichment analysis on pre-existing PGE$_2$-sensitive enhancers (see Methods) revealed an overrepresentation of the 5'-CTATTTTTGG-3' motif, corresponding to the binding site for the TF MEF2 (Figure 49). To assess genomic distribution of MEF2 TFs, we performed ChIP-Seq for MEF2 family members expressed in BMDMs, namely MEF2A, MEF2C and MEF2D. MEF2A and MEF2D bound the genome in a pervasive manner, with 26,472 and 18,709 peaks respectively, while MEF2C displayed lower occupancy (6,340 peaks) (Figure 53). Interestingly, MEF2A binding sites largely overlapped with those of LDTFs PU.1, IRF8 and C/EBP-β (Figure 54).

In accordance with motif enrichment analysis, binding of MEF2A and MEF2D at pre-existing PGE$_2$-sensitive enhancers was already evident in untreated cells, as well as at resistant enhancers at lower level, possibly reflecting occupancy via protein-protein interactions and not directly by DNA binding (Figure 50). Binding of MEF2 increased upon stimulation with LPS at sensitive and resistant enhancers and reduced in costimulated BMDMs selectively at PGE$_2$-sensitive regions (Figure 50). We conclude that MEF2 TFs display a broad occupancy in the genome and mark a set of enhancers targeted by PGE$_2$.

Figure 53

Figure 54

MEF2 ChIP-Seq

MEF2A ChIP-Seq

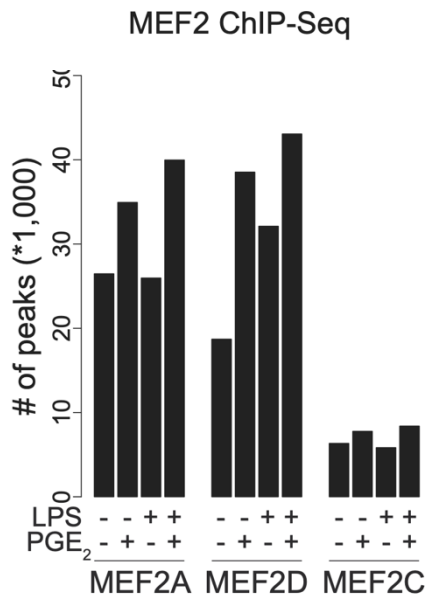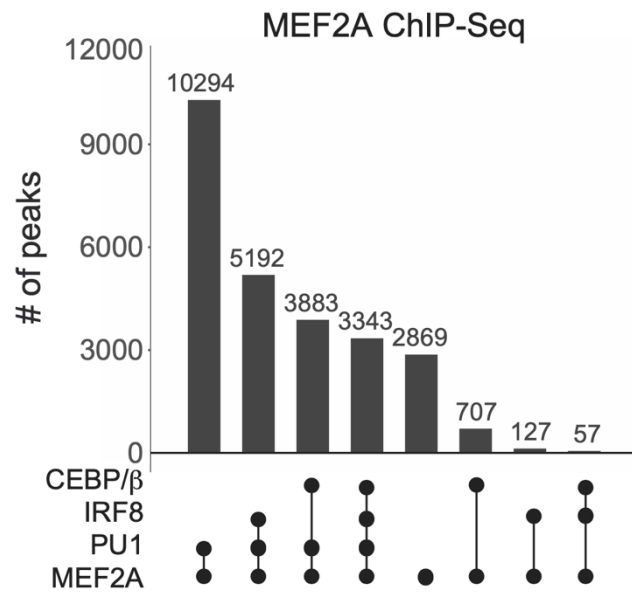**MEF2 TFs pervasively bind the genome in macrophages.**
Figure 53 – Number of ChIP-Seq peaks identified for MEF2A, MEF2D or MEF2C in BMDMs stimulated as indicated.
Figure 54 - Number of MEF2A ChIP-Seq peaks overlapping with the indicated TFs.

MEF2A controls the basal and the LPS-inducible enhancer landscape in macrophages

We next assessed the role of MEF2 TFs in regulating enhancer landscape and generated immortalized macrophages (iMacs, Figure 55) with single or combined edits in *Mef2a*, *Mef2c* and *Mef2d* genes (Figure 56). We focused on MEF2A since *Mef2a*$^{-/-}$ macrophages displayed defective induction of *Ifnb1* upon stimulation with LPS (Figure 56). Deficiency of MEF2A (Figure 57) resulted in altered basal and inducible epigenome, with hundreds of enhancers affected. *Mef2a*$^{-/-}$ macrophages showed reduced H3K27ac signal at enhancers of untreated (n=998) and LPS-treated (n=981) cells (Figure 57), indicating that loss of MEF2A profoundly altered *cis*-regulatory repertoire, particularly evident at the *Ifnb1* locus (Figure 59).

We then evaluated the impact of MEF2A deficiency on PGE$_2$-sensitive enhancers. Loss of MEF2A reduced basal histone acetylation, PU.1 binding and chromatin accessibility selectively at PGE$_2$-sensitive but not resistant enhancers, and this effect was even more exacerbated upon exposure to LPS (Figure 60). These results point out MEF2A as key regulator of basal and inducible epigenome in macrophages, particularly of PGE$_2$-sensitive enhancers.

Figure 55

Figure 56

clone ID	MEF2A	MEF2C	MEF2D
B5	+/-	+/+	+/+
B9	+/-	+/+	+/+
D7	-/-	+/+	+/+
H4	+/+	-/-	+/+
G4	+/+	+/+	-/-
D3	+/+	+/+	+/-
G1	+/-	+/+	+/-
A7	-/-	+/+	+/-
A8	-/-	+/+	-/-
C7	-/-	+/-	+/+
C1	+/-	-/-	-/-
G5	+/-	+/-	+/-
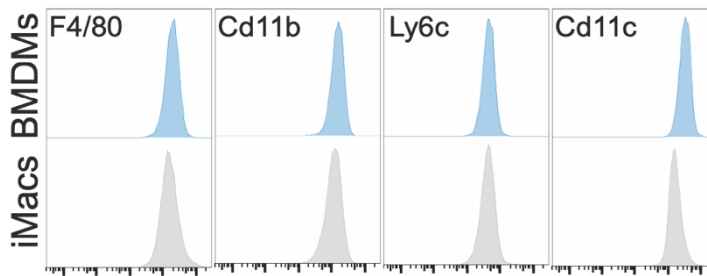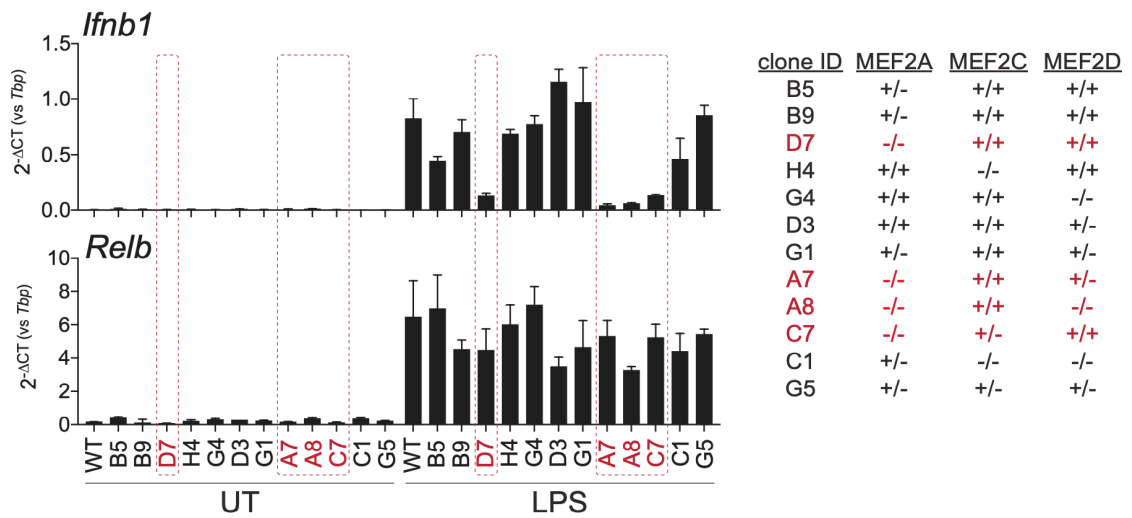
Generation of MEF2-deficient iMacs.

Figure 55 – Surface expression of the indicated markers in differentiated BMDMs (light blue) or iMacs (grey).

Figure 56 - RT-qPCR analysis (left) of *Ifnb1* and *Relb* on clones of iMacs in the indicated conditions. MEF2A-deficient clones are highlighted in red. The ID and genotype of each clone are shown on the right.

Figure 57
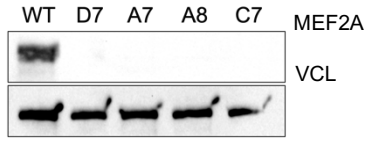
Figure 58
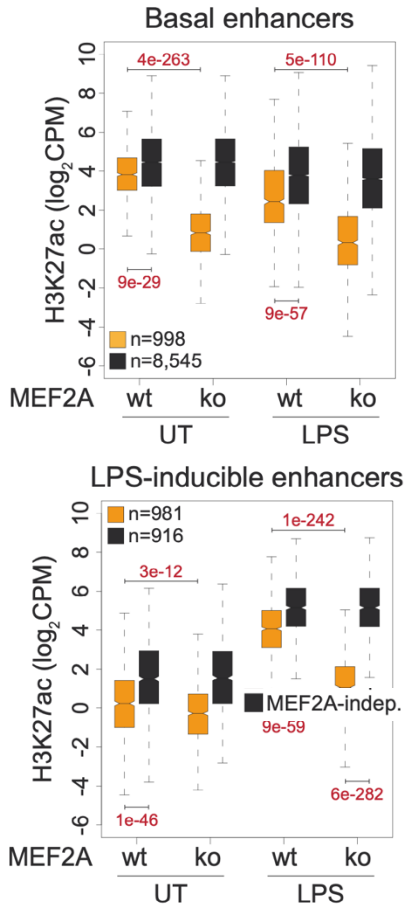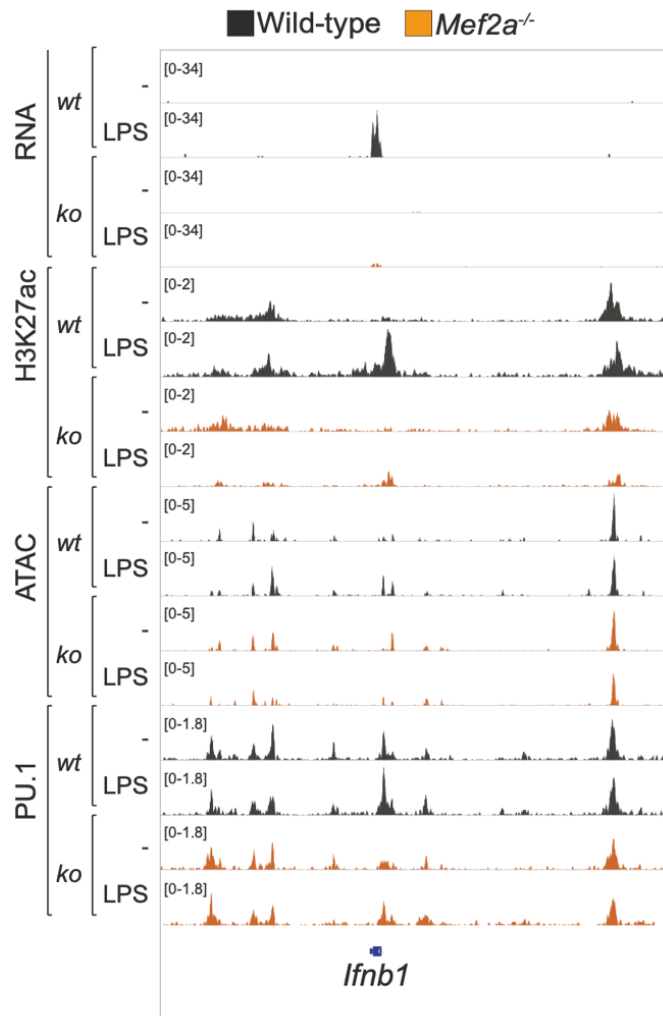
Basal enhancers

LPS-inducible enhancers

Figure 59

Figure 60

H3K27ac

ATAC-Seq

PU.1

PGE$_2$-sensitive enhancers
Resistant enhancers
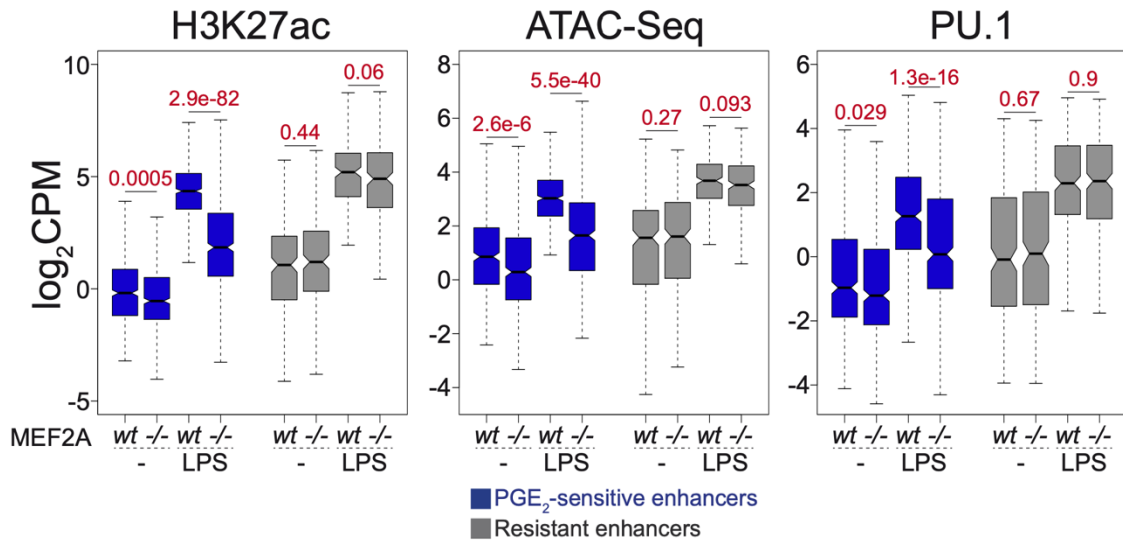
MEF2A controls the basal and the LPS-inducible enhancer landscape of macrophages.

Figure 57 - Western blot analyses of MEF2A and loading control (VCL) in wt and *Mef2a$^{-/-}$* iMacs clones. IDs of the individual clones are shown.

Figure 58 – H3K27Ac mean intensity values for basal (top) or LPS-inducible (bottom) MEF2A-dependent (orange) and MEF2A-independent (black) enhancers (see Methods). Data are shown for wt or MEF2A-deficient iMacs in the indicated conditions. Data from three biological replicates. Pearson correlation > 0.94 for all replicates. Numbers indicate p-values (Mann-Whitney U test) for the corresponding comparisons.

Figure 59 – IGV snapshot showing read coverage of the indicated datasets at *Ifnb1* genomic locus in wt (black) or *Mef2a$^{-/-}$* (orange) iMacs in the indicated experimental conditions.

Figure 60 – Box plot showing mean intensity values within PGE$_2$-sensitive (blue) or resistant (grey) enhancers in the indicated datasets, obtained in wt or MEF2A-deficient iMacs for the indicated conditions. Data from two biological replicates. Pearson correlation > 0.82 for all replicates. Numbers denote p-values (Mann-Whitney U test) for the indicated comparisons.

MEF2A controls TLR4-dependent induction of IFN I

To define the role of MEF2A in regulating inflammatory gene expression, we stimulated MEF2A-deficient macrophages with LPS and performed RNA-Seq. *Mef2a^-/-* macrophages showed defective induction of a large set of genes (n=94/312, see Methods) upon stimulation with LPS, including *Ifnb1*, *Cxcl9*, *Cxcl10* and *Il12b* (Figure 61). Impaired induction of *Ifnb1* resulted in defective production of IFN-β (Figure 62) and IFN-dependent gene expression, as resulted from gene set enrichment analysis on MEF2A-dependent transcripts (Figure 63). Such defective IFN I response could be partially restored in *Mef2a^-/-* macrophages by exogenous administration of recombinant IFN-β, as indicated by recovered induction of selected MEF2A-dependent genes (Figure 64). Impaired inflammatory gene expression of MEF2A deficient cells was not to ascribe to altered signalling pathways activated by LPS. Indeed, degradation of IkBα (Figure 65), nuclear translocation of NF-ϰB (Figure 66), internalization of TLR4 (Figure 67) and phosphorylation of TBK1 (Figure 68) were preserved in *Mef2a^-/-* macrophages upon exposure to LPS. Loss of MEF2A did not impact on the release of IL-10 or PGE$_2$ by activated macrophages (Figure 69), consistent with the defective inflammatory gene expression observed in *Mef2a^-/-* macrophages treated with IL-10R blocking antibody (Figure 70). Overall, these data indicate that MEF2A is a critical regulator of TLR4-driven IFN I response.

We next assessed the impact of MEF2A deficiency on the expression of PGE$_2$-sensitive genes. We found that MEF2A-dependent genes also comprised a significant fraction of PGE$_2$-sensitive genes (Figure 71). In line with this, PGE$_2$-sensitive transcripts were enriched in MEF2A-dependent genes, while resistant transcripts were not (Figure 72). Our data established MEF2A as key regulator of macrophage activation targeted by PGE$_2$. Loss of MEF2A, as well as treatment with PGE$_2$, resulted in altered basal and LPS-inducible gene expression of a fraction of sensitive genes enriched in IFN-induced transcripts. However, the overlap between MEF2A-dependent and PGE$_2$-sensitive genes was not complete, indicating an additional layer of control by PGE$_2$ not ascribable to MEF2A.

Figure 61
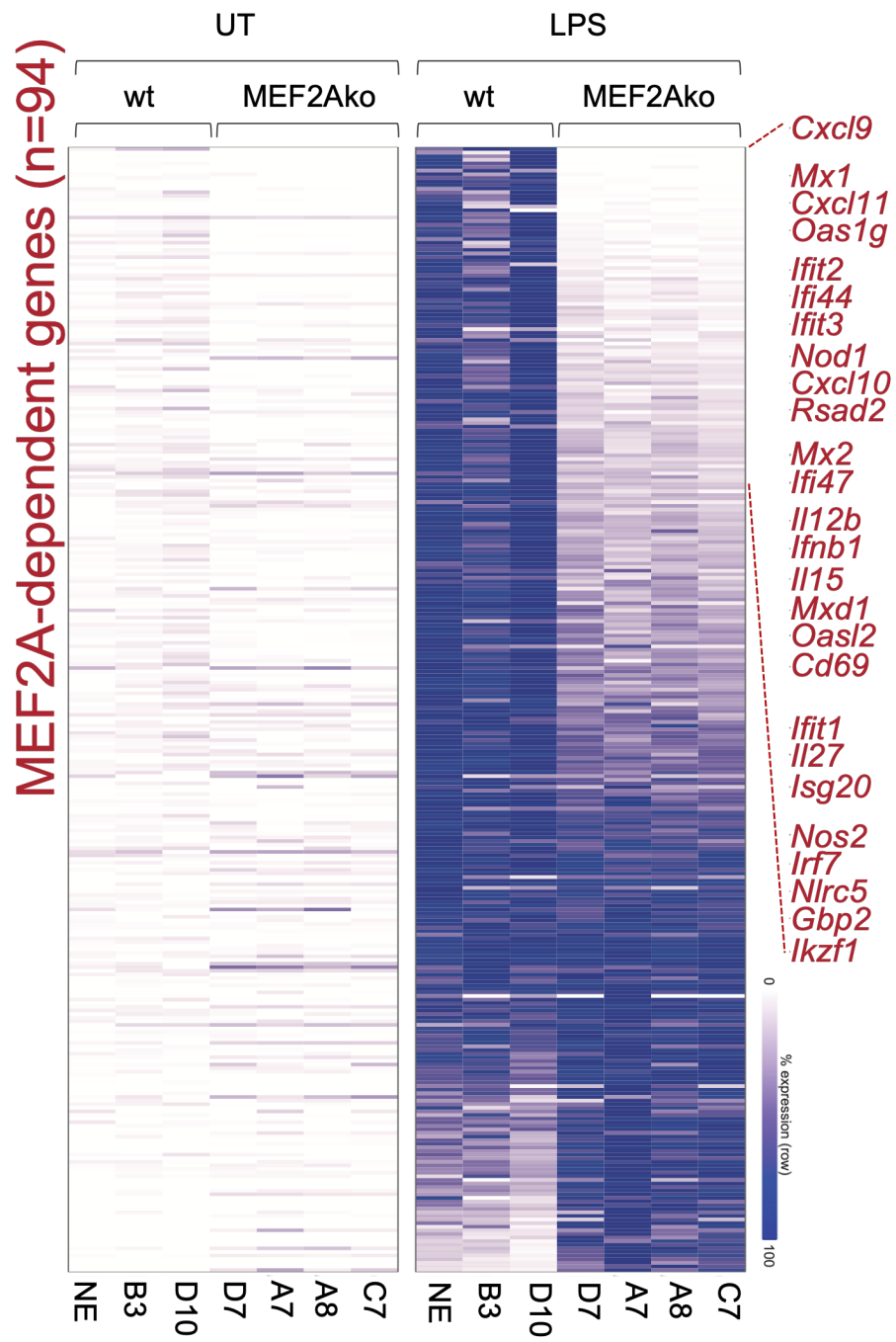
MEF2A is required for TLR4-driven induction of IFN I.

Figure 61 - Heatmap showing the behavior of LPS-inducible genes (n=312, see Methods) in wt or *Mef2a*$^{-/-}$ macrophages. The defined set of MEF2A-dependent genes (n=94, see Methods) is highlighted in red. Colors represent row-normalized percentage of gene expression. Selected gene names are shown on the right, color legends and clone IDs are shown on the right and on the bottom, respectively. Data from three biological replicates. Pearson correlation > 0.93 for all replicates.

Figure 62
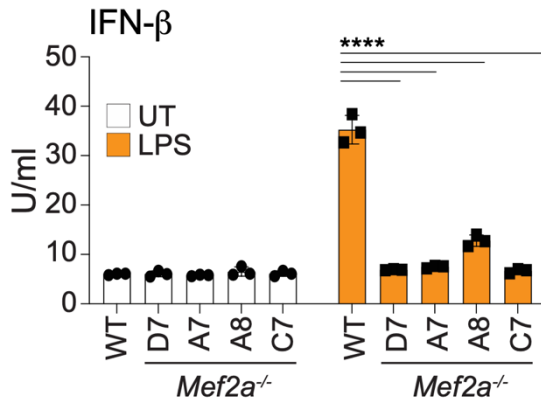
Figure 63
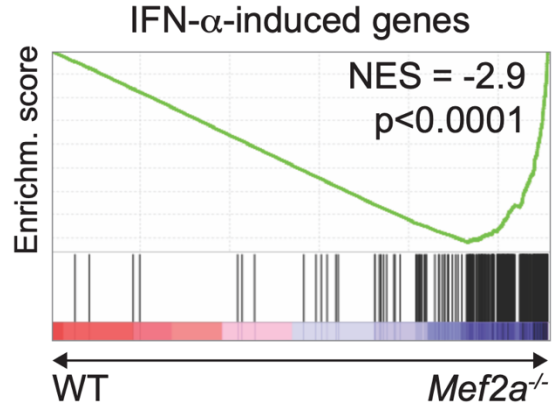
Figure 64
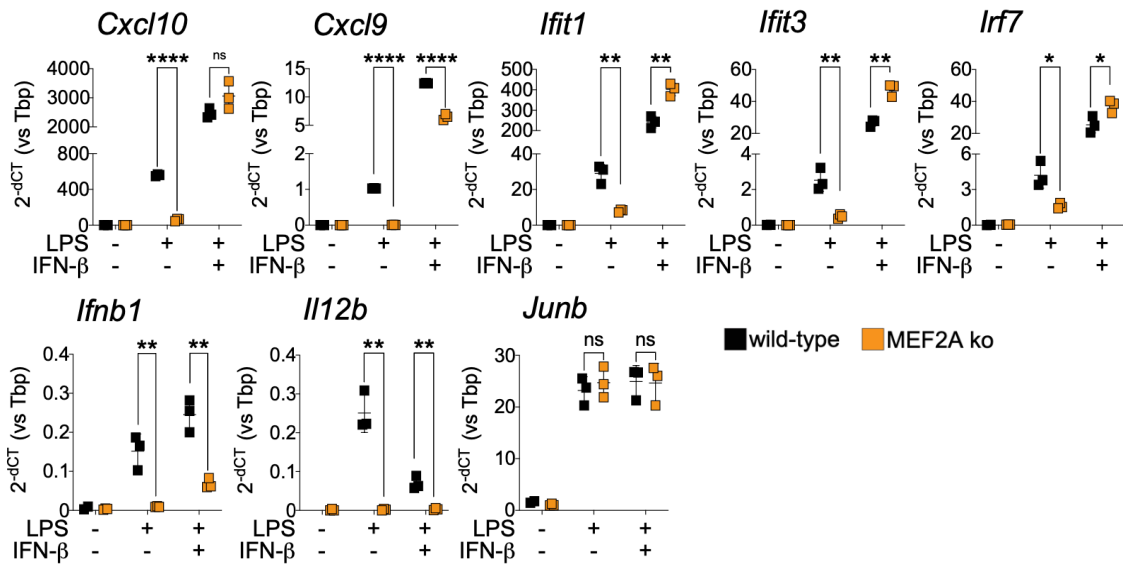
MEF2A is required for TLR4-driven induction of IFN I.

Figure 62 – IFN-β release by wt or *Mef2a⁻ᐟ⁻* iMacs stimulated with LPS. Genotypes and IDs of the individual clones are shown. Bar plot represents mean ± SD. Data from three biological replicates. **** p<0.0001 (two-way ANOVA test).

Figure 63 – GSEA of IFN-α-induced genes (gene set) in ranked gene lists obtained comparing LPS-stimulated *Mef2a⁻ᐟ⁻* versus wt iMacs. NES and p-value are shown.

Figure 64 – RT-qPCR analysis of a set of PGE₂-sensitive or resistant genes in wt (black) or *Mef2a⁻ᐟ⁻* (orange) iMacs stimulated as indicated. Dot plots represent mean ± SD. Data from three biological replicates. **** p< 0.0001, ** p< 0.01, * p<0.05, ns not significant (unpaired *t*-test).

Figure 65

Wild-type | MEF2Ako
(h) - 0.5 1 2 | - 0.5 1 2

IκBα

VCL

Figure 66

Nuclear p65

Figure 68

pTBK1 (IF)

Figure 67

TLR4 internalization

- - - Wild-type, UT
- - - MEF2Ako, UT
—— Wild-type, LPS
—— MEF2Ako, LPS

■ wild-type ■ MEF2A ko

Figure 69

IL-10

PGE$_2$

Figure 70

Ifnb1

Cxcl9

Il12b

Il6

Relb

Junb

■ wild-type
■ MEF2A ko
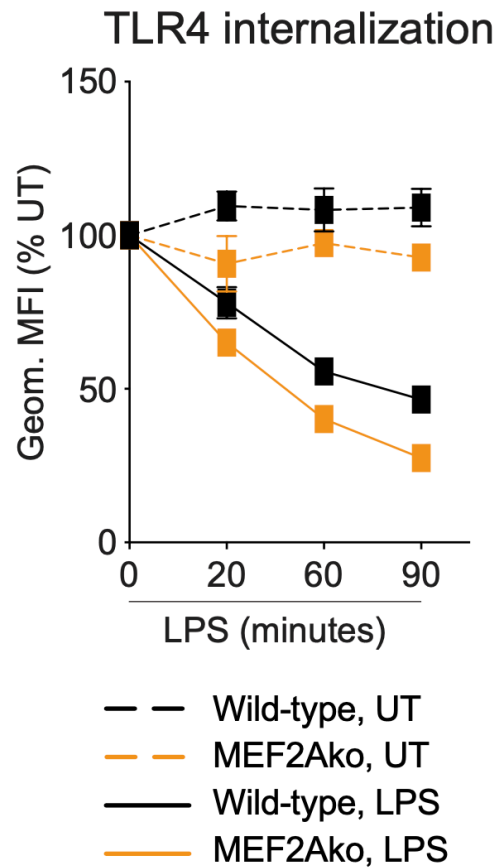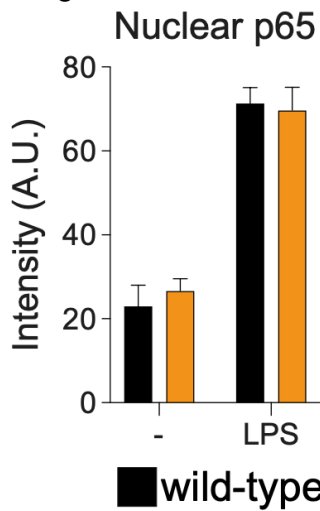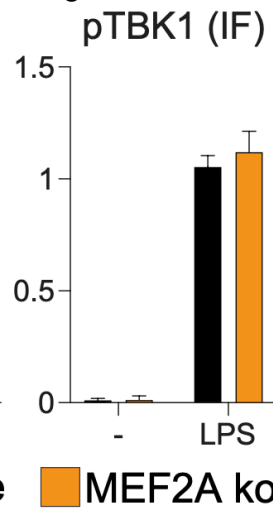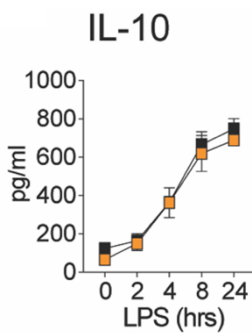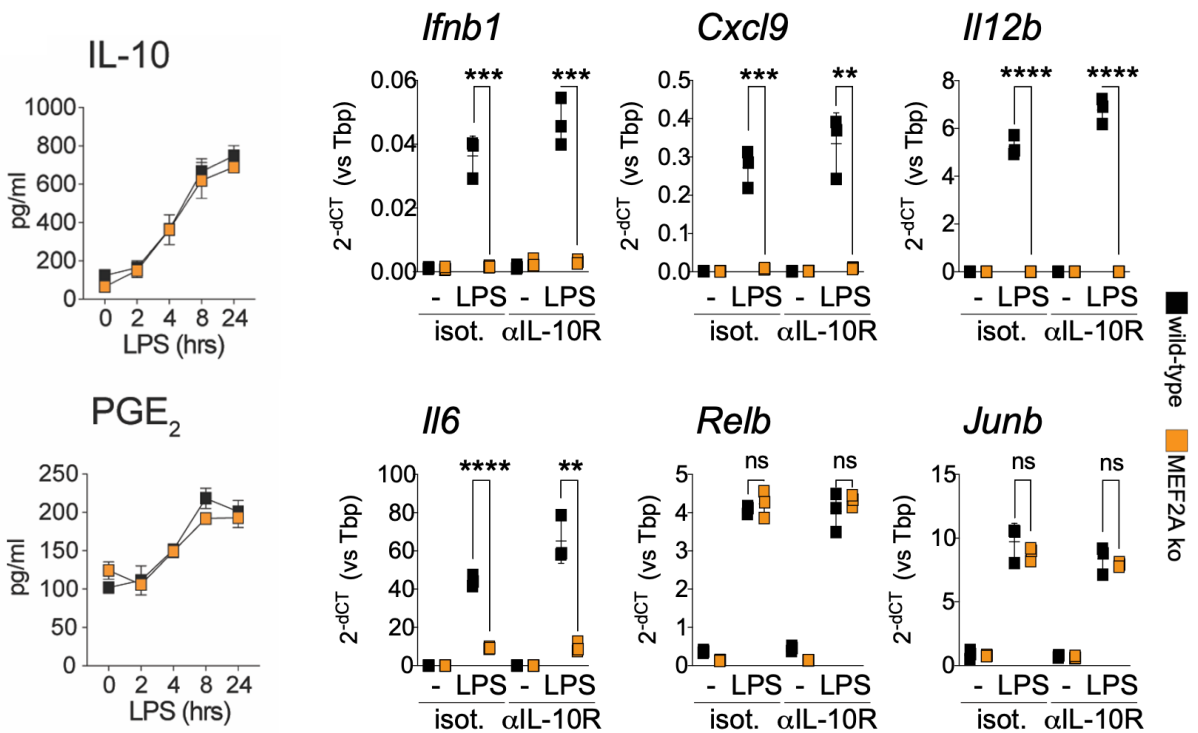
MEF2A deficiency does not alter the LPS-induced signalling pathways.

Figure 65 – Western blot analyses of IκBa and loading control (VCL) in whole cell extracts of wt or *Mef2a*$^{-/-}$ iMacs stimulated with LPS for the indicated time points.

Figure 66 – Immunofluorescence analyses of nuclear NF-κB p65 in wt (black) or *Mef2a*$^{-/-}$ (orange) iMacs stimulated with LPS for 30 minutes. Bar plots represent mean ± SD. Data from three biological replicates.

Figure 67 – Flow cytometry analysis of TLR4 internalization showing percentage of geometric Mean Fluorescence Intensity relative to the untreated condition in wt (black) or *Mef2a*$^{-/-}$ (orange) iMacs stimulated with control or LPS for the indicated time points. Line plot represents mean ± SD. Data from three biological replicates.

Figure 68 - Immunofluorescence analyses of or phosphorylated TBK1 (right) in wt (black) or *Mef2a*$^{-/-}$ (orange) iMacs stimulated with LPS for 30 minutes. Bar plots represent mean ± SD. Data from three biological replicates.

Figure 69 - IL-10 (top) or PGE$_2$ (bottom) release by wt (black) or *Mef2a*$^{-/-}$ (orange) iMacs stimulated for the indicated time points with LPS. Line plots represent mean ± SD. Data from three biological replicates.

Figure 70 - RT-qPCR analysis of a set of PGE$_2$-sensitive or resistant genes in wt (black) or *Mef2a*$^{-/-}$ (orange) iMacs, stimulated as indicated in the presence or absence of IL10R blocking antibody. Dot plots represent mean ± SD. Data from three biological replicates. **** $p < 0.0001$, *** $p < 0.001$, ** $p < 0.01$, ns not significant (unpaired *t*-test).
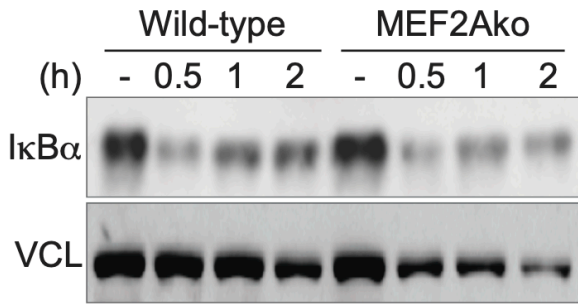
Figure 71
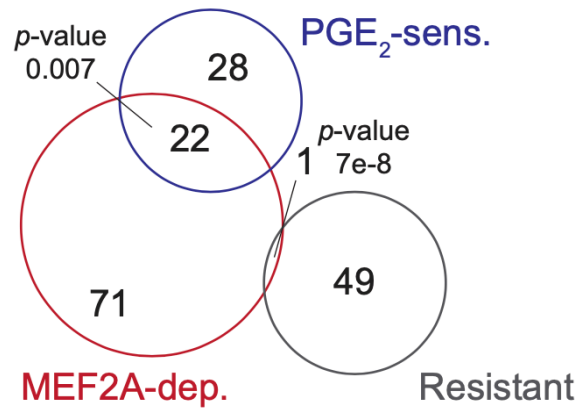
Figure 72
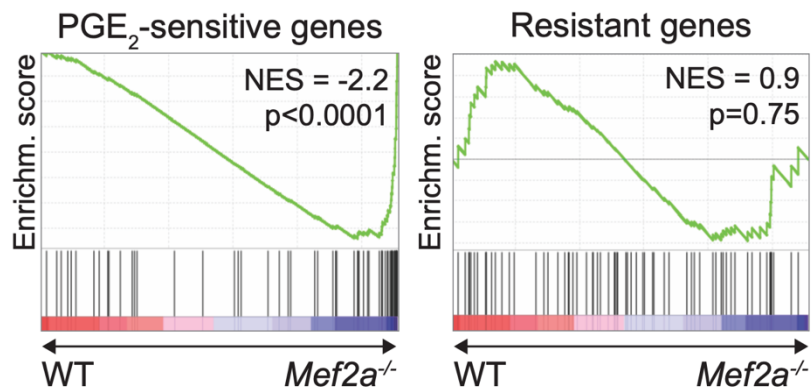
MEF2A-dependent and PGE$_2$-sensitive genes partly overlap.
Figure 71 - Venn diagram showing the overlap between MEF2A-dependent (red), PGE$_2$-sensitive (blue) or resistant (grey) genes (see Methods). p-values (hypergeometric test) for the indicated overlaps are shown.
Figure 72 - GSEA of PGE$_2$-sensitive or resistant genes (gene sets) in ranked gene lists obtained comparing LPS-stimulated *Mef2a*$^{-/-}$ versus wt iMacs. NES and p-value are shown for each plot.

MEF2A controls IFN I induction in response to multiple innate immune triggers

To elucidate whether MEF2A controls macrophage activation to other innate immune signals, we exposed *Mef2a$^{-/-}$* macrophages to synthetic activators of TLR3, TLR9 and cGAS, namely poly(I:C), CpG-ODN and DMXAA, respectively. Defective induction of IFN I was observed in MEF2A-deficient cells at the mRNA (Figure 73) and protein levels (Figure 74), analogously to impaired transcription of *Ifnb1* and deposition of H3K27ac at PGE$_2$-sensitive enhancers observed in BMDMs exposed to CpG-ODN or DMXAA in the presence of PGE$_2$ or forskolin (Figure 75). Moreover, *Mef2a$^{-/-}$* macrophages failed to induce IFN I at the mRNA (Figure 76) and protein levels (Figure 77) upon bacterial infection with *Mycobacterium tuberculosis* (*M.tb*) or Bacillus Calmette-Guérin (BCG) and viral infection with Vesicular Stomatitis Virus (VSV), indicating MEF2A as central regulator of IFN I production in macrophages in response to different immune signals and microbial pathogens.

Figure 73
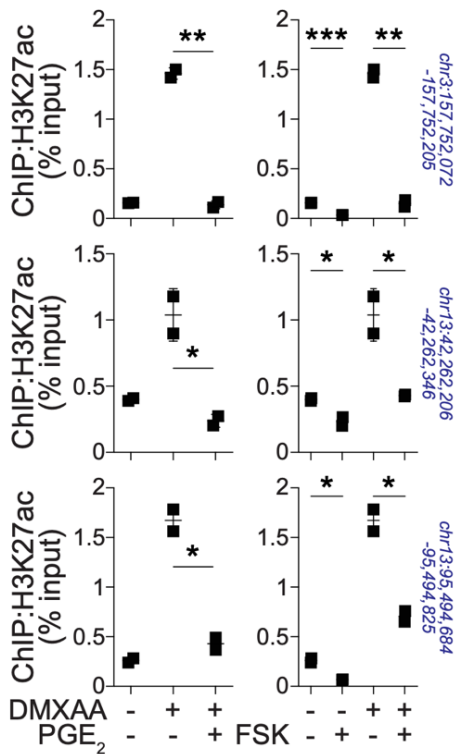
Figure 74
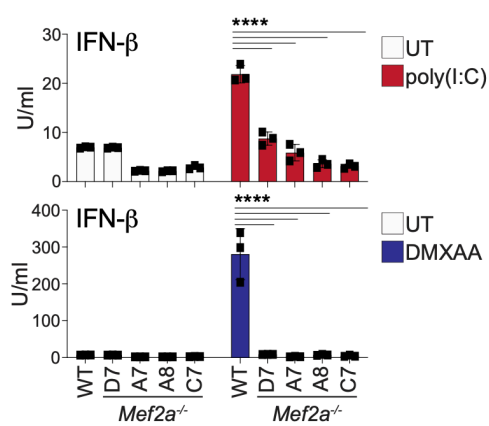
Figure 76
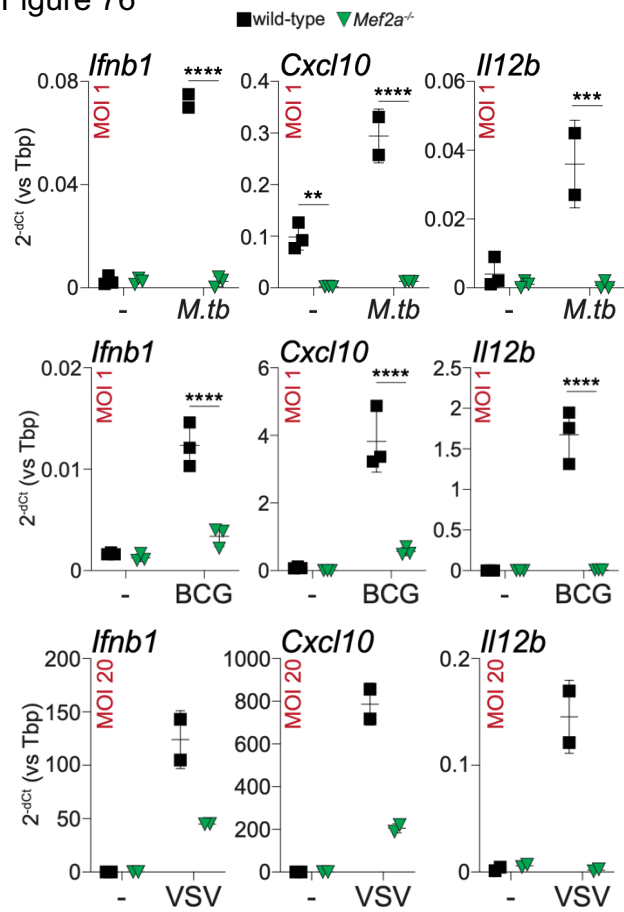
Figure 75
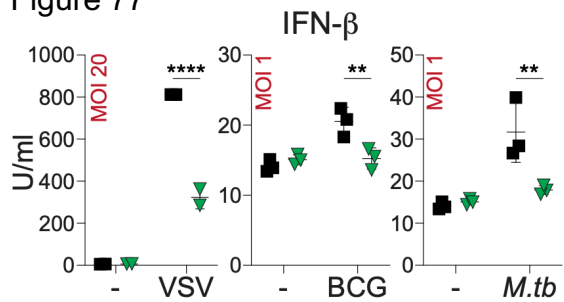
Figure 77

MEF2A controls IFN-β production upon multiple innate immune stimuli.

Figure 73 – RT-qPCR analysis of *Ifnb1* in wt or *Mef2a$^{-/-}$* iMacs stimulated for 4 hours with poly(I:C) (red, top), DMXAA (blue, center) or CpG (green, bottom). Genotypes and IDs of the individual clones are shown. Bar plots represent mean ± SD. Data from three biological replicates. **** $p<0.0001$ (two-way ANOVA test).

Figure 74 – IFN-β release by wt or *Mef2a$^{-/-}$* iMacs stimulated with poly(I:C) (red, top) or DMXAA (blue, bottom). Genotypes and IDs of the individual clones are shown. Bar plots represent mean ± SD. Data from three biological replicates. **** $p<0.0001$ (two-way ANOVA test).

Figure 75 – ChIP-qPCR analysis of a set of PGE$_2$-sensitive enhancers in BMDMs treated for 4 hours with DMXAA in the absence or presence of PGE$_2$ (left) or forskolin (right). Dot plots represent mean ± SD. Data from two biological replicates. *** $p<0.001$, ** $p<0.01$, * $p<0.05$ (unpaired *t*-test).

Figure 76 – RT-qPCR analysis of *Ifnb1*, *Cxcl10* or *Il12b* in wt (black) or *Mef2a$^{-/-}$* (green) iMacs infected with *M.tb.* (top), BCG (center) or VSV (bottom). MOI values are reported for each plot. Dot plots represent mean ± SD. Data from two or three biological replicates. **** $p< 0.0001$, *** $p< 0.001$ (two-way ANOVA test).

Figure 77 – IFN-β release by wt (black) or *Mef2a$^{-/-}$* (green) iMacs infected with VSV, BCG or *M.tb.* MOI values are reported for each plot. Dot plots represent mean ± SD. Data from two or three biological replicates. **** $p< 0.0001$, ** $p< 0.005$ (two-way ANOVA test).

IL-10 suppresses LPS-inducible gene expression via STAT3

We identified PGE_2 and IL-10 as potent suppressor of IFN I and we hypothesized that also IL-10 may modulate inflammatory gene expression by targeting MEF2A TF analogously to PGE_2. Exposure to IL-10 did not affect TLR4-induced signalling pathways (Figure 78) and caused reduced basal expression of IL-10-sensitive genes and basal histone acetylation at IL-10-sensitive enhancers (n=1,093, see Methods) (Figure 79, 80, 81), while chromatin accessibility and PU.1 occupancy remained largely unaffected (Figure 82). Analogously to PGE_2, IL-10-sensitive enhancers displayed poorly permissive chromatin and partially overlapped with PGE_2-sensitive enhancers (Figure 83).

Motif enrichment analysis on pre-existing and *de novo* IL-10-sensitive enhancers showed overrepresentation of IRF and PU.1:IRF sites, while MEF2A motif was exclusively retrieved from pre-existing PGE_2-sensitive enhancers and not from enhancers commonly sensitive to PGE_2 and IL-10 (Figure 84). These data demonstrate that MEF2A selectively control PGE_2-sensitive enhancers and underline a different mechanism of suppression by IL-10 on IRF-dependent enhancers. Indeed, we found that IL-10 suppressed inflammatory gene expression in a STAT3-dependent manner, since costimulated $Stat3^{-/-}$ BMDMs showed recovered induction of sensitive genes, including *Ifnb1*, *Il12b*, and *Il6* (Figure 85).
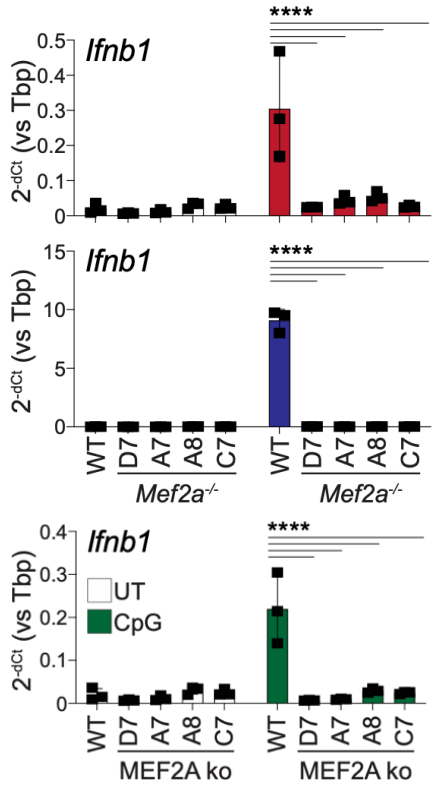
Figure 78
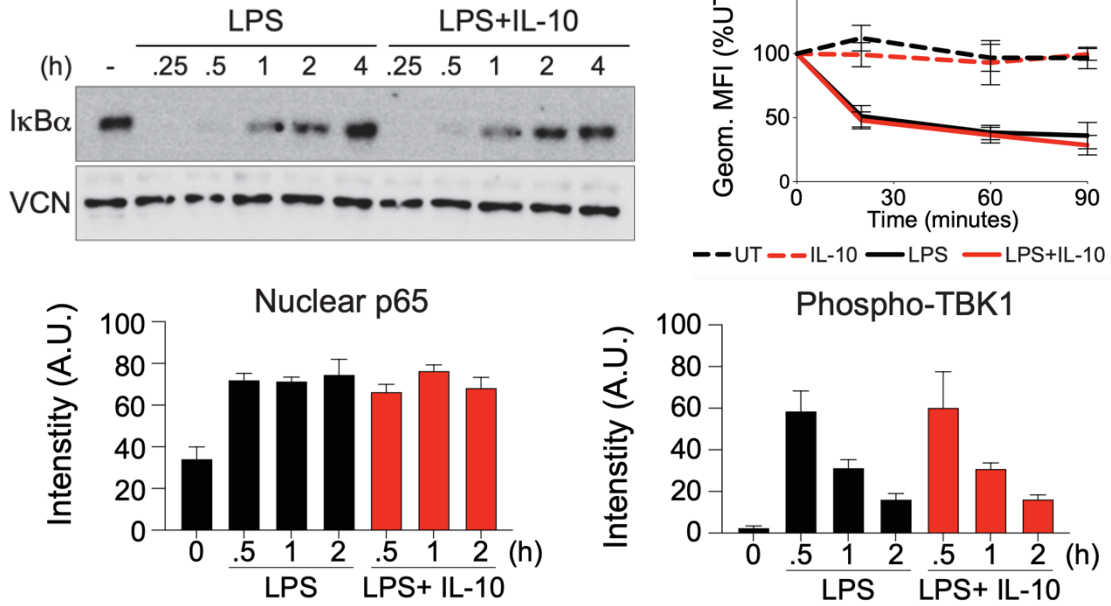
Figure 79
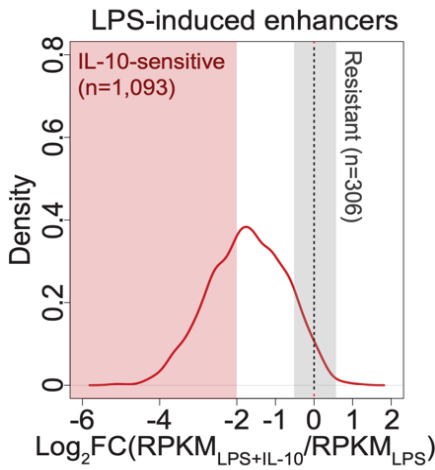
Figure 80
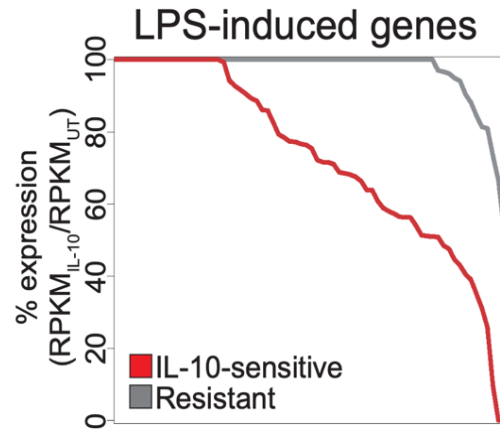
Figure 81
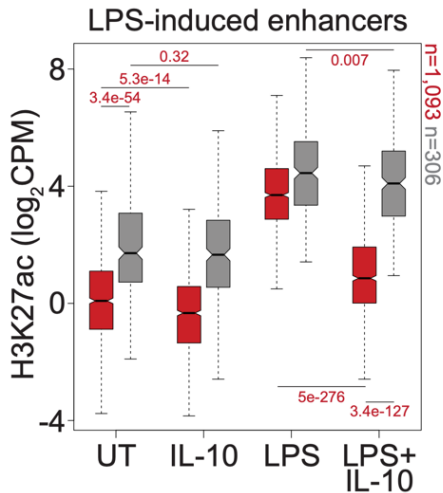
Figure 82
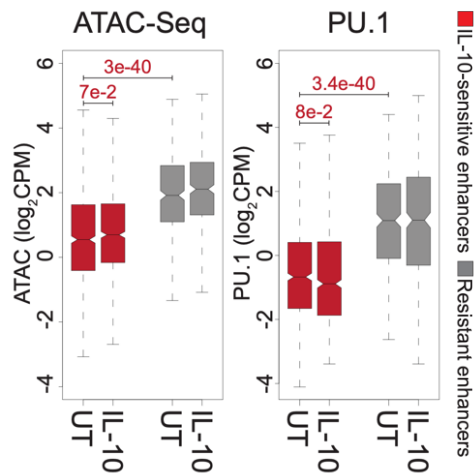
IL-10 functionally inactivates a set of inflammatory gene enhancers

Figure 78 – Western blot analyses of IκBa (top left) in whole cell extracts in BMDMs stimulated with LPS or LPS+IL-10 for the indicated time points.

Flow cytometry analysis of TLR4 internalization (top right) showing percentage of geometric Mean Fluorescence Intensity relative to the untreated condition in BMDMs stimulated with control, LPS, IL-10 or LPS+IL-10 for the indicated time points. Line plot represents mean ± SD. Data from three biological replicates.

Immunofluorescence analyses of nuclear NF-κB p65 (bottom left) or phosphorylated TBK1 (bottom right) in BMDMs stimulated as indicated. Bar plots represent mean ± SD. Data from three biological replicates.

Figure 79 – Density plot showing the effect of IL-10 costimulation on LPS-induced H3K27ac. Dotted line indicates lack of effect of the costimulation; red or grey shaded areas indicate values used to define IL-10-sensitive or resistant enhancers, respectively.

Figure 80 – Expression of IL-10-sensitive or resistant genes as percent ratio of BMDMs treated with IL-10 to untreated controls. Data from three biological replicates. Pearson correlation > 0.97 for all replicates.

Figure 81 – H3K27ac ChIP-Seq mean signal intensity within IL-10-sensitive (red) or resistant enhancers (grey) in the indicated conditions. Data from three biological replicates. Pearson correlation > 0.94 for all replicates. Numbers indicate p-values (Mann-Whitney U test) for the indicated comparisons.

Figure 82 - ATAC-Seq (left) and PU.1 ChIP-Seq (right) signal intensities within pre-existing and *de novo* OCRs in IL-10 sensitive (red) or resistant (grey) LPS-inducible enhancers. Numbers indicate p-values (Mann-Whitney U test) for the indicated comparisons.

Figure 83

IL-10-sensitive enhancers

PGE$_2$-sensitive enhancers

458   635   213

Figure 84

IL-10-sensitive enhancers

Pre-ex.	GAAASTGAAAST	IRF	p-val 1e-6 q-val 0.0001
	GCAASTGAAAST	IRF	p-val 1e-5 q-val 0.0003
de novo	GAAASTGAAAST	IRF	p-val 1e-14 q-val <0.0001
	GCAASTGAAAST	IRF	p-val 1e-11 q-val <0.0001
	GGAASTGAAAST	PU.1-IRF	p-val 1e-6 q-val <0.0001

IL-10-sensitive enhancers (pre-existing)

IL-10 only	GAAASTGAAAST	IRF	p-val 1e-4 q-val 0.016
	GAAASTGAAAST	IRF	p-val 1e-3 q-val 0.03
	GGAASTGAAAST	PU.1-IRF	p-val 1e-3 q-val 0.048
IL-10 and PGE$_2$	GAAASTGAAAST	IRF	p-val 1e-4 q-val 0.017
	ACAGGTGTAG	bHLH	p-val 1e-3 q-val 0.027
PGE$_2$ only	GCTATTTTTGGG	MEF2	p-val 1e-5 q-val 0.0019

Figure 85

STAT3 contributes to IL10-mediated suppression of inflammatory gene expression.
Figure 83 – Venn diagram showing the overlap between PGE$_2$-sensitive (blue) and IL-10-sensitive (red) enhancers.
Figure 84 – Motif enrichment analysis showing top-ranking motifs identified within pre-existing or *de novo* IL-10-sensitive enhancers (top) or within pre-existing sensitive enhancers targeted by IL-10 only, by both IL-10 and PGE$_2$, and by PGE$_2$ (bottom, see Methods). Putative cognate TF families and associated p-values and q-values are shown.
Figure 85 - RT-qPCR analysis of IL-10-sensitive and resistant genes in wt (black) or STAT3-deficient (orange) BMDMs stimulated as indicated. Dot plots represent mean ± SD. Data from two or three biological replicates. ** $p<0.01$, * $p<0.05$, ns not significant (unpaired *t*-test).

PGE$_2$ targets MEF2A-dependent gene expression by modulating ERK5 activity

We then aimed to dissect the molecular linking between PGE$_2$ and MEF2A and hypothesized that PGE$_2$ may alter transcriptional coregulators of MEF2A. We focused on class IIa HDACs, in particular on HDAC5 since induced after stimulation with PGE$_2$ (Figure 86) and known to interact with MEF TFs (Martin, Kettmann, and Dequiedt 2007). We found that CRISPR/Cas9-mediated disruption of *Hdac5* (Figure 87) did not result in restored induction of PGE$_2$-sensitive genes in costimulated BMDMs (Figure 88). We conclude that class II HDACs do not predominantly participate in suppression of LPS-inducible gene expression by PGE$_2$, although compensatory effects by other members cannot be excluded.

Next, we investigated the role of ERK5 in PGE$_2$-MEF2A axis, as described to interact with MEF2 (Pereira and Rodrigues 2020), to be modulated by cAMP-PKA pathway (Pearson, Earnest, and Cobb 2006) and to control the response of myeloid cells *in vivo* (Giurisato et al. 2018; Luiz et al. 2020). We found that LPS treatment induced a rapid and transient phosphorylation of ERK5, which was reduced in costimulated BMDMs (Figure 89). ERK5-deficient iMacs (Figure 89) stimulated with LPS showed reduced expression of a set of PGE$_2$-sensitive genes, including *Ifnb1*, *Il12b*, *Cxcl9*, but not of resistant transcripts (Figure 91), and defective production of IFN-β (Figure 92). These data indicate that PGE$_2$-mediated suppression of inflammatory gene expression is, at least in part, ascribable to modulation of LPS-induced activation of ERK5.

Figure 86

PGE₂ (h)

- 2 4

HDAC5

VCL

Figure 87

gRNA

ctrl   *Hdac5*

HDAC5

VCL
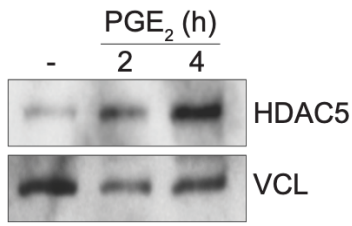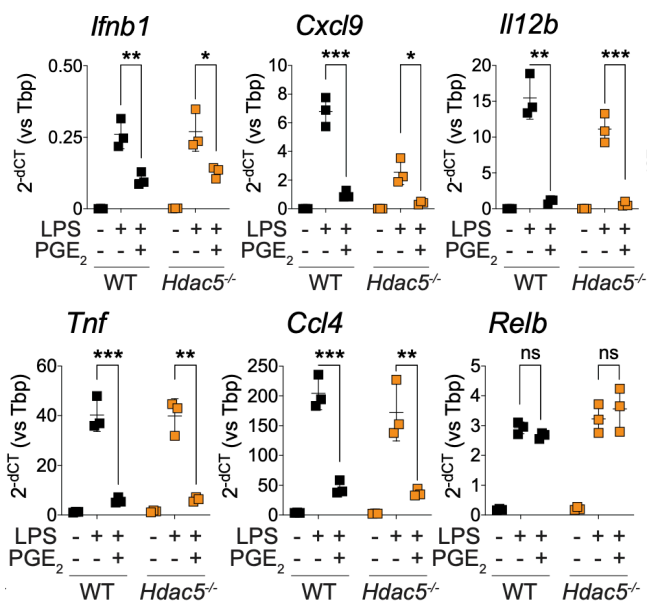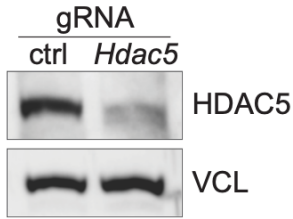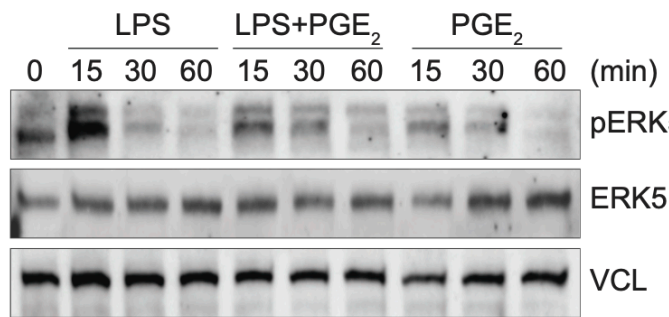
Figure 88
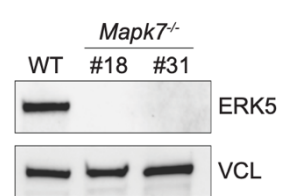
Figure 89

Figure 90

Figure 91
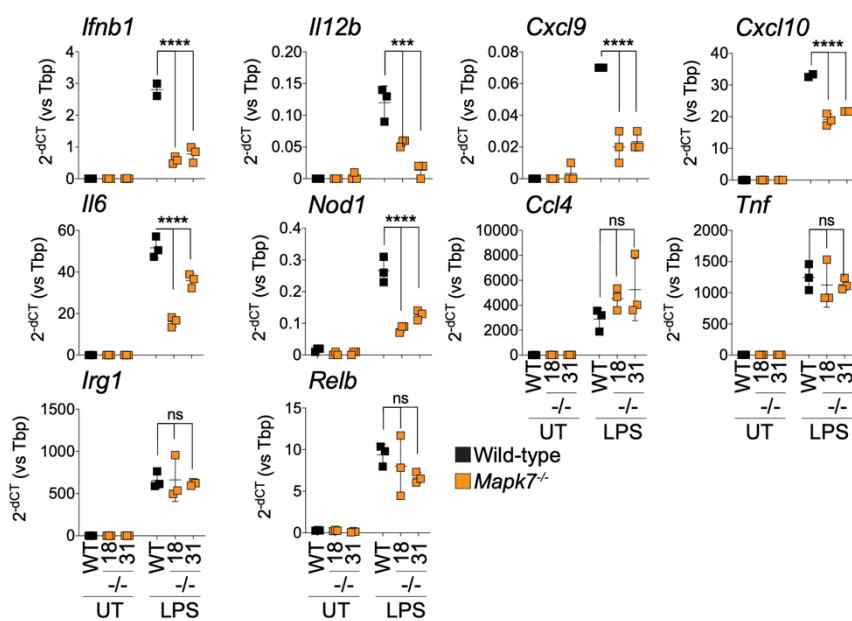
Figure 92
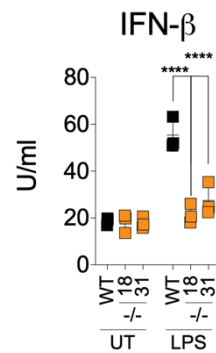
PGE₂ targets MEF2A-dependent gene expression by modulating ERK5 activity.
Figure 86 – Western blot analyses of HDAC5 and loading control (VCL) in BMDMs stimulated with PGE₂ for the indicated time points
Figure 87 – Western blot analyses of HDAC5 and loading control (VCL) in BMDMs upon CRISPR-Cas9-mediated targeting of *Hdac5*
Figure 88 – RT-qPCR analysis of PGE₂-sensitive and resistant genes in wt (black) or HDAC5-deficient (orange) BMDMs stimulated as indicated. Dot plots represent mean ± SD. Data from three biological replicates. *** $p<0.001$, ** $p<0.01$, * $p<0.05$, ns not significant (unpaired *t*-test).
Figure 89 – Western blot analyses for phosphorylated ERK5 (Thr218/Tyr220) as well as ERK5 and VCL as loading controls in BMDMs stimulated as indicated.
Figure 90 – Western blot analyses of ERK5 and loading control (VCL) in wt and *Mapk7*⁻/⁻ iMacs clones. Genotypes and IDs of the individual clones are shown.
Figure 91 – RT-qPCR analysis of PGE₂-sensitive and resistant genes in wt (black) or *Mapk7*⁻/⁻ (orange) iMacs clones stimulated as indicated. Genotypes and IDs of the individual clones are shown. Dot plots represent mean ± SD. Data from three biological replicates. **** $p<0.0001$, *** $p<0.001$, ns, not significant (unpaired *t*-test).
Figure 92 – IFN-β release by wt (black) and *Mapk7*⁻/⁻ (orange) iMacs stimulated as indicated. Dot plot represents mean ± SD. Data from three biological replicates. **** $p < 0.0001$ (two-way ANOVA test).

DISCUSSION

In this study, we uncovered principles of regulation of inflammatory gene expression by functionally antagonistic signals. Using stringent cut-offs to define modulated genes, our data indicated that immunomodulatory signals counteracted the expression of a substantial fraction of inflammatory genes (namely genes induced by LPS). The impact of LPS on gene expression program induced by immunomodulatory signals has not been characterized in this study and will be investigated in more detail in the future. Co-stimulated macrophages acquired a specific transcriptional profile, distinct from the one elicited by the single stimulations. These data reinforce the notion of the ability of these cells to integrate antagonistic stimuli and translate them into specific gene expression. However, the transcriptional profile of co-stimulated cells seemed to be more similar to the one induced by LPS, suggesting an overall dominance of the LPS-inducible program over the PGE_2-inducible one. Together with those of others (Muñoz-Rojas et al. 2021), our data provide support to the model of context-dependent activation and may exemplify the diversity of macrophages *in vivo*, whereby co-existence of opposing signals frequently occurs.

Transcriptional profiling of costimulated macrophages revealed that PGE_2, IL-10 and IL-4 supressed distinct sets of LPS-inducible transcripts, indicating stimulus-dependent modulation of inflammatory gene expression. Distinct signals displayed a selective impact on inducible gene expression likely through different mechanism(s). This concept is exemplified by the selective targeting of IFN-β and IFN I-dependent gene expression by PGE_2 and IL-10, but not by IL-4. Interestingly, PGE_2 and IL-10 did not suppress IFN-dependent gene expression when co-administered with IFN I. These data indicate that PGE_2 and IL-10 primarily hamper the induction of *Ifnb1* and that deficient IFN-dependent gene expression in co-stimulated cells results from impaired production of IFN-β and activation of the downstream response.

The suppressive effect of PGE$_2$ also occurred upon *ex vivo* and *in vivo* stimulation with LPS in distinct populations of myeloid cells and partly relies on enhanced production of IL-10 by costimulated cells. Increased production of PGE$_2$ and IL-10 upon stimulation with LPS, coupled with boosted production of IL-10 by co-stimulated macrophages, generate a negative feedback loop aimed at restraining excessive inflammatory response. In line with this, hyper-production of IL-10 was partly responsible for the suppressive effect of PGE$_2$ on inflammatory gene expression, and this effect was particularly evident for *Il12b* and *Il6*.

Genes dependent on TRIF-IRF3 pathway were over-represented in the set of sensitive transcripts, indicating a preferential targeting of the latter pathway by immunomodulatory signals. Activation of TRIF-IRF3 module requires endosomal internalization of TLR4 and therefore occurs with a delayed kinetics compared to MYD88 (Kagan et al. 2008), whose dependent genes were less represented among sensitive transcripts. Because of this differences, immunomodulatory signals may take advantage of this temporal delay and hamper chromatin remodelling events required for transcriptional induction. Analysis of genomic features of genes sensitive to PGE$_2$ further supported the importance of chromatin conformation for antagonism. Sensitive genes displayed low basal expression, poorly accessible promoters and enhancers and low PU.1 occupancy. In contrast, resistant genes were expressed at relatively high levels already in unstimulated macrophages and displayed more accessible chromatin status. Therefore, the degree of chromatin permissivity underlies differential sensitivity to modulation and defines basal chromatin organization as key determinant of vulnerability to antagonism. Because of poorly permissive chromatin configuration, sensitive genes require chromatin remodelling for their induction, while resistant genes were relatively unaffected by antagonism because basally accessible. Such features may ensure tight regulation of inflammatory gene expression and therefore may determine vulnerability to antagonistic signals.

Treatment with IFN-γ or IL-4 causes a loss of basal chromatin accessibility at regulatory regions of the antagonistic program (Czimmerer et al. 2018; Kyuho Kang et al. 2017). Analogously, PGE$_2$ elicited a loss of basal chromatin accessibility selectively at sensitive enhancers, which resulted in reduced basal transcription. In this context, PGE$_2$ may modulate the activity or alter the interaction networks of TFs and promote the recruitment of repressor complexes that contribute to reduce chromatin permissivity. As

a consequence, such functional inactivation of inflammatory gene enhancers resulted in impaired chromatin remodelling and induction upon stimulation with LPS.

The lack of interference at the signalling pathway level, also observed in other co-stimulation settings (Piccolo et al. 2017), is compatible with the selective suppressive effect of PGE$_2$ at a set of inflammatory gene enhancers, and points out chromatin as the main integration platform for antagonistic signals in macrophages. In this context, PGE$_2$ targeted inflammatory enhancers bound by MEF2 TFs. We identified MEF2A as a non-redundant regulator of inflammatory enhancers and, more specifically, of PGE$_2$-sensitive enhancers. Even though increased upon exposure to LPS, DNA occupancy by MEF2A occurred already at basal level and was higher at sensitive enhancers compared to resistant ones. MEF2A bound to thousands of genomic regions in unstimulated macrophages and a considerable number of them overlapped with those bound by macrophage LDTFs. These data may support the idea of MEF2A to cooperate with LDTFs in the establishment and maintenance of the basal landscape of *cis*-regulatory elements in macrophages. In this study, we particularly focused on the role of MEF2A at a specific set of gene enhancers, but several studies support MEF TFs as key driver of acquisition of cell identity and their activity highly dependent on the interactions with other TFs and co-factors. Structural analysis revealed that p300 directly binds the MADS-box/MEF2 domains of MEF2 proteins, resulting in transcriptional activation (He et al. 2011; Sartorelli et al. 1997). The same domains also mediate the association of MEF2 TFs to class II HDACs (Lu et al. 2000; Miska et al. 1999), indicating the dynamic role of MEF2 in positive and negative regulation of gene transcription. Therefore, the activity of MEF2 may be controlled not only by the chromatin context (i.e., cooperation with LDTFs and cell type-restricted TFs), but also by dynamic and context-dependent modulation of interaction partners.

In our context, loss of MEF2A overlapped with PGE$_2$ treatment, indicating the functional relevance of MEF2A-PGE$_2$ axis in macrophages. Deficiency of MEF2A resulted in chromatin compaction at sensitive inflammatory enhancers, impaired activation, and defective induction of IFN-β and IFN-dependent gene expression upon innate immune signals and viral or bacterial pathogens. The suppressive activity of PGE$_2$ on IFN I response was partly dependent on the interference with LPS-induced activation of ERK5 (Pereira and Rodrigues 2020), a known interactor of MEF2 and whose deletion

caused reduced production of IFN-β. However, the activity of PGE$_2$ was not entirely dependent on MEF2A since the induction of a group of sensitive genes still occurred upon MEF2A depletion, indicating the existence of MEF2A-independent mechanisms. The dissection of the complex immunomodulatory mechanisms of PGE$_2$ is incredibly relevant to modulate macrophage phenotype in disease contexts and will be further investigated in the future.

Immunomodulatory activities of PGE$_2$ on inflammatory gene expression overlapped with those of cAMP. Distinct cAMP-eliciting stimuli, including PGE$_2$ itself, as well as chemical activation of the pathway counteracted the production of IFN-β. IFN I response has been shown to promote anti-tumor immunity and contributes to tumor rejection (Demaria et al. 2019). De-regulated IFN I response also contributes to several chronic inflammatory manifestations and autoimmune diseases (Ivashkiv and Donlin 2014), pointing out the critical role of INF I in the inflammatory process. Multiple environmental cues activate cAMP as second messenger to modulate immune responses in homeostatic conditions and its aberrant regulation has been involved in several pathological conditions, such as in cancer (Bohn et al. 2018; Colegio et al. 2014). The role of PGE$_2$ in cancer progression can be ascribed to its dual effect. On one hand, PGE$_2$ promotes the establishment of a detrimental form of inflammation that fuel immune evasion by tumor cells, while, on the other hand, acts on immune cells to suppresse anti-tumor immunity. Because of the relevance of cAMP and MEF2A in the control of IFN I, it is tempting to speculate that multiple cAMP-eliciting signals may share a common mechanism of modulation in macrophages, namely by negatively targeting MEF2A. Therefore, the identification of PGE$_2$-MEF2A axis raises the possibility to modulate this pathway in different pathological contexts. To this aim, in the next future we are planning to identify and validate possible interactors of MEF2A whose activity may be modulated by PGE$_2$. Such studies will end up with potential candidates whose targeting may be relevant to modulate the activation state of macrophages. We are also generating LysM-Cre Mef2a$^{flox/flox}$ mice to study the role of MEF2A *in vivo* in the myeloid compartment during tissue homeostasis, as well as in pathological conditions, as in a mouse model of pancreatic cancer recently employed in the laboratory.

MATERIALS AND METHODS

The following information has been published in Cilenti, Barbiera et al., Immunity, 2021

Animal models used in this study

Animal experiments were performed in accordance with the Italian Laws (D.L.vo 116/92), which enforce the EU 86/609 Directive (approved by the Italian Ministry of Health, #449/2018-PR). C57BL/6 mice were purchased from Charles River Italy. Rosa26-Cas9 genetically targeted mice (MGI, J:213550) were obtained from Luigi Naldini. Bone marrow cells from STAT3-deficient (*Stat3$^{fl/fl}$ Mx1-Cre*) or STAT3-proficient (*Stat3$^{fl/fl}$*) mice were provided by Valeria Poli (University of Turin).

Differentiation and culture of murine cells

Bone marrow cells were collected from femurs and tibias in 50 mL PBS, filtered through a 70 μm cell strainer and centrifuged 450 x g for 5 minutes. Red blood cells were lysed using 0.2% NaCl solution, followed by 1.6% NaCl solution. Cells were filtered through a 70 μm cell strainer and centrifuged 450 x g for 5 minutes. For BMDM differentiation, 5 x 10^4 – 5 x 10^6 bone marrow cells were plated and cultured in IMDM supplemented with 10% FBS, 20% L929-conditioned medium containing M-CSF, antibiotics (penicillin G 100 U/ml and streptomycin sulfate 100 U/ml), 2 mM L-glutamine and 5 μM 2-mercaptoethanol. After six days of culture, adherent cells were >99% Cd11b$^+$ F4/80$^+$, as assessed by flow cytometry, and were stimulated as described below. For BMDC differentiation, 1.5 x 10^6 bone marrow cells were plated and cultured in IMDM supplemented with 10% FBS, 5 μM 2-mercaptoethanol, antibiotics (penicillin G 100 U/ml and streptomycin sulfate 100 U/ml), 2 mM L-glutamine and 15% of FLT3 ligand-containing supernatant, produced from an SP2/0 transfected cell line that secretes murine recombinant FLT3 ligand. To achieve BMDC differentiation, medium was replaced every three days. At day 7 of culture cells were harvested, plated at 2 x 10^5 cells/100 μl in 96-well U-bottom plates as previously described (Caronni et al. 2018).

Conditionally immortalized Hoxb8-FL cells (Redecke et al. 2013) were cultured in RPMI-1640 supplemented with 10% FBS, 5% of FLT3 ligand-containing supernatant,

antibiotics (penicillin G 100 U/ml and streptomycin sulfate 100 U/ml), 2 mM L-glutamine, 5 μM 2-mercaptoethanol and 1 μM b-estradiol. For iMac differentiation, Hoxb8-FL cells were washed twice with PBS and plated in IMDM supplemented with 10% FBS, 20% L929-conditioned medium containing M-CSF, antibiotics (penicillin G 100 U/ml and streptomycin sulfate 100 U/ml), 2 mM L-glutamine and 5 μM 2-mercaptoethanol. At day 5 of culture, fresh L929-conditioned medium was added. After 7 days of culture, adherent cells were >99% Cd11b^{+} F4/80[+], as assessed by flow cytometry, and were stimulated as indicated below.

Peritoneal macrophages were obtained by flushing the peritoneal cavity with 5 mL of cold PBS supplemented with 2% of Fetal Bovine Serum (FBS) and centrifuged 400 x g for 5 minutes. Cells were cultured in Iscove's Modified Dulbecco's Medium (IMDM) supplemented with 10% FBS, 20% L929-conditioned medium containing M-CSF, antibiotics (penicillin G 100 U/ml and streptomycin sulfate 100 U/ml), 2 mM L-glutamine and 5 μM 2-mercaptoethanol. After 24 hours, cells were washed twice with PBS to remove non-adherent cells and macrophages stimulated as described below.

Generation and culture of gene-edited cells

Single guide RNAs (sgRNAs) were designed using CHOPCHOP (Labun et al. 2019), and generated by *in vitro* transcription using GeneArt Precision gRNA Synthesis kit following manufacturer's instructions. Ribonucleoprotein (RNP) complexes of Cas9-sgRNAs were obtained by incubating 30 μg or 5 μg of Cas9 (produced in-house or commercial, respectively) with 12 μg or 6 μg sgRNA for 15 minutes at room temperature. Hoxb8-FL cells (2.5 x 10^{5}) or BMDMs (5 x 10^{5}, day 4 of differentiation) were resuspended in P3 solution of P3 Primary Cell 4D-Nucleofector kit, mixed with RNP complex and electroporated using ED-113 program of the 4D-Nucleofector System (Lonza). BMDMs were washed 24 hours after nucleofection and stimulated after additional 24 hours. Hoxb8-FL cells were FAC-sorted as single clones in 96-well U-bottom plates (FACSAria II, BD Biosciences) 5 days after nucleofection and expanded in culture.

Gene-editing efficiency and clone screening were assessed via Non-Homologous End Joining (NHEJ) at targeted sites. Briefly, genomic DNA was purified using QIAamp DNA Micro kit and targeted regions were amplified by PCR. PCR products were purified with AMPure XP beads, quantified by NanoDrop 8000 and mixed 1:1 with PCR product

from wild type cells. Annealed PCR products (500 ng) were digested with T7 Endonuclease for 30 minutes at 37°C and subjected to capillary electrophoresis using D1000 TapeStation kit (Agilent 4200 TapeStation). NHEJ efficiency was defined by calculating the percentage of cleavage of the PCR product. Gene-edited Hoxb8-FL clones were validated by Sanger Sequencing using TOPO-TA Cloning Kit following manufacturer's instructions. Protein disruption was validated by Western Blot analyses either in BMDMs or in Hoxb8 clones upon differentiation in iMacs.

Differentiation of human monocyte derived macrophages (hMDMs)

Human peripheral blood leukocyte concentrates from healthy donors were obtained in accordance with the Declaration of Helsinki and with Ospedale San Raffaele ethics committee approval (TIGET09 protocol). Peripheral blood mononuclear cells (PBMCs) were isolated by density centrifugation over Lymphoprep gradient. CD14$^+$ cells were obtained from PBMC by positive selection with CD14 MicroBeads according to the manufacturer's instructions. 3 x 10^6 CD14$^+$ cells were plated in 6-well plate in Dulbecco's Modified Eagle medium (DMEM) supplemented with 10% FBS, 5% human type AB serum male, antibiotics (penicillin G 100 U/ml and streptomycin sulfate 100 U/ml) and 2mM L-glutamine. At day 7 of culture, macrophage differentiation was assessed by morphological analyses.

***Ex vivo* stimulation of mouse and human cells**

Cells were stimulated with reagents at the following concentrations: LPS (10 ng/ml for mouse and human macrophages; 1 µg/ml for BMDCs and for IFN-β quantification in BMDMs or iMacs), PGE$_2$ (1µM), IL-10 (10 ng/ml), IL-4 (10 ng/ml), IFN-α (10 U/ml), IFN-β (100U/ml), DMXAA (10 µg/ml), poly(I:C) (10 µg/ml), CpG (100 nM), PFI-1 (10 µM, 2-hour pre-treatment), SGC-CBP30 (10 µM, 2-hour pre-treatment), forskolin (50 µM, 2-hour pre-treatment), 6-Bnz-cAMP (250 µM, 2-hour pre-treatment), db-cAMP (50 µM, 2-hour pre-treatment), salmeterol xinafoate (2.5 µM), BAY60-6583 (10 µM), anti-IL10-R antibody or isotype control (10μg/ml, 40-minute pre-treatment).

***In vivo* stimulation of peritoneal macrophages or bronchoalveolar lavage fluid (BALF) cells**

C57BL/6 mice were intraperitoneally injected with PGE$_2$ (2 μg per mouse) or an equal volume of PBS. After 1 hour, mice were intraperitoneally injected with LPS (10 μg per mouse) given alone or in combination with PGE$_2$ (2 μg per mouse). Mice were sacrificed 2 hours post injection and peritoneal lavage was collected as described above. Peritoneal macrophages (CD11b+ F4/80+) were FAC-sorted in RLT buffer (Qiagen) on a FACSAria II instrument (BD Biosciences). Total RNA was extracted as described below. For the stimulation of BALF cells, C57BL/6 mice were anesthetized and intranasally administered PGE$_2$ (2 μg per mouse) or an equal volume of PBS. After 1 hour, mice were intranasally administered LPS (10 μg per mouse) alone or in combination with PGE$_2$ (2 μg per mouse). Mice were sacrificed 2 hours post treatment and BALF cells collected in 3 mL of cold PBS. To assess the percentage of alveolar macrophages, cells were stained with Cd11c (1:100) and SiglecF (1:100). Total RNA was extracted as described below.

Flow cytometry

To assess macrophages differentiation, cells were washed with cold PBS and incubated for 30 minutes at 4°C with conjugated antibodies at the indicated concentrations: F4/80 (1:100), Cd11b (1:100), Cd11c (1:100), Ly6c (1:100). To assess cell apoptosis and viability, cells were washed with cold PBS and resuspended in AnnexinV binding buffer (PE AnnexinV Apoptosis Detection kit). Cells were stained following manufacturer's instructions. Cells were washed, resuspended in PBS-BSA 1% and analyzed on a FACSCanto II (BD Bioscience). Data were analyzed with FlowJo Software 10.6.0.

Production of lentiviral vectors and transduction of BMDMs

Single gRNAs targeting *Hdac5* gene were designed using tools available from the Genetic Perturbation Platform (Broad Institute) and cloned into lentiGuide-Puro plasmid. Lentiviral vectors (LV) were obtained transfecting 293T cells with a solution containing a mix of the selected LV genome transfer plasmid, the packaging plasmids pMDLg/pRRE and pCMV.REV, pMD2.G and pAdvantage, as previously described (Milani et al. 2019). Medium was changed 14 to 16 hours after transfection and supernatant collected 30 hours after medium change. Vector-containing supernatants were sterilized through a 0.22-μm filter, transferred into sterile polyallomer tubes and centrifuged at 20,000 x g for 120 min at 20°C (Beckman Optima XL-100 K Ultracentrifuge). LV pellet was dissolved in the

appropriate volume of PBS to allow 500× to 1000× concentrations. 2.5 x 10^5/well Cas9-expressing BMDMs were transduced twice at day 5 and 6 of differentiation with a multiplicity of infection (MOI) of 10 in L929-conditioned medium supplemented with polybrene (8 μg/ml). After the second hit, transduced cells were selected with puromycin (5 μg/ml) for 48 hours and then stimulated as indicated.

Immunofluorescence

BMDMs or iMacs were seeded in a 6-well plate at a density of 3.5 x 10^5 cells/well and differentiated for 5 days as described above. Cells were then detached with trypsin and plated on coverslips within a 6-well plate at a density of 10^6 cells/well. After 24 hours, cells were stimulated as indicated, washed with PBS and fixed in 1% paraformaldehyde (PFA) in PBS at room temperature for 10 minutes. Fixed cells were then permeabilized with cold methanol 100% for 10 minutes at −20°C, washed three times with 0.3% Triton X-100 in PBS, and blocked for 1 h with 5% BSA in 0.3% Triton-X100/PBS. Then, cells were stained with anti-NFκB (1:100) or anti-phospho TBK1 (1:50) overnight at 4°C. Cells were incubated with Alexa Fluor 488 Goat anti-Rabbit antibody (1:2,000), counterstained with DAPI (1:10,000) for 10 minutes at room temperature and mounted with Aqua/Poly mount on slides. Images were taken on a Nikon Eclipse E600 microscope (1024 × 1024, 40hex) and analyzed with Fiji ImageJ software (v 2.0.0-rc-69).

TLR4 internalization assay

2 x 10^5 BMDMs or iMacs were subjected to the indicated treatments and then washed with cold PBS. Cells were stained with anti-TLR4 antibody (1:200) as previously described (Zanoni et al. 2011) and LYVEDEAD Fixable Yellow (1:1,000) for dead-cell exclusion for 20 minutes on ice and then washed with cold PBS. Cells were resuspended in PBS and analyzed on FACSCanto II (BD Bioscience). Data were analyzed with FlowJo Software 10.6.0.

Western Blot analyses

5 x 10^6 BMDMs or iMacs were subjected to the indicated treatments and lysed with a buffer containing 10 mM Tris-HCl pH 8, 1 mM EDTA pH 8, 140 mM NaCl, 1% Triton X-100, 0.1% SDS, 0.1% deoxycholate and protease/phosphatase inhibitors. Lysates were

electrophoresed and immunoblotted with the following antibodies: anti-β-ACTIN (1:2,000), anti-VINCULIN (1:1,000), anti-IκBa (1:1,000), anti-p38 MAPK (1:1,000), anti-phospho p38 MAPK (Thr180/Tyr 182, 1:1,000), anti-SAPK/JNK (1:1,000), anti-phospho SAPK/JNK (Thr183/Tyr185, 1:1,000), anti-IRF1 (1:1,000), anti-phospho STAT1 (Tyr 701, 1:1,000), anti-phospho STAT2 (Tyr689, 1:100), anti-MEF2A (1:1,000), anti-CREB (1:1,000), anti-phospho CREB (Ser133, 1:500), anti-HDAC5 (1:500), anti ERK5 (1:1,000), anti-phospho ERK5 (Thr218/Tyr220, 1:500).

To analyze nuclear translocation of IRF3, 10^7 BMDMs were lysed with a buffer containing 50 mM Hepes, 1 mM EDTA pH 8, 140 mM NaCl, 0.25% Triton X-100, 0.5% NP-40, 10% glycerol and protease/phosphatase inhibitors. Lysates were incubated 10 minutes in ice and centrifuged 450 x g for 5 minutes. Supernatant was collected as cytosolic fraction and nuclei were washed with a buffer containing 10 mM Tris-HCl pH 8, 1 mM EDTA pH 8, 200 mM NaCl, 0.5 mM EGTA and protease/phosphatase inhibitors, incubated 10 minutes at room temperature on rotation and centrifuged 450 x g for 5 minutes. Nuclei were lysed with a buffer containing 10 mM Tris-HCl pH 8, 1 mM EDTA pH 8, 140 mM NaCl, 1% Triton X-100, 0.1% SDS, 0.1% deoxycholate and protease/phosphatase inhibitors. Lysates were electrophoresed and immunoblotted with the following antibodies: anti-IRF3 (1:1,000), anti-LAMINB1 (1:500).

Real-Time Quantitative PCR

If not differently stated, total RNA was extracted using ReliaPrep RNA Cell Miniprep System and quantified using NanoDrop 8000. Single-stranded cDNA was synthesized using ImProm-II Reverse Transcription System starting from 500 ng total RNA. For *in vivo* stimulated peritoneal macrophages, total RNA was extracted by RNeasy plus micro kit, following manufacturer's instructions. Single-stranded cDNA was synthesized using SuperScript IV Vilo Master Mix. Amplification of target genes was performed using Fast SYBR Green Master Mix on a ViiA 7 Real-Time PCR System.

Quantification of IFN-β

Cells were stimulated as indicated for 24 hours and supernatant was collected and centrifuged to remove cellular debris. L929 cells transfected with an interferon-sensitive luciferase construct (ISRE-Luc) (Jiang et al., 2005) were plated at 4 x 10^4 cells/well in

96-well plate and after 8 hours were incubated over-night with conditioned supernatant and luminescence was measured using Bright-Glo Luciferase Assay System. Recombinant IFN-β was used for standard curve calibration.

Quantification of PGE$_2$, IL-10, cyclic AMP

For the quantification of PGE$_2$ or IL-10 release, cells were stimulated for the indicated time and supernatant was collected and centrifuged to remove cellular debris. IL-10 (Mouse IL-10 DuoSet ELISA kit) or PGE$_2$ (Prostaglandin E$_2$ Express ELISA Kit) were measured following manufacturer's instructions. For the quantification of intracellular cyclic AMP, cells were stimulated as indicated and lysed in 0.1 M HCl. cAMP was quantified using Direct cAMP ELISA kit following manufacturer's instructions. Absorbance was measured on a Multiskan GO Microplate Spectrophotometer.

Bacterial infections and CFU assay

3×10^5 macrophages/well were infected in L929-conditioned medium without antibiotics at MOI 1 with *M. tuberculosis* H37Rv NCTC7416 or *M. bovis* BCG (OncoTICE MSD). Bacterial stocks were pre-quantified for colony forming unit (CFU) values and maintained at $-80°C$ in Middlebrook 7H9, 10% OADC, 0.05% Tween80 supplemented with 20% glycerol. Upon thawing, bacterial stocks were centrifuged 17,000x g for 5 minutes, washed with PBS, resuspended in L929-conditioned medium without antibiotics, de-clumped by 10 passages through a 21-gauge needle and diluted in L929-conditioned medium immediately before the infection. Four hours or one day after infection, macrophages were lysed for RNA analyses or supernatant collected for IFN-β quantification, respectively.

VSV infection

5×10^5 iMacs were infected with Vesicular Stomatitis Virus (VSV) at MOI of 20 or 2 in DMEM without serum for 1 hour at 37°C and then were supplemented with L929-conditioned medium. Three hours or one day after infection, macrophages were lysed for RNA analyses or supernatant collected for IFN-β quantification, respectively.

Generation and processing of bulk RNA-Seq data

RNA-Seq data generation. Total RNA was purified using the ReliaPrep RNA Cell Miniprep System and RNA-Seq libraries were generated using the Smart-seq2 method (Picelli et al. 2014). Five ng of RNA were retrotranscribed, cDNA was PCR-amplified (15 cycles) and purified with AMPure XP beads. After purification, the concentration was determined using Qubit 3.0 and size distribution was assessed using Agilent 4200 TapeStation system. Then, the tagmentation reaction was performed starting from 0.5 ng of cDNA for 30 minutes at 55°C and the enrichment PCR was carried out using 12 cycles. Libraries were then purified with AMPure XP beads, quantified using Qubit 3.0, assessed for fragment size distribution on an Agilent 4200 TapeStation system. Sequencing was performed on an Illumina NextSeq500 or NovaSeq6000 (single-end, 75bp read length) following manufacturer's instruction.

RNA-Seq data processing. Reads were aligned to the mm10 reference genome using STAR aligner (v 2.5.3) (Dobin et al. 2013); the `featureCounts` function from Rsubread package (v 1.24.2) (Liao, Smyth, and Shi 2019)was used to compute reads over RefSeq *Mus musculus* transcriptome (mm10) (Pruitt, Tatusova, and Maglott 2007), setting minMQS option to 255. Further analyses were performed in R environment (v 3.4.1) with edgeR R package (v. 3.20.7) (Robinson, McCarthy, and Smyth 2009). Read counts of expressed genes were normalized with the Trimmed Mean of M-values (TMM) method (Robinson and Oshlack 2010) using `calcNormFactors` function. Dispersion was estimated with the `estimateDisp` function. Differential expression across different conditions was evaluated fitting a negative binomial generalized linear model on the dataset with `glmQLFit` function and then performing a quasi-likelihood (QL) F-test with `glmQLFTest` function. Sample replicates were included in the design as covariates. Reads per kilo base per million (RPKM) values were computed for each gene with `rpkm` function. For published RNA-Seq datasets, fastq files were downloaded from GEO repository using fastq-dump from SRA Toolkit (v. 2.8) and processed as described above.

RNA-Seq analyses of costimulated BMDMs

Definition of stimulus-inducible genes. After RNA-Seq data processing, as described above, genes with RPKM > 1 in at least two samples in the datasets were retained. We defined induced genes by comparing their expression in the LPS, IFN-α, PGE$_2$, IL-10 or IL-4 conditions setting $\log_2$FC(RPKM) $\geq$ 2 and FDR < 0.05 versus untreated (UT)

controls as cut-offs. After filtering out genes not reaching RPKM > 1.5 in at least two replicates within each comparison, we obtained 468 LPS-induced, 291 IFN-α-induced, 138 PGE$_2$-induced, 28 IL-10-induced and 118 IL-4-induced genes.

Definition of induced genes sensitive or resistant to costimulation. For the analysis of LPS-stimulated transcription, we filtered out genes induced by PGE$_2$, IL-10 or IL-4, leading to the definition of a final set of 421 LPS-inducible genes. These were classified as 'PGE$_2$-sensitive' if having log$_2$FC(RPKM) $\leq$ -2 and FDR < 0.05 in the LPS+PGE$_2$ versus LPS condition (n=70); using the same analytical strategy and cut-offs, we defined 'IL-10-sensitive' (n=72) and 'IL-4-sensitive' genes (n=42). Genes were classified as 'resistant' (n=72) if their expression was preserved in all costimulation conditions (LPS+PGE$_2$, LPS+IL-10, LPS+IL-4) as compared to LPS alone, setting a cut-off of -1 < log$_2$FC(RPKM$_{LPS+costim}$/RPKM$_{LPS}$) < 1. For the analysis of IFN-α-stimulated transcription, we focused on 283 genes that were induced by IFN-α but not by PGE$_2$ and IL-10. We classified 5 genes as PGE$_2$-sensitive and 0 as IL-10 sensitive [(log$_2$FC(RPKM$_{costim}$ /RPKM$_{IFN-a}$) $\leq$ -2 and FDR < 0.05] and 251 genes as resistant [-1 < log$_2$FC(RPKM$_{costim}$ /RPKM$_{IFN-a}$) < 1].

Nascent RNA-Seq analyses of lipid A-stimulated BMDMs

Definition of MYD88-, TRIF-, IRF3- or IFNAR-dependent genes. We downloaded and processed RNA-Seq datasets (GSE67357) from wt or gene-deficient BMDMs stimulated with lipid A for 120 minutes (WT0, WT0 Rep2, WT120, WT120 Rep2, MYD88-120, MYD88-120 Rep2, TRIF-120, TRIF-120 Rep2, IRF3-120, IRF3-120 Rep2, IFNAR-120, IFNAR-120 Rep2) (Tong et al. 2016). Genes with RPKM > 1 in at least two samples in the datasets were retained for further analyses. For each expressed gene and for each experimental condition we computed mean expression (RPKM) across replicates. For each of the previously defined set of 421 LPS-induced genes, we calculated the percentage of expression in *MyD88*$^{-/-}$, *Ticam1*$^{-/-}$, *Irf3*$^{-/-}$ or *Ifnar*$^{-/-}$ versus wt BMDMs stimulated with lipid A (RPKM$_{KO\_lipidA}$*100/RPKM$_{WT\_lipidA}$). We set the percentage of expression to 100 for those LPS-induced genes that were not expressed in this dataset (we assumed no difference between the considered conditions). Genes whose expression in genetically ablated versus wt BMDMs was below 30% were classified as MYD88-, TRIF-, IRF3- or IFNAR-dependent, respectively.

Gene set enrichment analysis (GSEA). For each genotype, expressed genes were ranked by decreasing order of $\log_2\mathrm{FC}(\mathrm{RPKM})$ in lipid A-stimulated genetically ablated versus wt BMDMs. GSEA (v. 4.0.3) (Subramanian et al. 2005) was performed on ranked gene lists using previously defined PGE_2-sensitive and resistant transcripts as Gene Sets, with number of permutations set to 10,000.

RNA-Seq analyses of BMDMs treated with exogenous IFN-β

Definition of IFNβ-restored genes. After RNA-Seq data processing, genes with RPKM > 1 in at least two samples in the datasets were retained. Previously defined PGE_2-sensitive genes were classified as 'restored' (n=33) if having $\log_2\mathrm{FC}(\mathrm{RPKM}) \geq 1$ in the LPS+PGE_2+IFN-β versus LPS+PGE_2 condition. Genes with $0{,}5 \leq \log_2\mathrm{FC}(\mathrm{RPKM}_{LPS+PGE2+IFNb}/\mathrm{RPKM}_{LPS+PGE2}) < 1$ were classified as 'partially restored' and genes with $\log_2\mathrm{FC}(\mathrm{RPKM}_{LPS+PGE2+IFNb}/\mathrm{RPKM}_{LPS+PGE2}) < 0{,}5$ were classified as 'not restored'. We calculated also a percentage of restoration in LPS+PGE_2+IFN-β versus LPS+PGE_2 treated BMDMs $[(\mathrm{RPKM}_{LPS+PGE2+IFNb} - \mathrm{RPKM}_{LPS+PGE2})/(\mathrm{RPKM}_{LPS} - \mathrm{RPKM}_{LPS+PGE2})]$ .We set the percentage of restoration to 0 for those LPS-induced genes that were not expressed in this dataset (we assumed no difference between the considered conditions).

RNA-Seq analyses of BMDMs treated with IL-10R blocking antibody

Definition of anti-IL-10R-restored genes. After RNA-Seq data processing, genes with RPKM > 1 in at least two samples in the datasets were retained. We calculated a percentage of restoration for each of the previously defined PGE_2-sensitive genes $[(\mathrm{RPKM}_{LPS+PGE2+aIL\text{-}10R} - \mathrm{RPKM}_{LPS+PGE2})/(\mathrm{RPKM}_{LPS} - \mathrm{RPKM}_{LPS+PGE2})]$. Genes were classified as 'restored' (n=9) if having percentage of restoration $\geq 0{,}8$ and 'partially restored' if having $0{,}2 \leq$ percentage of restoration $< 0{,}8$. Genes with percentage of restoration $< 0{,}2$ were classified as 'not restored'.

RNA-Seq analyses of LPS-stimulated BMDMs with BRD2-4 or CBP-p300 inhibitors

RNA-Seq data were generated and pre-processed as described above. Genes not passing the expression cut-off of RPKM > 1 in at least three samples in the datasets were filtered out. For each gene and for each experimental condition we computed mean expression

(RPKM) across replicates. For each of the previously defined set of 421 LPS-induced genes, we calculated the percentage of expression in BMDMs stimulated with LPS in the presence or absence of BRD2-4 or CBP-p300 inhibitors ($RPKM_{inhibitor\_LPS}*100/RPKM_{Ctrl\_LPS}$). We set the percentage of expression to 100 for those LPS-induced genes that were not expressed in this dataset. Genes whose expression was below 30% in LPS-stimulated BMDMs treated with inhibitors versus controls were classified as BRD2-4 or CBP-p300 dependent, respectively.

RNA-Seq analyses of wt or MEF2A-deficient iMacs

Definition of LPS-inducible genes in wt iMacs. RNA-Seq data were generated and pre-processed as described above. Genes not passing the expression cut-off of RPKM > 1 in at least one sample in the dataset were filtered out. Differential gene expression was performed considering MEF2A-deficient iMac clones (D7, A7, A8, C7) and MEF2A-proficient (referred to as wt) iMac clones (NE, B3 and D10) as sets of biological replicates. We defined LPS-inducible genes in wt iMacs by comparing their expression in the LPS versus UT conditions, setting $log_2FC(RPKM) \geq 2$ and FDR < 0.05 as cut-offs. After filtering out genes not reaching RPKM > 1.5 in two samples within each comparison, and genes that did not pass the cut-off for induction by LPS also in wt BMDMs, we defined a set of 312 LPS-inducible genes in iMacs.

Definition of MEF2A-dependent or MEF2A-independent genes in LPS-treated iMacs. We compared expression of LPS-inducible genes in MEF2A-deficient versus wt iMacs upon LPS-stimulation. Of the previously defined set of 312 LPS-inducible in iMacs, 94 were classified as MEF2A-dependent, setting $log_2FC(RPKM_{MEF2Ako\_LPS}/RPKM_{WT\_LPS}) \leq -2$ and FDR < 0.05 as cut-offs. As a control group of MEF2A-independent transcripts, we selected 118 genes whose expression in response to LPS was not affected in MEF2A-deficient as compared to wt iMacs, setting $-1 < log_2FC(RPKM_{MEF2Ako\_LPS}/RPKM_{WT\_LPS}) < 1$ as cut-offs.

Overlap between PGE$_2$-sensitive or resistant and MEF2A-dependent or MEF2A-independent genes. Of the previously defined sets of PGE$_2$-sensitive or resistant genes in BMDMs, only those that were induced by LPS in iMacs were retained (50/70 and 50/72 genes, respectively) for these analyses. We calculated the overlap between these sets of genes and those, previously defined, of MEF2A-dependent or MEF2A-independent genes

in iMacs, an hypergeometric tests was performed in order to assess significance of these overlaps. Out of 50 PGE_2-sensitive genes (induced by LPS in both BMDMs and iMacs), 22 (44%) were MEF2A-dependent and 14 (28%) were MEF2A-independent. Conversely, out of 50 resistant genes (induced by LPS in both BMDMs and iMacs) 1 (2%) was MEF2A-dependent and 34 (68%) were MEF2A-independent.

Gene set enrichment analysis. For each genotype, expressed genes were ranked by decreasing order of $log_2FC(RPKM_{MEF2Ako\_LPS}/RPKM_{WT\_LPS})$ in LPS-stimulated MEF2A-deficient versus wt iMacs. GSEA (v. 4.0.3) (Subramanian et al. 2005)was performed on ranked gene lists using PGE_2-sensitive (n=70) and resistant (n=72) transcripts as Gene Sets, with number of permutations set to 10,000.

Generation and analysis of single-cell RNA-Seq data

Data generation. BMDMs were stimulated for 4 hours as indicated above, and scRNA-Seq libraries were generated using a microfluidics-based approach on Chromium Single-Cell Controller (10X Genomics) using the Chromium Single Cell 3′ Reagent Kit v2 according to the manufacturers' instructions. Briefly, single cells were partitioned in Gel Beads in Emulsion (GEMs) and lysed, followed by RNA barcoding, reverse transcription and PCR amplification (12 cycles). The concentration of the scRNA-seq libraries was determined using Qubit 3.0 and size distribution was assessed using an Agilent 4200 TapeStation system. Libraries were sequenced on an Illumina NextSeq500 instrument (paired-end, 150bp read length).

Data processing. Fastq files were processed with Cell Ranger (v 2.0) (Zheng et al. 2017)using default parameters. Reads were aligned to reference genome mm10 and quantified using ENSEMBL genes (Hubbard et al. 2002) as gene model. Only confidently mapped reads, non-PCR duplicates, with valid barcodes and unique molecular identifiers (UMIs) were retained to compute a gene expression matrix containing the number of UMI for every cell and gene. Gene counts were imported in R environment (v. 3.5.2) and processed with Seurat (v 3.1.2) (https://satijalab.org/seurat/). Cells expressing less than 1000 unique genes were discarded. Genes with a mean expression (counts normalized with `NormalizeData` function) lower than 0.01 were excluded. Cells with a ratio of mitochondrial versus endogenous genes expression exceeding 0.1 were also excluded, resulting in 3,935 retained cells. Raw expression data were then scaled using

`SCTransform` function, regressing on percentage of mitochondrial gene expression and cell cycle scores. Cell cycle scores were calculated using `CellCycleScoring` function.

Graph-based clustering and differential gene expression analyses. Shared Nearest Neighbor (SNN) graph was constructed using the `FindNeighbors` function taking as input the first 30 principal components, computed with `RunPCA` function. Cell clusters were defined using a resolution r = 0.4, calculated with the `FindCluster` function and were visualized in 2 dimensions using uniform manifold approximation and projection (UMAP) (Becht et al. 2019). Cluster-specific genes were identified using `FindMarkers` function with option only.pos=TRUE, setting a cut-off of FDR < 0.05. Additional, separate graph-based clustering analyses were performed on filtered sub-datasets including cells from the UT, PGE$_2$, LPS and LPS+PGE$_2$ samples (3,102 cells, sub-dataset A) as well as the UT, PGE$_2$, IFN-α and IFN-α+PGE$_2$ samples (2,162 cells, sub-dataset B). For each cell within sub-dataset A we computed the mean expression of LPS-induced or PGE$_2$-induced genes, as well as PGE$_2$-sensitive or resistant genes previously defined by bulk RNA-Seq analyses. For each cell within sub-dataset B we computed the mean expression of IFN-α-induced or PGE$_2$-induced genes. Only genes expressed in the single cell dataset were considered.

Single-cell trajectories. The dataset (genes and cells filtered as described above) was then reanalyzed with Monocle3 (v. 0.1.3) (Trapnell et al. 2014) (https://cole-trapnell-lab.github.io/monocle3/). Data were normalized and principal component analysis was performed with `preprocess_cds` function with num_dim parameter set to 30. Dimensionality reduction was performed with `reduce_dimension` function using UMAP. Finally, trajectories were constructed using `cluster_cells` function and `learn_graph` function with `use_partition` parameter set to FALSE.

Generation and processing of ChIP-Seq data

ChIP-Seq data generation. Cells were stimulated for 4 hours (H3K27ac, IRF1, STAT1 ChIP-Seq) or 2 hours (PU.1, MEF2A, MEF2D, JUNB, NF-κB p65 ChIP-Seq). 6 x 10^6 (H3K27ac or PU.1 ChIP-Seq) or 10^8 (MEF2A, MEF2D, IRF1, STAT1, JUNB, NF-κB p65 ChIP-Seq) cells were fixed with 1% formaldehyde, and nuclear fractions isolated and lysed as described previously (Ostuni et al. 2013). Fragmented chromatin was obtained using Covaris E220 focused-ultrasonicator and nuclear extracts were incubated overnight

at 4°C with Dynabeads Protein G, previously coupled with 3 μg (for H3K27ac), 5 μg (for PU.1) or 15 μg (for MEF2A, MEF2D, IRF1, STAT1, JUNB, NF-κB p65) of antibody. Beads were recovered using a 96-well magnet, washed, and DNA de-crosslinked overnight at 65°C. DNA was purified with AMPure XP beads and quantified with Qubit 3.0. ChIP or input DNA (1 µl) were used for ChIP-qPCR experiments. ChIP DNA (5 ng) was used for library preparation with Illumina TruSeq ChIP Library Prep kit and sequenced on Illumina NextSeq500 or NovaSeq6000 (single-end, 75bp read length).

ChIP-Seq data processing, peak calling and normalization. Reads from fastq files were aligned to the mm10 reference genome using BWA aligner (v. 0.7.15) (Li and Durbin 2009). Bam files were processed using samtools (v.1.4) (Li et al. 2009) and BEDTools (v. 2.24.0) (Quinlan and Hall 2010) suites. Reads with a mapping quality lower than 15 or duplicated reads were discarded. For published ChIP-Seq datasets, fastq files were downloaded from GEO repository using fastq-dump from SRA Toolkit (v. 2.8) and processed as described above. All regions of interest were annotated using ChIPpeakAnno R package (v 3.16.1) (Zhu et al. 2010) and defined as proximal or distal if located within or beyond 5kb from an annotated TSS, respectively. Distal regions were further classified as intragenic or intergenic. Read counts were computed on all regions of interest using `multiBamCov` function from BEDTools. Further analyses were performed in R environment (v 3.4.1) with edgeR package (v. 3.20.7).

For H3K27ac ChIP-Seq, peak calling was performed using MACS2 (v. 2.2.1) (Y. Zhang et al. 2008) `callpeak` function with parameters -g mm -q 0.01 --broad --nomodel --extsize 147. Peaks with a q-value lower than 1e-3 were selected and resulting peaks with a distance lower than 1,000bp were merged using `mergeBed` function form BEDTools. Resulting peaks from all samples were then merged. Read counts were computed on resulting regions as described above and normalized with the TMM method using `calcNormFactors` function. Dispersion was estimated with the `estimateDisp` function. Differences in signal intensities across different conditions were evaluated fitting a negative binomial generalized linear model on the dataset with `glmQLFit` function and then performing a quasi-likelihood (QL) F-test with `glmQLFTest` function. Sample replicates were included in the design as covariates. CPM (counts per million) values were computed for each region with `cpm` function.

For PU.1, MEF2A, MEF2D, IRF1, STAT1, JUNB or NF-κB p65 ChIP-Seq, peak calling was performed using MACS2 (v. 2.2.1) (Y. Zhang et al. 2008) `callpeak` function with parameters -g mm. For each sample, peaks with a q-value lower than 1e-5 were selected. Read counts were computed on regions of interest as described above. For PU.1, MEF2A and MEF2D ChIP-Seq data, CPM values were estimated by normalizing counts on total reads mapping within merged peaks for each TF. For the other transcription factors, which are LPS-inducible and thus displayed limited binding in untreated samples, counts were normalized by total library size.

Generation and processing of ATAC-Seq data

ATAC-Seq data generation. ATAC-Seq was performed as described (Corces et al. 2016) with slight modifications. Briefly, 50,000 cells were collected and centrifuged at 450 x g for 5 minutes. Then, the transposition reaction was performed using digitonin 1%, Tn5 transposase and TD Buffer for 45 minutes at 37°C. Immediately following transposition, the reaction was stopped using a solution of 900 mM NaCl and 300 mM EDTA, 5% SDS and Proteinase K for 30 minutes at 40°C. Transposed DNA fragments were purified using AMPure XP beads, barcoded with Illumina Nextera dual indexes and PCR amplified with KAPA HiFi PCR Kit. Then, the concentration of the library was determined using Qubit 3.0 and size distribution was assessed using Agilent 4200 TapeStation system. Libraries were sequenced on Illumina NextSeq 500 or NovaSeq6000 instruments (single-end, read length 75 bp).

ATAC-Seq data processing, peak calling and normalization. Reads were aligned to the mm10 reference genome using BWA aligner (v. 0.7.15) (Li and Durbin 2009). Bam files were processed using samtools (v.1.4) (Y. Zhang et al. 2008) and BEDTools (v. 2.24.0) (Quinlan and Hall 2010) suites. Duplicated reads, reads with mapping quality below 15, unassigned reads or reads mapped on chromosomes Y and M were removed. Peak calling was performed using MACS2 (v. 2.2.1) (Y. Zhang et al. 2008) `callpeak` function with parameters -g mm --nomodel --shift -100 --extsize 200 and setting q-value lower than 1e-5 as cut-off. Obtained peaks were merged using `mergeBed` function and resulting regions were termed open chromatin regions (OCRs). All regions were annotated using ChIPpeakAnno R package (v 3.16.1) (Zhu et al. 2010) and defined as proximal or distal if located within or beyond 5kb from an annotated TSS, respectively. Read counts were

computed using `multiBamCov` function from BEDTools and normalized with the TMM method using `calcNormFactors` function. Dispersion was estimated with the `estimateDisp` function. Differences in signal intensities across different conditions were evaluated fitting a negative binomial generalized linear model on the dataset with `glmQLFit` function and then performing a quasi-likelihood (QL) F-test with `glmQLFTest` function. Sample replicates were included in the design as covariates. CPM (counts per million) values were computed for each region with `cpm` function. For published ATAC-Seq datasets, fastq files were downloaded from GEO repository using fastq-dump from SRA Toolkit (v. 2.8) and processed as described above.

Re-analysis of published ChIP-Seq and ATAC-Seq datasets

We downloaded ATAC-Seq datasets form untreated or LPS-treated (6h) BMDMs (GSE67357, WT_unstimulated_ATAC_rep1, WT_unstimulated_ATAC_rep2, WT_LPS_6h_ATAC_rep1, WT_LPS_6h_ATAC_rep2). We downloaded H3K4me3, H3K27ac and PU.1 ChIP-Seq datasets from untreated or LPS-treated (4h) BMDMs (GSE38377, H3K4me3_UT, H3K4me3_LPS_4h, H3K27ac_UT, H3K27ac_LPS_4h, PU.1_UT, PU.1_LPS_4h). Samples were processed as described above. Using `computeMatrix` function from deepTools (v. 2.4.0) suite, we computed mean read coverages (CPM) over intervals of 10bp within larger regions surrounding each TSS of PGE_2-sensitive, IL-4-sensitive, IL-10-sensitive or resistant genes (TSS +/- 1,000bp for ATAC-Seq data and PU.1 ChIP-Seq; TSS +/- 3,000bp for H3K4me3 ChIP-Seq; TSS +/- 5,000bp for H3K27ac ChIP-Seq).

Analysis of LPS-inducible enhancers in BMDMs

Definition of LPS-inducible enhancers, sensitive or resistant to costimulation. We obtained a set of 53,925 H2K27ac ChIP-Seq regions after merging peaks from all samples, as described above. We focused on distal H3K27ac regions (n=39,606), which we operationally defined as enhancers. LPS-inducible enhancers were defined by comparing H3K27ac levels (CPM) in the LPS versus UT condition, setting $log_2FC(CPM_{LPS}/CPM_{UT}) \geq 2$ and FDR < 0.05 as cut-offs. Only regions passing MACS2 q-value cutoff in at least three samples in the comparison were selected, leading to the identification of 2,850 LPS-inducible enhancers. We then classified these regions as

PGE$_2$-sensitive (n=848) if having log$_2$FC(CPM$_{\text{LPS+PGE2}}$/CPM$_{\text{LPS}}$) ≤ -2 and FDR < 0.05 in the LPS+PGE$_2$ versus LPS comparison. Analogously, we defined IL-10-sensitive enhancers (n=1,093) by comparing the LPS+IL-10 to the LPS condition. We then identified PGE$_2$-resistant (n=322) and IL-10-resistant (n=306) enhancers setting -0.5 < log$_2$FC(CPM$_{\text{LPS+co-stimulus}}$/CPM$_{\text{LPS}}$) < 0.5 as cut-off.

Definition of pre-existing or de novo OCRs within LPS-inducible enhancers. To define pre-existing OCRs within LPS-inducible enhancers, we first selected OCRs (n=76,203) merging ATAC-Seq peaks passing MACS2 q-value cutoff in all three replicates of UT BMDMs, and then retained those OCRs (n=1,265) mapping within previously defined LPS-inducible enhancers (based on H3K27ac ChIP-Seq). These enhancers were classified as pre-existing enhancers. To define *de novo* OCRs within LPS-inducible enhancers, we first selected OCRs merging ATAC-Seq peaks passing MACS2 q-value cutoff in all three replicates of LPS BMDMs; then, we discarded regions overlapping with previously defined pre-existing OCRs; finally, we retained those OCRs (n=1,476) mapping within previously defined LPS-inducible enhancers. These enhancers were classified as *de novo* enhancers. Read counts were computed on pre-existing or *de novo* OCRs and CPM estimated as described above. We assigned a summit to each *pre-existing* or *de novo* OCR. We retained OCRs in which peak summits from all three replicates (UT or LPS) mapped within 120bp and computed the mean position of summits. These analyses defined two sets of 177 and 221 pre-existing OCRs summits and two sets of 433 and 595 *de novo* OCRs summits within PGE$_2$-sensitive and IL-10-sensitive LPS-inducible enhancers, respectively; and 176 and 213 pre-existing OCRs summits and 182 and 119 *de novo* OCRs summits within PGE$_2$-resistant and IL-10-resistant LPS-inducible enhancers respectively.

PU.1 occupancy within LPS-inducible enhancers, sensitive or resistant to costimulation. We computed PU.1 read counts on pre-existing and *de novo* OCRs summits (+/- 100bp) within PGE$_2$-sensitive and IL-10-sensitive or PGE$_2$-resistant IL-10-resistant enhancers; as well as number of overlapping peaks for the untreated BMDMs.

TF binding in pre-existing or de novo OCRs within LPS-inducible enhancers. We used `computeMatrix` function from deepTools (v. 2.4.0) (Ramírez et al. 2014) suite to compute mean read coverages (CPM) within previously defined OCR summits +/- 1,000bp. Heatmap was produced with `plotHeatmap` function. For all transcription

factors, we also reported cpm computed over pre-existing and *de novo* OCRs summits (+/- 100bp) within PGE_2-sensitive or PGE_2-resistant enhancers.

Motif enrichment analysis within OCRs. We first defined genomic regions spanning 200bp from previously defined OCRs summits and performed analyses with HOMER (v. 4.10) (Sven Heinz et al. 2010), using the `findMotifsGenome.pl` script with parameters -size given -mask -h.

Analysis of LPS-inducible enhancers in wt or MEF2A-deficient iMacs

Definition of LPS-inducible enhancers in iMacs. Following the procedure described above for H3K27ac ChIP-Seq on BMDMs, we defined a set of 42,251 regions (29,596 distal) merging peaks from all samples. To estimate differences in signal intensities in these regions, MEF2A-deficient iMac clones (D7, A7, A8, C7) and MEF2A-proficient (referred to as wt) iMac clones (NE, B3 and D10) were considered as sets of biological replicates. LPS-inducible enhancers were defined in wt iMacs by comparing H3K27ac levels (CPM) in the LPS versus UT condition, setting $\log_2FC(CPM_{LPS}/CPM_{UT}) \geq 2$ and FDR < 0.05 as cut-offs. Only distal regions passing MACS2 q-value cutoffs in at least two samples in the comparison were selected, leading to the definition of 3,421 LPS-inducible enhancers in iMacs. We then classified these regions as MEF2A-dependent (n=981) if having $\log_2FC(CPM_{MEF2Ako\_LPS}/CPM_{WT\_LPS}) \leq -2$ and FDR < 0.05 in MEF2A-deficient vs wt LPS treated iMacs comparison. As a control group of MEF2A-independent enhancers, we selected 916 regions whose acetylation in response to LPS was not affected in MEF2A-deficient as compared to wt iMacs, setting $-0,5 < \log_2FC(CPM_{MEF2Ako\_LPS}/CPM_{WT\_LPS}) < 0,5$ as cut-offs.

Analogously, we defined MEF2A-dependent enhancers in untreated iMacs (n=998), setting $\log_2FC(CPM_{MEF2Ako\_UT}/CPM_{WT\_UT}) \leq -2$ and FDR < 0.05 and selecting distal regions passing MACS2 q-value cutoffs in at least two untreated samples (Basal enhancers). As a control group of MEF2A-independent enhancers, we selected 8545 regions passing MACS2 q-value cutoffs in at least two untreated samples and whose acetylation was not affected in MEF2A-deficient as compared to wt untreated iMacs, setting $-0,5 < \log_2FC(CPM_{MEF2Ako\_UT}/CPM_{WT\_UT}) < 0,5$ as cut-offs.

We then focused on PGE_2-sensitive (n=551) or PGE_2-resistant enhancers (n=190) that were LPS-inducible in both BMDMs and iMacs. Read counts were computed and CPM

values estimated as described above. We also computed CPM values for BMDMs on MEF2A-dependent (LPS) (n=669) and MEF2A-independent (LPS) (n=377) enhancers that were LPS-inducible in both BMDMs and iMacs.

Definition of pre-existing or de novo OCRs in iMacs. ATAC-Seq data were processed as described above. We defined pre-existing OCRs merging ATAC-Seq peaks passing MACS2 q-value cutoff in all replicates of UT wt iMacs. To define *de novo* OCRs we first merged ATAC-Seq peaks passing MACS2 q-value cutoff in all four replicates of LPS wt iMacs; then, we discarded regions overlapping with previously defined pre-existing OCRs. We then assigned a summit to each *pre-existing* or *de novo* OCR as described above for BMDMs. These analyses defined two sets of 279 and 3500 pre-existing OCRs summits within MEF2A-dependent (UT) and MEF2A-independent (UT) basal enhancers, respectively; and two sets of 404 and 628 *de novo* OCRs summits within MEF2A-dependent (LPS) and MEF2A-independent (LPS) LPS-inducible enhancers, respectively.

CPM were computed on pre-existing and *de novo* OCRs (previously defined in BMDMs) within PGE$_2$-sensitive or PGE$_2$-resistant enhancers that were LPS-inducible in both BMDMs and iMacs.

Motif enrichment analysis within OCRs. We first defined genomic regions spanning 200bp from previously defined OCRs summits and performed analyses with HOMER (v. 4.10) (Sven Heinz et al. 2010), using the `findMotifsGenome.pl` script with parameters -size given -mask -h. We compared motif enrichment within MEF2A-dependent versus MEF2A-independent enhancers. For MEF2A-independent basal enhancers we selected the top 1000 regions with lower absolute values of logFC($CPM_{MEF2Ako\_UT}/CPM_{WT\_UT}$) in order to have a comparable number of regions with basal MEF2A-dependent enhancers.

PU.1 signal intensity on pre-existing or de novo OCRs within LPS-inducible enhancers in iMacs. We computed PU.1 read counts from all samples on *pre-existing* and *de novo* OCRs summits (+/- 100bp) (defined in BMDMs) within PGE$_2$-sensitive or PGE$_2$-resistant enhancers that were LPS-inducible in both BMDMs and iMacs.

QUANTIFICATION AND STATISTICAL ANALYSIS

Results are illustrated as mean ± SD. Graphs show data from at least two independent repeats. Significance was defined as $p < 0.05$. Statistical analysis was conducted either

using GraphPad Prism v9.0 (GraphPad Software) or R v3.4.1 (R project). The specific statistical tests, exact value of n, what n represents are mentioned in the figure legends.

References

Alver, Burak H. et al. 2017. "The SWI/SNF Chromatin Remodelling Complex Is Required for Maintenance of Lineage Specific Enhancers." *Nature Communications* 8. 14648 (2017). https://doi.org/10.1038/ncomms14648

Andersson, Robin, and Albin Sandelin. 2020. "Determinants of Enhancer and Promoter Activities of Regulatory Elements." *Nature Reviews Genetics* 21(2): 71–87. http://dx.doi.org/10.1038/s41576-019-0173-8.

Andzelm, Milena M. et al. 2015. "MEF2D Drives Photoreceptor Development through a Genome-Wide Competition for Tissue-Specific Enhancers." *Neuron* 86(1): 247–63. http://dx.doi.org/10.1016/j.neuron.2015.02.038.

Azizi, Elham et al. 2018. "Single-Cell Map of Diverse Immune Phenotypes in the Breast Tumor Microenvironment." *Cell* 174(5): 1293-1308.e36. https://doi.org/10.1016/j.cell.2018.05.060.

Bannister, Andrew J., and Tony Kouzarides. 2011. "Regulation of Chromatin by Histone Modifications." *Cell Research* 21(3): 381–95.

Barrat, Franck J., Mary K. Crow, and Lionel B. Ivashkiv. 2019. "Interferon Target-Gene Expression and Epigenomic Signatures in Health and Disease." *Nature Immunology* 20(12): 1574–83. http://dx.doi.org/10.1038/s41590-019-0466-2.

Becht, Etienne et al. 2019. "Dimensionality Reduction for Visualizing Single-Cell Data Using UMAP." *Nature Biotechnology* 37(1): 38–47.

Bohn, Toszka et al. 2018. "Tumor Immunoevasion via Acidosis-Dependent Induction of Regulatory Tumor-Associated Macrophages." *Nature Immunology* 19(12): 1319–29. http://dx.doi.org/10.1038/s41590-018-0226-8.

Bonavita, Eduardo et al. 2020. "Antagonistic Inflammatory Phenotypes Dictate Tumor Fate and Response to Immune Checkpoint Blockade." *Immunity* 53(6): 1215-1229.e8. https://doi.org/10.1016/j.immuni.2020.10.020.

Bonham, Kevin S. et al. 2014. "A Promiscuous Lipid-Binding Protein Diversifies the Subcellular Sites of Toll-like Receptor Signal Transduction." *Cell* 156(4): 705–16. http://dx.doi.org/10.1016/j.cell.2014.01.019.

Bonnardel, Johnny et al. 2019. "Stellate Cells, Hepatocytes, and Endothelial Cells Imprint the Kupffer Cell Identity on Monocytes Colonizing the Liver Macrophage Niche." *Immunity* 51(4): 638-654.e9. https://doi.org/10.1016/j.immuni.2019.08.017.

Böttcher, Jan P. et al. 2018. "NK Cells Stimulate Recruitment of CDC1 into the Tumor Microenvironment Promoting Cancer Immune Control." *Cell* 172(5): 1022-1037.e14.

Buenrostro, Jason D. et al. 2013. "Transposition of Native Chromatin for Fast and Sensitive Epigenomic Profiling of Open Chromatin, DNA-Binding Proteins and Nucleosome Position." *Nature Methods* 10(12): 1213–18.

Burn, John et al. 2011. "Long-Term Effect of Aspirin on Cancer Risk in Carriers of Hereditary Colorectal Cancer: An Analysis from the CAPP2 Randomised Controlled Trial." *The Lancet* 378(9809): 2081–87. http://dx.doi.org/10.1016/S0140-6736(11)61049-0.

Caglio, Giulia, Elena Torlai Triglia, and Ana Pombo. 2017. "Keep Them Close: PRC2 Poises Enhancer-Promoter Interactions at Anterior Neuronal Genes." *Cell Stem Cell* 20(5): 573–75. http://dx.doi.org/10.1016/j.stem.2017.04.006.

Caronni, Nicoletta et al. 2018. "Downregulation of Membrane Trafficking Proteins and Lactate Conditioning Determine Loss of Dendritic Cell Function in Lung Cancer." *Cancer Research* 78(7): 1685–99.

Chakarov, Svetoslav et al. 2019. "Two Distinct Interstitial Macrophage Populations Coexist across Tissues in Specific Subtissular Niches." *Science* 363(6432).

Chen, Yi Chuan et al. 2016. "Foxp2 Controls Synaptic Wiring of Corticostriatal Circuits and Vocal Communication by Opposing Mef2c." *Nature Neuroscience*.

Cheng, Christine S. et al. 2017. "Iterative Modeling Reveals Evidence of Sequential Transcriptional Control Mechanisms." *Cell Systems* 4(3): 330-343.e5. http://dx.doi.org/10.1016/j.cels.2017.01.012.

Cheng, Quen et al. 2019. "Sequential Conditioning-Stimulation Reveals Distinct Gene- and Stimulus-Specific Effects of Type I and II IFN on Human Macrophage Functions." *Scientific Reports* 9(1): 1–14.

Cheng, Shih Chin et al. 2014. "MTOR- and HIF-1α-Mediated Aerobic Glycolysis as Metabolic Basis for Trained Immunity." *Science* 345(6204).

Cheng, Tse Chang, Mia C. Wallace, John P. Merlie, and Eric N. Olson. 1993. "Separable Regulatory Elements Governing Myogenin Transcription in Mouse Embryogenesis." *Science* 261(5118): 215-18.

Choudhary, Chunaram et al. 2009. "Lysine Acetylation Targets Protein Complexes and Co-Regulates Major Cellular Functions." *Science* 325(5942): 834–40.

Clapier, Cedric R., Janet Iwasa, Bradley R. Cairns, and Craig L. Peterson. 2017. "Mechanisms of Action and Regulation of ATP-Dependent Chromatin-Remodelling Complexes." *Nature Reviews Molecular Cell Biology* 18(7): 407–22. http://dx.doi.org/10.1038/nrm.2017.26.

Clark, Rebecca I. et al. 2013. "MEF2 Is an in Vivo Immune-Metabolic Switch." *Cell* 155(2): 435-447.

Cole, Christina J. et al. 2012. "MEF2 Negatively Regulates Learning-Induced Structural Plasticity and Memory Formation." *Nature Neuroscience* 15(9):1255-64.

Colegio, Oscar R. et al. 2014. "Functional Polarization of Tumour-Associated Macrophages by Tumour-Derived Lactic Acid." *Nature* 513(7519): 559–63.

Corces, M. Ryan et al. 2016. "Lineage-Specific and Single-Cell Chromatin Accessibility Charts Human Hematopoiesis and Leukemia Evolution." *Nature Genetics* 48(10): 1193–1203.

Creemers, Esther E. et al. 2006. "Coactivation of MEF2 by the SAP Domain Proteins Myocardin and MASTR." *Molecular Cell* 23(1):83-96.

Crispatzu, Giuliano et al. 2021. "The Chromatin, Topological and Regulatory Properties of Pluripotency-Associated Poised Enhancers Are Conserved in Vivo." *Nature Communications* 12(1): 1–17. http://dx.doi.org/10.1038/s41467-021-24641-4.

Crittenden, Siobhan et al. 2021. "Prostaglandin E2 Promotes Intestinal Inflammation via Inhibiting Microbiota-Dependent Regulatory T Cells." *Science Advances* 7(7): 1–17.

Cruz-Molina, Sara et al. 2017. "PRC2 Facilitates the Regulatory Topology Required for Poised Enhancer Function during Pluripotent Stem Cell Differentiation." *Cell Stem Cell* 20(5): 689-705.e9. http://dx.doi.org/10.1016/j.stem.2017.02.004.

Cuartero, Sergi et al. 2018. "Control of Inducible Gene Expression Links Cohesin to Hematopoietic Progenitor Self-Renewal and Differentiation." *Nature Immunology* 19(9). http://dx.doi.org/10.1038/s41590-018-0184-1.

Czimmerer, Zsolt et al. 2018. "The Transcription Factor STAT6 Mediates Direct Repression of Inflammatory Enhancers and Limits Activation of Alternatively Polarized Macrophages." *Immunity* 48(1): 75-90.e6.

Dakic, Aleksandar et al. 2005. "PU.1 Regulates the Commitment of Adult Hematopoietic Progenitors and Restricts Granulopoiesis." *Journal of Experimental Medicine* 201(9): 1487–1502.

Deczkowska, Aleksandra et al. 2017. "Mef2C Restrains Microglial Inflammatory Response and Is Lost in Brain Ageing in an IFN-I-Dependent Manner." *Nature Communications* 8(1):717.

Demaria, Olivier et al. 2019. "Harnessing Innate Immunity in Cancer Therapy." *Nature* 574(7776): 45–56.

Dey, Anup et al. 2019. "BRD4 Directs Hematopoietic Stem Cell Development and Modulates Macrophage Inflammatory Responses." *The EMBO Journal* 38(7): 1–17.

Dobin, Alexander et al. 2013. "STAR: Ultrafast Universal RNA-Seq Aligner." *Bioinformatics* 29(1): 15–21.

Fenouil, Romain et al. 2012. "CpG Islands and GC Content Dictate Nucleosome Depletion in a Transcription-Independent Manner at Mammalian Promoters." *Genome Research* 22(12): 2399–2408.

Fitzgerald, Katherine A., and Jonathan C. Kagan. 2020. "Toll-like Receptors and the Control of Immunity." *Cell* 180(6):1044-1066.

Flavell, Steven W. et al. 2006. "Activity-Dependent Regulation of MEF2 Transcription Factors Suppresses Excitatory Synapse Number." *Science* 311(5763):1008-12.

Foster, Simmie L., Diana C. Hargreaves, and Ruslan Medzhitov. 2007. "Gene-Specific Control of Inflammation by TLR-Induced Chromatin Modifications." *Nature* 447(7147): 972–78.

Fujisawa, Takao, and Panagis Filippakopoulos. 2017. "Functions of Bromodomain-Containing Proteins and Their Roles in Homeostasis and Cancer." *Nature Reviews Molecular Cell Biology* 18(4): 246–62.

Gabanyi, Ilana et al. 2016. "Neuro-Immune Interactions Drive Tissue Programming in Intestinal Macrophages." *Cell* 164(3): 378–91. http://dx.doi.org/10.1016/j.cell.2015.12.023.

Gay, Nicholas J., Monique Gangloff, and Luke A.J. O'Neill. 2011. "What the Myddosome Structure Tells Us about the Initiation of Innate Immunity." *Trends in Immunology* 32(3): 104–9. http://dx.doi.org/10.1016/j.it.2010.12.005.

Gaykalova, Daria A. et al. 2011. "A Polar Barrier to Transcription Can Be Circumvented by Remodeler-Induced Nucleosome Translocation." *Nucleic Acids Research* 39(9): 3520–28.

Ghisletti, Serena et al. 2010. "Identification and Characterization of Enhancers Controlling the Inflammatory Gene Expression Program in Macrophages." *Immunity* 32(3): 317–28. http://dx.doi.org/10.1016/j.immuni.2010.02.008.

Gieseck, Richard L., Mark S. Wilson, and Thomas A. Wynn. 2018. "Type 2 Immunity in Tissue Repair and Fibrosis." *Nature Reviews Immunology* 18(1): 62–76. http://dx.doi.org/10.1038/nri.2017.90.

Giladi, Amir et al. 2018. "Single-Cell Characterization of Haematopoietic Progenitors and Their Trajectories in Homeostasis and Perturbed Haematopoiesis." *Nature Cell Biology* 20(July). http://dx.doi.org/10.1038/s41556-018-0121-4.

Gioannini, Theresa L. et al. 2004. "Isolation of an Endotoxin-MD-2 Complex That Produces Toll-like Receptor 4-Dependent Cell Activation at Picomolar Concentrations." *Proceedings of the National Academy of Sciences of the United States of America* 101(12): 4186–91.

Giurisato, Emanuele et al. 2018. "Myeloid ERK5 Deficiency Suppresses Tumor Growth by Blocking Protumor Macrophage Polarization via STAT3 Inhibition." *Proceedings of the National Academy of Sciences of the United States of America* 115(12): E2801–10.

Goodwin, Megan M., Susan Canny, Ashley Steed, and Herbert W. Virgin. 2010. "Helminth Infection Reactivates Latent γ-Herpesvirus via Cytokine Competition at a Viral Promoter." *Journal of Virology* 84(7): 3711–17.

Gosselin, David et al. 2014. "Environment Drives Selection and Function of Enhancers Controlling Tissue-Specific Macrophage Identities." *Cell* 159(6):1327-40.

Gossett, L A, D J Kelvin, E A Sternberg, and E N Olson. 1989. "A New Myocyte-Specific Enhancer-Binding Factor That Recognizes a Conserved Element Associated with Multiple Muscle-Specific Genes." *Molecular and Cellular Biology* 9(11):5022-33.

Guilliams, Martin, Guilhem R. Thierry, Johnny Bonnardel, and Marc Bajenoff. 2020. "Establishment and Maintenance of the Macrophage Niche." *Immunity* 52(3): 434–51. https://doi.org/10.1016/j.immuni.2020.02.015.

Haberle, Vanja, and Alexander Stark. 2018. "Eukaryotic Core Promoters and the Functional Basis of Transcription Initiation." *Nature Reviews Molecular Cell Biology* 19(10): 621–37. http://dx.doi.org/10.1038/s41580-018-0028-8.

Hammond, Colin M. et al. 2017. "Histone Chaperone Networks Shaping Chromatin Function." *Nature Reviews Molecular Cell Biology* 18(3): 141–58.

Hargreaves, Diana C., Tiffany Horng, and Ruslan Medzhitov. 2009. "Control of Inducible Gene Expression by Signal-Dependent Transcriptional Elongation." *Cell* 138(1): 129–45. http://dx.doi.org/10.1016/j.cell.2009.05.047.

Harrison, Oliver J. et al. 2019. "Commensal-Specific T Cell Plasticity Promotes Rapid Tissue Adaptation to Injury." *Science* 363(6422): 1–18.

Harzenetter, Marit D. et al. 2007. "Negative Regulation of TLR Responses by the Neuropeptide CGRP Is Mediated by the Transcriptional Repressor ICER." *The Journal of Immunology* 179(1): 607–15.

He, Ju et al. 2011. "Structure of P300 Bound to MEF2 on DNA Reveals a Mechanism of Enhanceosome Assembly." *Nucleic Acids Research* 39(10):4464-74.

Heintzman, Nathaniel D. et al. 2007. "Distinct and Predictive Chromatin Signatures of Transcriptional Promoters and Enhancers in the Human Genome." *Nature Genetics* 39(3): 311–18.

Heintzman, Nathaniel D. et al. 2009. "Histone Modifications at Human Enhancers Reflect Global Cell-Type-Specific Gene Expression." *Nature* 459(7243): 108–12.

Heinz, S. et al. 2013. "Effect of Natural Genetic Variation on Enhancer Selection and Function." *Nature* 503(7477): 487–92. http://dx.doi.org/10.1038/nature12615.

Heinz, Sven et al. 2010. "Simple Combinations of Lineage-Determining Transcription Factors Prime Cis-Regulatory Elements Required for Macrophage and B Cell Identities." *Molecular Cell* 38(4): 576–89. http://dx.doi.org/10.1016/j.molcel.2010.05.004.

Hinz, Michael, and Claus Scheidereit. 2014. "The IκB Kinase Complex in NF-KB Regulation and Beyond." *EMBO Reports* 15(1): 46–61.

Hole, Camaron R. et al. 2019. "Induction of Memory-like Dendritic Cell Responses in

Vivo." *Nature Communications* 10(1): 1–13. http://dx.doi.org/10.1038/s41467-019-10486-5.

Hoogenkamp, Maarten et al. 2009. "Early Chromatin Unfolding by RUNX1: A Molecular Explanation for Differential Requirements during Specification versus Maintenance of the Hematopoietic Gene Expression Program." *Blood* 114(2): 299–309.

Van Hove, Hannah et al. 2019. "A Single-Cell Atlas of Mouse Brain Macrophages Reveals Unique Transcriptional Identities Shaped by Ontogeny and Tissue Environment." *Nature Neuroscience* 22(6): 1021–35. http://dx.doi.org/10.1038/s41593-019-0393-4.

Hu, Xiaoyu, and Lionel B. Ivashkiv. 2009. "Cross-Regulation of Signaling Pathways by Interferon-γ: Implications for Immune Responses and Autoimmune Diseases." *Immunity* 31(4): 539–50. http://dx.doi.org/10.1016/j.immuni.2009.09.002.

Hubbard, T. et al. 2002. "The Ensembl Genome Database Project." *Nucleic Acids Research* 30(1): 38–41.

Ivashkiv, Lionel B., and Laura T. Donlin. 2014. "Regulation of Type i Interferon Responses." *Nature Reviews Immunology* 14(1): 36–49.

Jaitin, Diego Adhemar et al. 2014. "Massively Parallel Single-Cell RNA-Seq for Marker-Free Decomposition of Tissues into Cell Types." *Science* 343(6172):776-9.

Kagan, Jonathan C. et al. 2008. "TRAM Couples Endocytosis of Toll-like Receptor 4 to the Induction of Interferon-β." *Nature Immunology* 9(4): 361–68.

Kaikkonen, Minna U. et al. 2013. "Remodeling of the Enhancer Landscape during Macrophage Activation Is Coupled to Enhancer Transcription." *Molecular Cell* 51(3): 310–25. http://dx.doi.org/10.1016/j.molcel.2013.07.010.

Kang, Kihwa et al. 2008. "Adipocyte-Derived Th2 Cytokines and Myeloid PPARδ Regulate Macrophage Polarization and Insulin Sensitivity." *Cell Metabolism* 7(6): 485–95.

Kang, Kyuho et al. 2017. "Interferon-γ Represses M2 Gene Expression in Human Macrophages by Disassembling Enhancers Bound by the Transcription Factor MAF." *Immunity* 47(2): 235-250.e4. http://dx.doi.org/10.1016/j.immuni.2017.07.017.

Kang, Kyuho et al. 2019. "IFN-γ Selectively Suppresses a Subset of TLR4-Activated Genes and Enhancers to Potentiate Macrophage Activation." *Nature Communications* 10(1). http://dx.doi.org/10.1038/s41467-019-11147-3.

Kaufmann, Eva et al. 2018. "BCG Educates Hematopoietic Stem Cells to Generate Protective Innate Immunity against Tuberculosis." *Cell* 172(1–2): 176-190.e19.

Kazemian, Majid et al. 2013. "Widespread Evidence of Cooperative DNA Binding by Transcription Factors in Drosophila Development." *Nucleic Acids Research* 41(17): 8237–52.

Kujirai, Tomoya, and Hitoshi Kurumizaka. 2020. "Transcription through the Nucleosome." *Current Opinion in Structural Biology* 61: 42–49. https://doi.org/10.1016/j.sbi.2019.10.007.

Kulaeva, Olga I., Fu Kai Hsieh, and Vasily M. Studitsky. 2010. "RNA Polymerase Complexes Cooperate to Relieve the Nucleosomal Barrier and Evict Histones." *Proceedings of the National Academy of Sciences of the United States of America* 107(25): 11325–30.

van de Laar, Lianne et al. 2016. "Yolk Sac Macrophages, Fetal Liver, and Adult Monocytes Can Colonize an Empty Niche and Develop into Functional Tissue-Resident Macrophages." *Immunity* 44(4): 755–68. http://dx.doi.org/10.1016/j.immuni.2016.02.017.

Labun, Kornel et al. 2019. "CHOPCHOP v3: Expanding the CRISPR Web Toolbox beyond Genome Editing." *Nucleic Acids Research* 47(W1): W171–74.

Lan, Fei et al. 2007. "Recognition of Unmethylated Histone H3 Lysine 4 Links BHC80 to LSD1-Mediated Gene Repression." *Nature* 448(7154): 718–22.

Lavin, Yonit et al. 2014. "Tissue-Resident Macrophage Enhancer Landscapes Are Shaped by the Local Microenvironment." *Cell* 159(6):1312-26.

Lavin, Yonit et al. 2017. "Innate Immune Landscape in Early Lung Adenocarcinoma by Paired Single-Cell Analyses." *Cell* 169(4): 750-765.e17. http://dx.doi.org/10.1016/j.cell.2017.04.014.

Li, Heng et al. 2009. "The Sequence Alignment/Map Format and SAMtools." *Bioinformatics* 25(16): 2078–79.

Li, Heng, and Richard Durbin. 2009. "Fast and Accurate Short Read Alignment with Burrows-Wheeler Transform." *Bioinformatics* 25(14): 1754–60.

Liao, Yang, Gordon K. Smyth, and Wei Shi. 2019. "The R Package Rsubread Is Easier, Faster, Cheaper and Better for Alignment and Quantification of RNA Sequencing Reads." *Nucleic Acids Research* 47(8).

Lichtinger, Monika et al. 2012. "RUNX1 Reshapes the Epigenetic Landscape at the Onset of Haematopoiesis." *EMBO Journal* 31(22): 4318–33.

Link, Verena M. et al. 2018. "Analysis of Genetically Diverse Macrophages Reveals Local and Domain-Wide Mechanisms That Control Transcription Factor Binding and Function." *Cell* 173(7): 1796-1809.e17. http://dx.doi.org/10.1016/j.cell.2018.04.018.

Liu, Siqi et al. 2015. "Phosphorylation of Innate Immune Adaptor Proteins MAVS, STING, and TRIF Induces IRF3 Activation." *Science* 347(6227).

Lu, Jianrong, Timothy A. McKinsey, Chun Li Zhang, and Eric N. Olson. 2000. "Regulation of Skeletal Myogenesis by Association of the MEF2 Transcription Factor with Class II Histone Deacetylases." *Molecular Cell* 6(2):233-44.

Luan, Bing et al. 2015. "CREB Pathway Links PGE2 Signaling with Macrophage Polarization." *Proceedings of the National Academy of Sciences of the United States of America* 112(51): 15642–47.

Luiz, João Paulo M. et al. 2020. "MEK5/ERK5 Signaling Mediates IL-4-Induced M2 Macrophage Differentiation through Regulation of c-Myc Expression." *Journal of Leukocyte Biology* 108(4): 1215–23.

Lumeng, Carey N., Jennifer L. Bodzin, and Alan R. Saltiel. 2007. "Obesity Induces a Phenotypic Switch in Adipose Tissue Macrophage Polarization." *Journal of Clinical Investigation* 117(1): 175–84.

MacKenzie, Kirsty F. et al. 2013. " PGE 2 Induces Macrophage IL-10 Production and a Regulatory-like Phenotype via a Protein Kinase A–SIK–CRTC3 Pathway ." *The Journal of Immunology* 190(2): 565–77.

Mancino, Alessandra et al. 2015. "A Dual Cis-Regulatory Code Links IRF8 to Constitutive and Inducible Gene Expression in Macrophages." *Genes and Development* 29(4):394-408

Martin, M., R. Kettmann, and F. Dequiedt. 2007. "Class IIa Histone Deacetylases: Regulating the Regulators." *Oncogene* 26(37): 5450–67.

Mass, Elvira et al. 2016. "Specification of Tissue-Resident Macrophages during

Organogenesis." *Science* 353(6304).

Matheis, Fanny et al. 2020. "Adrenergic Signaling in Muscularis Macrophages Limits Infection-Induced Neuronal Loss." *Cell* 180(1): 64-78.e16. https://doi.org/10.1016/j.cell.2019.12.002.

Mavrich, Travis N. et al. 2008. "A Barrier Nucleosome Model for Statistical Positioning of Nucleosomes throughout the Yeast Genome." *Genome Research* 18(7): 1073–83.

Milani, Michela et al. 2019. "Phagocytosis-Shielded Lentiviral Vectors Improve Liver Gene Therapy in Nonhuman Primates." *Science Translational Medicine* 11(493): 1–14.

Mills, Charles D. et al. 2000. "M-1/M-2 Macrophages and the Th1/Th2 Paradigm." *The Journal of Immunology* 164(12): 6166–73.

Mills, Charles D. et al. 2012. "M1 and M2 Macrophages: Oracles of Health and Disease." *Critical Reviews in Immunology* 32(6): 463–88.

Miska, Eric A. et al. 1999. "HDAC4 Deacetylase Associates with and Represses the MEF2 Transcription Factor." *EMBO Journal* 18(18):5099-107.

Mitroulis, Ioannis et al. 2018. "Modulation of Myelopoiesis Progenitors Is an Integral Component of Trained Immunity." *Cell* 172(1–2): 147-161.e12.

Molkentin, J D, B L Black, J F Martin, and E N Olson. 1996. "Mutational Analysis of the DNA Binding, Dimerization, and Transcriptional Activation Domains of MEF2C." *Molecular and Cellular Biology* 16(6):2627-36

Molkentin, Jeffery D., Brian L. Black, James F. Martin, and Eric N. Olson. 1995. "Cooperative Activation of Muscle Gene Expression by MEF2 and Myogenic BHLH Proteins." *Cell* 83(7):1125-36

Mossadegh-Keller, Noushine et al. 2013. "M-CSF Instructs Myeloid Lineage Fate in Single Haematopoietic Stem Cells." *Nature* 497(7448): 239–43.

Muñoz-Rojas, Andrés R. et al. 2021. "Co-Stimulation with Opposing Macrophage Polarization Cues Leads to Orthogonal Secretion Programs in Individual Cells." *Nature Communications* 12(1): 1–12. http://dx.doi.org/10.1038/s41467-020-20540-2.

Murakami, Koichi et al. 2021. "A RUNX–CBFβ-Driven Enhancer Directs the Irf8 Dose-Dependent Lineage Choice between DCs and Monocytes." *Nature*

Immunology 22(3): 301–11. http://dx.doi.org/10.1038/s41590-021-00871-y.

Murray, Peter J., and Stephen T. Smale. 2012. "Restraint of Inflammatory Signaling by Interdependent Strata of Negative Regulatory Pathways." *Nature Immunology* 13(10): 916–24.

Nakanishi, Masako, and Daniel W. Rosenberg. 2013. "Multifaceted Roles of PGE2 in Inflammation and Cancer." *Seminars in Immunopathology* 35(2): 123–37.

Natoli, Gioacchino, and Renato Ostuni. 2019. "Adaptation and Memory in Immune Responses." *Nature Immunology* 20(7): 783–92. http://dx.doi.org/10.1038/s41590-019-0399-9.

Nicodeme, Edwige et al. 2010. "Suppression of Inflammation by a Synthetic Histone Mimic." *Nature* 468(7327): 1119–23.

Nitsch, Sandra, Lara Zorro Shahidian, and Robert Schneider. 2021. "Histone Acylations and Chromatin Dynamics: Concepts, Challenges, and Links to Metabolism." *EMBO reports* 22(7): 1–13.

Novakovic, Boris et al. 2016. "β-Glucan Reverses the Epigenetic State of LPS-Induced Immunological Tolerance." *Cell* 167(5): 1354-1368.e14. http://dx.doi.org/10.1016/j.cell.2016.09.034.

Ooi, Steen K.T. et al. 2007. "DNMT3L Connects Unmethylated Lysine 4 of Histone H3 to de Novo Methylation of DNA." *Nature* 448(7154): 714–17.

Osborne, Lisa C. et al. 2014. "Virus-Helminthcoinfection Reveals a Microbiota-Independent Mechanism of Immunomodulation." *Science* 345(6196): 578–82.

Ostuni, Renato et al. 2013. "Latent Enhancers Activated by Stimulation in Differentiated Cells." *Cell* 152(1-2):157-71

Oudelaar, A. Marieke, and Douglas R. Higgs. 2021. "The Relationship between Genome Structure and Function." *Nature Reviews Genetics* 22(3): 154–68. http://dx.doi.org/10.1038/s41576-020-00303-x.

Ouyang, Wenjun, and Anne O'Garra. 2019. "IL-10 Family Cytokines IL-10 and IL-22: From Basic Science to Clinical Translation." *Immunity* 50(4): 871–91. https://doi.org/10.1016/j.immuni.2019.03.020.

Park, Beom Seok, and Jie Oh Lee. 2013. "Recognition of Lipopolysaccharide Pattern by TLR4 Complexes." *Experimental and Molecular Medicine* 45(12).

Park, Sung Ho et al. 2017. "Type i Interferons and the Cytokine TNF Cooperatively

Reprogram the Macrophage Epigenome to Promote Inflammatory Activation." *Nature Immunology* 18(10): 1104–16.

Pearson, Gray W., Svetlana Earnest, and Melanie H. Cobb. 2006. "Cyclic AMP Selectively Uncouples Mitogen-Activated Protein Kinase Cascades from Activating Signals." *Molecular and Cellular Biology* 26(8): 3039–47.

Pereira, Diane M., and Cecília M.P. Rodrigues. 2020. "Targeted Avenues for Cancer Treatment: The MEK5–ERK5 Signaling Pathway." *Trends in Molecular Medicine* 26(4): 394–407. https://doi.org/10.1016/j.molmed.2020.01.006.

Perkins, Darren J. et al. 2018. "Autocrine–Paracrine Prostaglandin E 2 Signaling Restricts TLR4 Internalization and TRIF Signaling." *Nature Immunology* 19(12): 1309–18. http://dx.doi.org/10.1038/s41590-018-0243-7.

Piccolo, Viviana et al. 2017. "Opposing Macrophage Polarization Programs Show Extensive Epigenomic and Transcriptional Cross-Talk." *Nature Immunology* 18(5):530-540.

Picelli, Simone et al. 2014. "Full-Length RNA-Seq from Single Cells Using Smart-Seq2." *Nature Protocols* 9(1):171-81

Porta, Chiara et al. 2020. "Tumor-Derived Prostaglandin E2 Promotes P50 NF-KB-Dependent Differentiation of Monocytic MDSCs." *Cancer Research* 80(13): 2874–88.

Pruitt, Kim D., Tatiana Tatusova, and Donna R. Maglott. 2007. "NCBI Reference Sequences (RefSeq): A Curated Non-Redundant Sequence Database of Genomes, Transcripts and Proteins." *Nucleic Acids Research* 35(SUPPL. 1): 61–65.

Qiao, Yu et al. 2013. "Synergistic Activation of Inflammatory Cytokine Genes by Interferon-γ-Induced Chromatin Remodeling and Toll-like Receptor Signaling." *Immunity* 39(3): 454–69. http://dx.doi.org/10.1016/j.immuni.2013.08.009.

Qiao, Yu et al. 2016. "IFN-γ Induces Histone 3 Lysine 27 Trimethylation in a Small Subset of Promoters to Stably Silence Gene Expression in Human Macrophages." *Cell Reports* 16(12): 3121–29. http://dx.doi.org/10.1016/j.celrep.2016.08.051.

Quinlan, Aaron R., and Ira M. Hall. 2010. "BEDTools: A Flexible Suite of Utilities for Comparing Genomic Features." *Bioinformatics* 26(6): 841–42.

Quintin, Jessica et al. 2012. "Candida Albicans Infection Affords Protection against Reinfection via Functional Reprogramming of Monocytes." *Cell Host and Microbe*

12(2): 223–32.

Rada-Iglesias, Alvaro et al. 2011. "A Unique Chromatin Signature Uncovers Early Developmental Enhancers in Humans." *Nature* 470(7333): 279–85.

Ramirez-Carrozzi, Vladimir R. et al. 2006. "Selective and Antagonistic Functions of SWI/SNF and Mi-2β Nucleosome Remodeling Complexes during an Inflammatory Response." *Genes and Development* 20(3): 282–96.

Ramirez-Carrozzi, Vladimir R. et al. 2009. "A Unifying Model for the Selective Regulation of Inducible Transcription by CpG Islands and Nucleosome Remodeling." *Cell* 138(1):114-28.

Ramírez, Fidel et al. 2014. "DeepTools: A Flexible Platform for Exploring Deep-Sequencing Data." *Nucleic Acids Research* 42(W1): 187–91.

Redecke, Vanessa et al. 2013. "Hematopoietic Progenitor Cell Lines with Myeloid and Lymphoid Potential." *Nature Methods* 10(8): 795–803.

Robinson, Mark D., Davis J. McCarthy, and Gordon K. Smyth. 2009. "EdgeR: A Bioconductor Package for Differential Expression Analysis of Digital Gene Expression Data." *Bioinformatics* 26(1): 139–40.

Robinson, Mark D., and Alicia Oshlack. 2010. "Deseq2论文附录." *Genome Biology* 11(3): 1–9. http://genomebiology.com/2010/11/3/R25.

Rodríguez-Ubreva, Javier et al. 2017. "Prostaglandin E2 Leads to the Acquisition of DNMT3A-Dependent Tolerogenic Functions in Human Myeloid-Derived Suppressor Cells." *Cell Reports* 21(1): 154–67.

Roers, Axel, Björn Hiller, and Veit Hornung. 2016. "Recognition of Endogenous Nucleic Acids by the Innate Immune System." *Immunity* 44(4): 739–54.

Ryu, Je Kyung et al. 2017. "Reconstruction of LPS Transfer Cascade Reveals Structural Determinants within LBP, CD14, and TLR4-MD2 for Efficient LPS Recognition and Transfer." *Immunity* 46(1): 38–50. http://dx.doi.org/10.1016/j.immuni.2016.11.007.

Sabio, Guadalupe, and Roger J. Davis. 2014. "TNF and MAP Kinase Signalling Pathways." *Seminars in Immunology* 26(3): 237–45. http://dx.doi.org/10.1016/j.smim.2014.02.009.

Saeed, Sadia et al. 2014. "Epigenetic Programming of Monocyte-to-Macrophage Differentiation and Trained Innate Immunity." *Science* 345(6204).

Sakai, Mashito et al. 2019. "Liver-Derived Signals Sequentially Reprogram Myeloid Enhancers to Initiate and Maintain Kupffer Cell Identity." *Immunity* 51(4):655-670.e8.

Sandmann, Thomas et al. 2006. "A Temporal Map of Transcription Factor Activity: Mef2 Directly Regulates Target Genes at All Stages of Muscle Development." *Developmental Cell* 10(6):797-807.

Sanin, David E. et al. 2018. "Mitochondrial Membrane Potential Regulates Nuclear Gene Expression in Macrophages Exposed to Prostaglandin E2." *Immunity* 49(6): 1021-1033.e6.

Sartorelli, V, J Huang, Y Hamamori, and L Kedes. 1997. "Molecular Mechanisms of Myogenic Coactivation by P300: Direct Interaction with the Activation Domain of MyoD and with the MADS Box of MEF2C." *Molecular and Cellular Biology* 17(2):1010-26.

Schulz, Christian et al. 2012. "A Lineage of Myeloid Cells Independent of Myb and Hematopoietic Stem Cells." *Science* 335(6077): 86–90.

Sebastian, Soji et al. 2013. "Tissue-Specific Splicing of a Ubiquitously Expressed Transcription Factor Is Essential for Muscle Differentiation." *Genes and Development* 27(11):1247-59.

Seeley, John J., and Sankar Ghosh. 2017. "Molecular Mechanisms of Innate Memory and Tolerance to LPS." *Journal of Leukocyte Biology* 101(1): 107–19.

Segal, Eran et al. 2006. "A Genomic Code for Nucleosome Positioning." *Nature* 442(7104): 772–78.

Shalizi, Aryaman et al. 2006. "A Calcium-Regulated MEF2 Sumoylation Switch Controls Postsynaptic Differentiation." *Science* 311(5763):1012-7.

Shen, Chen et al. 2015. "NSD3-Short Is an Adaptor Protein That Couples BRD4 to the CHD8 Chromatin Remodeler." *Molecular Cell* 60(6): 847–59. http://dx.doi.org/10.1016/j.molcel.2015.10.033.

Smale, Stephen T. 2010. "Selective Transcription in Response to an Inflammatory Stimulus." *Cell* 140(6): 833–44. http://dx.doi.org/10.1016/j.cell.2010.01.037.

Subramanian, Aravind et al. 2005. "Gene Set Enrichment Analysis: A Knowledge-Based Approach for Interpreting Genome-Wide Expression Profiles." *Proceedings of the National Academy of Sciences of the United States of America* 102(43):

15545–50.

Tan, Yunhao et al. 2015. "Mechanisms of Toll-like Receptor 4 Endocytosis Reveal a Common Immune-Evasion Strategy Used by Pathogenic and Commensal Bacteria." *Immunity* 43(5): 909–22. http://dx.doi.org/10.1016/j.immuni.2015.10.008.

Taniguchi, Koji, and Michael Karin. 2018. "NF-B, Inflammation, Immunity and Cancer: Coming of Age." *Nature Reviews Immunology* 18(5): 309–24. http://dx.doi.org/10.1038/nri.2017.142.

Tong, Ann Jay et al. 2016. "A Stringent Systems Approach Uncovers Gene-Specific Mechanisms Regulating Inflammation." *Cell* 165(1): 165–79. http://dx.doi.org/10.1016/j.cell.2016.01.020.

Trapnell, Cole et al. 2014. "The Dynamics and Regulators of Cell Fate Decisions Are Revealed by Pseudotemporal Ordering of Single Cells." *Nature Biotechnology* 32(4): 381–86.

Treger, Rebecca S. et al. 2019. "The Lupus Susceptibility Locus Sgp3 Encodes the Suppressor of Endogenous Retrovirus Expression SNERV." *Immunity* 50(2): 334-347.e9. https://doi.org/10.1016/j.immuni.2018.12.022.

Uematsu, Satoshi, Makoto Matsumoto, Kiyoshi Takeda, and Shizuo Akira. 2002. " Lipopolysaccharide-Dependent Prostaglandin E 2 Production Is Regulated by the Glutathione-Dependent Prostaglandin E 2 Synthase Gene Induced by the Toll-Like Receptor 4/MyD88/NF-IL6 Pathway ." *The Journal of Immunology* 168(11): 5811–16.

Vierbuchen, Thomas et al. 2017. "AP-1 Transcription Factors and the BAF Complex Mediate Signal-Dependent Enhancer Selection." *Molecular Cell* 68(6):1067-1082.e12.

Walsh, Jonathan C. et al. 2002. "Cooperative and Antagonistic Interplay between PU.1 and GATA-2 in the Specification of Myeloid Cell Fates." *Immunity* 17(5): 665–76.

Wang, Zhong et al. 2021. "Interdependence between Histone Marks and Steps in Pol II Transcription." (607).

Weber, Axel, Peter Wasiliew, and Michael Kracht. 2010. "Interleukin-1 (IL-1) Pathway." *Science Signaling* 3(105).

Xue, Jia et al. 2014. "Transcriptome-Based Network Analysis Reveals a Spectrum

Model of Human Macrophage Activation." *Immunity* 40(2): 274–88. http://dx.doi.org/10.1016/j.immuni.2014.01.006.

Yadav, Tejas, Jean Pierre Quivy, and Geneviève Almouzni. 2018. "Chromatin Plasticity: A Versatile Landscape That Underlies Cell Fate and Identity." *Science* 361(6409): 1332–36.

Yang, Xiang Jiao, and Edward Seto. 2008. "Lysine Acetylation: Codified Crosstalk with Other Posttranslational Modifications." *Molecular Cell* 31(4): 449–61.

Zanoni, Ivan et al. 2009. "CD14 Regulates the Dendritic Cell Life Cycle after LPS Exposure through NFAT Activation." *Nature* 460(7252): 264–68. http://dx.doi.org/10.1038/nature08118.

Zanoni, Ivan et al. 2011. "CD14 Controls the LPS-Induced Endocytosis of Toll-like Receptor 4." *Cell* 147(4): 868–80. http://dx.doi.org/10.1016/j.cell.2011.09.051.

Zaret, Kenneth S. 2020. "Pioneer Transcription Factors Initiating Gene Network Changes." *Annual Review of Genetics* 54: 367–85.

Zelenay, Santiago et al. 2015. "Cyclooxygenase-Dependent Tumor Growth through Evasion of Immunity." *Cell* 162(6): 1257–70.

Zhang, Tiantian et al. 2020. "Histone H3K27 Acetylation Is Dispensable for Enhancer Activity in Mouse Embryonic Stem Cells." *Genome Biology* 21(1): 1–7.

Zhang, Yong et al. 2008. "Model-Based Analysis of ChIP-Seq (MACS)." *Genome Biology* 9(9).

Zheng, Grace X.Y. et al. 2017. "Massively Parallel Digital Transcriptional Profiling of Single Cells." *Nature Communications* 8.

Zhu, Lihua J. et al. 2010. "ChIPpeakAnno: A Bioconductor Package to Annotate ChIP-Seq and ChIP-Chip Data." *BMC Bioinformatics* 11.